Agrociencia

eISSN: 2521-9766

VOLUME 60, NUMBER 2 | February 16 - March 31, 2026 | MEXICO

AGRICULTURA
SECRETARÍA DE AGRICULTURA

COPYRIGHT AND RELATED RIGHTS, **Volume 60, Number 2, February 16 - March 31, 2026**, Agrociencia is a semi-monthly publication edited by Colegio de Postgraduados. Carretera Mexico-Texcoco, Km 36.5, Montecillo, Texcoco, State of Mexico. C. P. 56264. Phone: 5959284427. www.colpos.mx. Editor in chief: Dr. Fernando Carlos Gómez Merino. Reservations of Rights to Exclusive Use 04-2021-031913431800-203. eISSN: 2521-9766, granted by the National Copyright Institute. Last modification date, **March 31, 2026**.

The opinions expressed by the authors do not necessarily reflect the position of the editor of the publication.

All correspondence (subscription information, sales, advertising, author contributions, etc.) should be addressed to:

Central Office:

Agrociencia
Guerrero No. 9, Esquina con Avenida Hidalgo,
San Luis Huexotla, Texcoco 56220,
State of Mexico. MEXICO
Tel.: +52-595 92 84427

https://agrociencia-colpos.org/index.php/agrociencia

Cover: Geese
Designed by Pixabay

AGRICULTURA
SECRETARÍA DE AGRICULTURAY DESARROLLO RURAL

Contents

Volume 60, Number 2 | February 16 - March 31, 2026

Agrociencia

DYNAMIC CHARACTERISTICS OF MEMBRANE-TYPE AIR SPRINGS WITH AUXILIARY CHAMBER

Chunyan **Kong***, Xiaotong **Liu,** Xian **Wang,** Shunyao **Wang,** Guangli **Liu,** Mingkun **Yang,** Shuangshuang **Li**

Xihua University. School of Mechanical Engineering. Chengdu 610039, China.
* Author for correspondence: kongcy@mail.xhu.edu.cn

Citation: Kong C, Liu X, Wang X, Wang S, Liu G, Yang M, Li S. 2026. Dynamic characteristics of membrane-type air springs with auxiliary chamber. **Agrociencia** 60(2): 175-194. https://doi.org/ 10.47163/agrociencia.v60i2.3579

Editor in Chief:
Dr. Fernando C. Gómez Merino

Received: November 19, 2025.
Approved: March 10, 2026.
Published in Agrociencia: March 24, 2026.

ABSTRACT

Air springs with auxiliary chambers are widely used by automobile manufacturers due to their lightweight design, low noise, superior shock absorption performance, and adjustable stiffness. The structural parameters of the auxiliary chamber and connecting pipeline play a decisive role in the shock absorption performance of air springs. This paper established a numerical simulation model for air springs with auxiliary chambers and studied the influence of the connecting pipeline diameter and the auxiliary chamber volume on the dynamic characteristics of air springs. The results indicate that, under the same initial internal pressure, the position where the stiffness tends to flatten shifts to higher frequencies as the pipeline diameter increases. As the pipeline diameter increased, the auxiliary chamber affected the stiffness over a broader frequency range. At lower loading frequencies, smaller pipeline diameters had a greater impact on stiffness, while larger pipeline diameters had a lesser impact. As the frequency increases, larger pipeline diameters gradually exert a stronger influence on stiffness. Between 2 and 6 Hz, the stiffness under different initial internal pressures decreased as the auxiliary chamber volume increased, while between 14 and 30 Hz, the opposite trend was observed. At all loading frequencies, the stiffness under different initial internal pressures decreased with increasing auxiliary chamber volume at 2 Hz, but as the loading frequency increased, this trend gradually reversed.

Keywords: Agricultural engineering, agricultural machinery, numerical simulation, stiffness, connecting pipe, finite element analysis.

INTRODUCTION

At present, the springs used in vehicles are mainly divided into two categories: ordinary springs and air springs (Figure 1). Ordinary springs include leaf springs, helical springs, and torsion bar springs. As modern automotive design and manufacturing have become increasingly aware of the importance of passenger comfort, air springs are increasingly being adopted by automakers due to their lightweight design, low noise, superior shock absorption performance, and road friendliness. Based on different structures of their air bags, air springs can be classified into three types: membrane-type, bellows-type, and sleeve-type (Kong *et al.*, 2025).

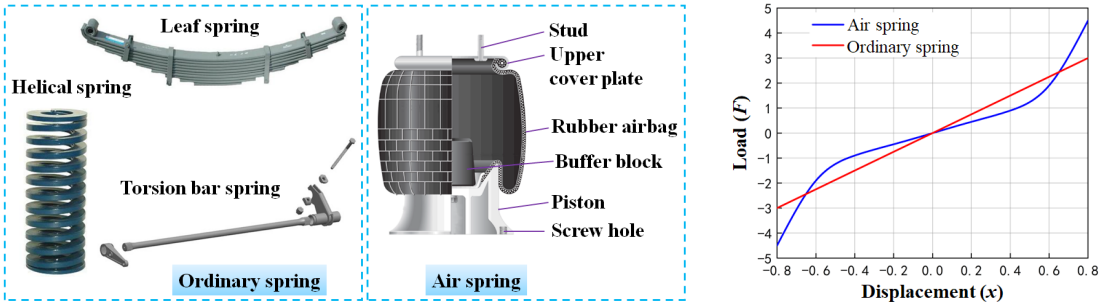

Figure 1. Comparison of springs used in vehicles.

Membrane-type air springs are commonly utilized in passenger vehicles due to their lower stiffness compared to bellows-type air springs. They also possess a straightforward structure, which allows for variations in elastic characteristics by simply adjusting structural parameters (Atindana *et al.*, 2023; Van and Tung, 2023). However, traditional single-chamber air springs are now struggling to meet people's demands for vehicle ride smoothness. Therefore, this paper focused on the study of membrane-type air springs with auxiliary chambers (ASWAC). Due to the influence of connecting pipelines and auxiliary chambers, the stiffness characteristics of ASWAC differ significantly from those of single-chamber air springs. The structural parameters of the connecting pipeline and auxiliary chamber present major challenges in ASWAC research (Zheng *et al*., 2016).

Numerous scholars, both domestically and internationally, have investigated this topic. Toyofuku *et al*. (1999) proposed a model to analyze the dynamic characteristics of air springs equipped with auxiliary chambers and pipelines, considering the relationship between vibration frequency and spring response and examining the effect of the pipeline on the dynamic spring constant. Zhang *et al*. (2020) verified the effectiveness of a proposed semi-active control system for air suspensions through numerical simulations. Mendia-García *et al*. (2022) used the Abaqus software to analyze the effects of selected structural parameters and initial internal pressure on the load-bearing performance of the main air chamber. These studies offer limited information on the structural parameters of ASWAC. As a result, it is challenging to accurately characterize the relationships and variation patterns between the structural parameters of the connecting pipelines and auxiliary chambers, as well as their dynamic stiffness.

This paper takes the air spring of a certain Mercedes-Benz model as the structural basis and adds an auxiliary chamber to it (Figure 2). By utilizing the Fluent software, a finite element simulation model is established to explore the variation patterns between the auxiliary chamber and its connecting pipeline and the dynamic characteristics of the air spring. This provides a certain theoretical foundation for the design and development of membrane-type ASWAC.

Figure 2. Structural configuration of the modified air suspension assembly.

MATERIALS AND METHODS

Theoretical basis of air springs with auxiliary chambers

The physical model of the air spring system with an auxiliary chamber (Figure 3) consists of a main chamber that includes a rubber bladder, an upper cover plate, and a piston. The auxiliary chamber comprises a cavity, and the main chamber is connected to the auxiliary chamber through a pipeline (Piller *et al*., 2002). Wherein P_1, V_1, and T_1 represent the absolute pressure, gas volume, and gas temperature in the main chamber, respectively; P_2, V_2, and T_2 represent the absolute pressure, gas volume, and gas temperature in the auxiliary chamber, respectively; and P_g, V_g, and T_g represent

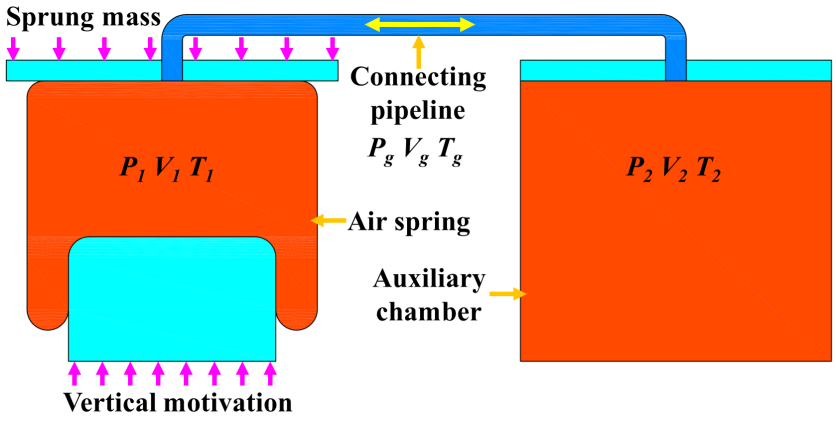

Figure 3. Physical model of the air spring system with auxiliary chamber and connecting pipeline.

the absolute pressure, gas volume, and gas temperature in the pipeline, respectively. During the operation of an air spring, its primary load comes from forces acting in the vertical direction (Chen *et al*., 2011; Wong *et al*., 2024). In this study, only the vertical motion of the air spring was considered.

While a vehicle is driving on the road, it experiences vibrations due to road irregularities or other external excitations. These vibrations are transmitted to the air spring through the vehicle's suspension system, causing deformation of the bladder in the main chamber. As the excitation intensifies, the air spring undergoes significant up-and-down vibrations, which alter its internal volume and pressure. At this point, changes in the internal pressure of the bladder will cause gas to flow between the main chamber and the auxiliary chamber, which are connected by a pipeline or orifice. The auxiliary chamber, serving as an additional volume, can accommodate more gas, thereby buffering the changes in pressure within the main chamber to a certain extent. The orifice or pipeline plays a crucial role in the process of gas flow (Karpenko *et al*., 2023; Mehmood *et al*., 2023). They not only restrict the gas flow velocity but also create a certain damping effect during the flow. This damping effect helps to attenuate vibrations, enabling the air spring to better absorb and disperse impacts from the road surface (Karachinskii and Timofeev, 2023). Through the synergistic effect of the main chamber, auxiliary chamber, and orifice or pipeline, the ASWAC can maintain stable performance under different vibration conditions.

The energy conservation equation for the main chamber of an ASWAC was defined as follows (Wissink, 2003; Zhang *et al*., 2005; Zhu *et al*., 2008):

$$dQ_1 + d(h_{1in} - h_{1out}) + dW_1 = dE_1$$

where Q_1 represents the heat exchange between the main chamber of the air spring and the external environment; h_{1in} is the inflow enthalpy of the main chamber; h_{1out} is the outflow enthalpy of the main chamber; W_1 is the work done by external forces on the main chamber; and E_1 is the total energy of the gas within the main chamber.

Similarly, based on the energy conservation equation for the main chamber, the energy conservation equation for the auxiliary chamber can be expressed as:

$$dQ_2 + d(h_{2in} - h_{2out}) + dW_2 = dE_2$$

where Q_2 represents the heat exchange between the auxiliary chamber of the air spring and the external environment; h_{2in} is the inflow enthalpy of the auxiliary chamber; h_{2out} is the outflow enthalpy of the auxiliary chamber; W_2 is the work done by external forces on the auxiliary chamber; and E_2 is the total energy of the gas within the auxiliary chamber.

When an ASWAC is in operation, due to the presence of the connecting pipeline, an exchange of gas and energy occurs between the main chamber and the auxiliary

chamber (Berg, 2000; Quaglia and Sorli, 2001). Therefore, the energy conservation equation and the gas state equation were used to describe the process of air changes within the air spring and the auxiliary reservoir. The gas flow rate equation was utilized to describe the mass exchange of air between the air spring and the auxiliary reservoir. To simplify the problem, discussions were held regarding the following scenarios:

1) During the operation of an air spring, as the frequency of displacement excitation increases, heat exchange between the air spring and the auxiliary chamber with the external environment becomes extremely difficult. When the amplitude of displacement excitation in the main chamber of the air spring is limited to ±10 mm, the gas exchange between the main and auxiliary chambers decreases (Williams, 1997; Mao *et al*., 2023).
2) In general, the air spring and the auxiliary chamber are installed in a basically horizontal position on a vehicle, with almost zero height difference between them. Therefore, the potential and kinetic energy between the main chamber of the air spring and the auxiliary chamber can be ignored.
3) According to the static experimental results of automotive air springs (Liu and Lee, 2011), when the excitation amplitude is ±10 mm, the relative error in the effective area change is only 6.37 %. Therefore, when conducting theoretical modeling, the effective area can be treated as a constant.

Establishment of a finite element model

According to Kong *et al*. (2024), the characteristics of the main chamber of the air spring under different initial internal pressures and displacements were analyzed. The loads and actual internal pressures of the main chamber under these conditions were obtained. Therefore, the equivalent area of the air spring at different initial internal pressures and displacements could be calculated (Table 1).

The equivalent area of the air spring within an excitation amplitude of ±10 mm was calculated under different initial internal pressures (Figure 4). At the same initial internal pressure, the equivalent area of the air spring varies slightly within a certain range for different displacements. The maximum difference in area occurs at an initial pressure of 0.25 MPa, with a value of 693.0939 mm², which is relatively small. Furthermore, taking the equivalent area at a displacement of 0 mm as the reference value, it can be determined that the maximum relative error in the equivalent area of the air spring appears at an initial internal pressure of 0.2 MPa, and it is only 2.45 %. Therefore, in this simulation experiment, when the excitation amplitude is ±10 mm, the effective area of the air spring can be considered a constant value.

The overall structure of the ASWAC is relatively simple, consisting solely of the main air chamber, connecting pipeline, and auxiliary chamber. By simplifying this structure and only considering the internal flow field, the finite element model was obtained (Figure 5).

Table 1. Equivalent effective area of the air spring within ±10 mm displacement under varying initial internal pressures (0.1–0.3 MPa).

Pressure Displacement	0.1 MPa	0.15 MPa	0.2 MPa	0.25 MPa	0.3 MPa
-10	21 740.45	22 413.26	23 934.71	25 121.07	25 908.84
-8	21 868.72	22 443.53	23 762.01	25 049.99	26 009.93
-6	21 996.99	22 546.37	23 578.05	24 983.17	26 058.25
-4	22 038.93	22 649.20	23 394.09	24 916.34	26 106.57
-2	22 080.87	22 642.92	23 377.77	24 827.99	26 093.62
0	22 048.19	22 636.65	23 361.45	24 739.63	26 080.67
2	22 015.51	22 684.95	23 409.42	24 623.80	26 076.54
4	22 018.78	22 733.26	23 457.39	24 507.96	26 072.40
6	22 022.05	22 792.23	23 527.75	24 467.97	26 045.27
8	22 094.48	22 851.20	23 598.10	24 427.97	26 018.13
10	22 166.91	22 851.12	23 587.41	24 476.50	25 961.50
Maximum area (mm^2)	426.45	437.94	573.26	693.09	197.74
Maximum relative error	1.40 %	0.99 %	2.45 %	1.54 %	0.66 %

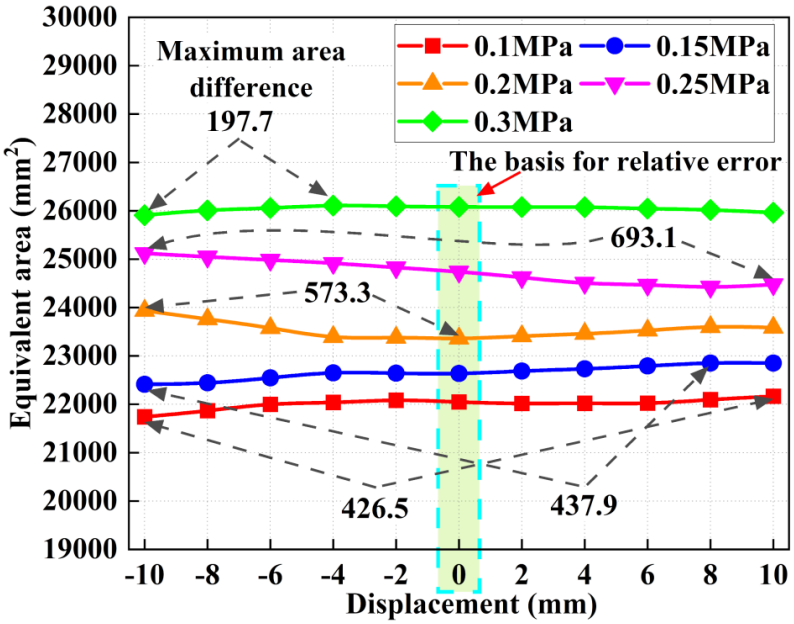

Figure 4. Variation of equivalent effective area within ±10 mm excitation amplitude under different initial internal pressures.

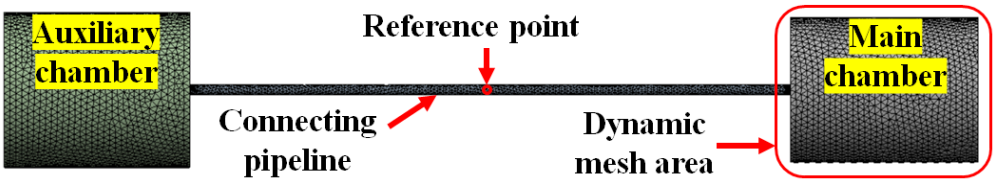

Figure 5. Simplified finite element model of the air spring with auxiliary chamber (ASWAC) internal flow field.

Mesh generation for the computational domain

A conformal algorithm was adopted to ensure the accuracy and efficiency of the simulation (Papkov *et al*., 2023). From the finite element model of the ASWAC, the entire computational domain can be divided into three parts: the main chamber, the auxiliary chamber, and the connecting pipeline. The dimensions of these three parts vary significantly, and the internal gas flow patterns are also different. Therefore, different mesh sizes were selected to discretize each region. Due to the small size of the connecting pipeline and the complexity of its internal flow field, a finer mesh size was required. Thus, preliminary mesh sizes of 1, 2, 3, 4, and 5 mm were selected. The main chamber and the auxiliary chamber have larger dimensions and simpler internal flow fields, allowing for larger mesh sizes. Hence, preliminary mesh sizes of 6, 8, 10, 12, and 14 mm were selected.

Mesh convergence analysis for the computational domain

When the mesh size was reduced to 2 mm, the stiffness was 33.157 N mm^{-1}, requiring approximately 600 min of simulation time (Figure 6). When the mesh size was further reduced to 1mm, the stiffness was 33.139 N mm^{-1}, showing a minimal difference compared to the stiffness at 2 mm, but the simulation time increased to 690 min. Considering both the accuracy and computational efficiency of the simulation, 2 mm was selected as the optimal mesh size for the pipeline. When the piping mesh size was 2 mm, its element quality and skewness were both within acceptable ranges (Table 2). As the mesh size decreased, the stiffness gradually diminished (Figure 7). When the mesh size was reduced to 6 and 8 mm, the stiffness remained stable, and no significant changes were observed, indicating that the influence of mesh size on the simulation results can be neglected at these sizes. The element quality and skewness were both within reasonable ranges when the mesh size was 6 and 8 mm (Table 3). Considering both the accuracy and efficiency of the simulation, the 8 mm mesh size was selected for the chamber.

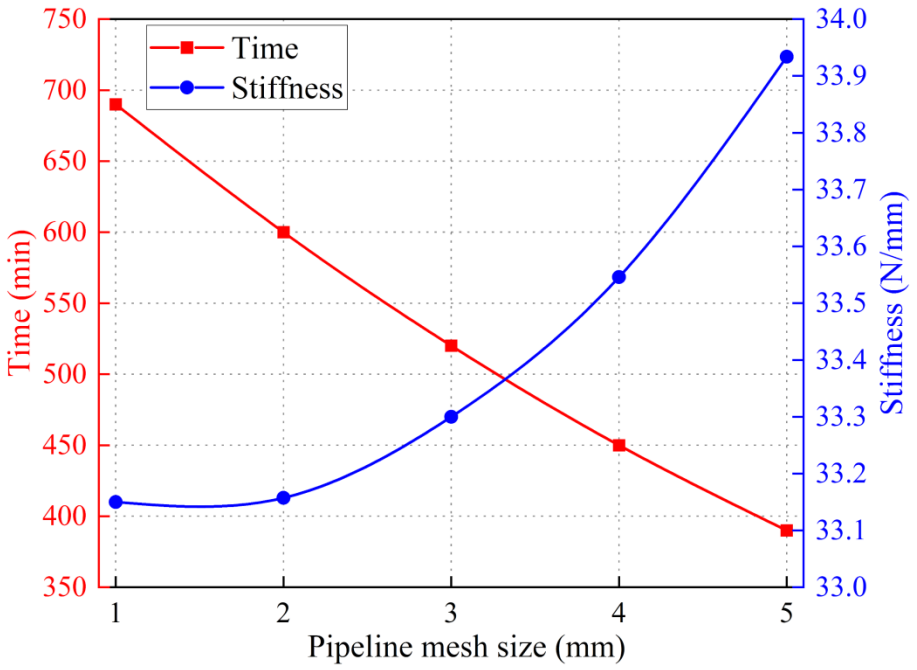

Figure 6. Pipeline mesh independence analysis based on dynamic stiffness and computational time.

Table 2. Element quality and skewness metrics of the pipeline mesh under different mesh sizes.

Mesh size (mm)	1	2	3	4	5
Element quality	0.85082	0.8439	0.84113	0.83949	0.83953
Skewness	0.20701	0.21777	0.22253	0.22565	0.22568

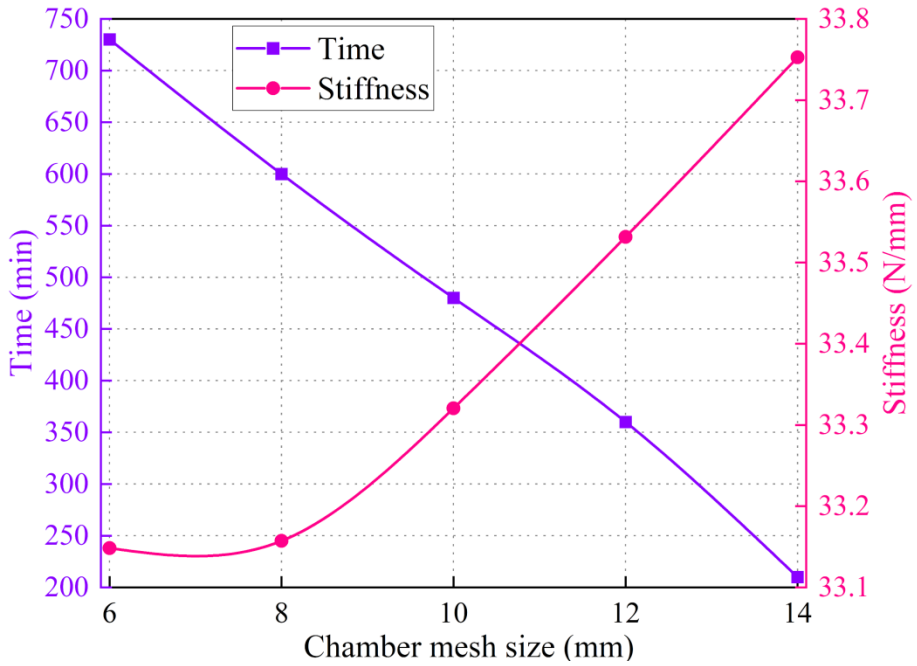

Figure 7. Chamber mesh independence analysis of chamber discretization based on dynamic stiffness response.

Table 3. Element quality and skewness evaluation of the chamber mesh under different mesh sizes.

Mesh size (mm)	6	8	10	12	14
Element quality	0.8438	0.8439	0.8457	0.8464	0.8467
Skewness	0.21808	0.21777	0.21477	0.21363	0.21327

Parameters for the simulation model

Loading pressure

To ensure that the ASWAC had the same load-bearing capacity as the main chamber of the air spring under the same initial internal pressure, the actual internal pressure at the design height of the main chamber of the air spring was considered as the loading pressure for the ASWAC at its design height. The correspondence table details the relationship between the initial internal pressure and the actual internal pressure at the design height (Table 4).

Table 4. Initial internal pressure and actual internal pressure at design height.

Initial internal pressure (MPa)	0.1	0.15	0.2	0.25	0.3
Actual internal pressure (MPa)	0.1497	0.2037	0.2551	0.3066	0.3590

Selection of the auxiliary chamber

Studies have indicated that the air spring performs optimally when the volume ratio of the auxiliary chamber to the main chamber does not exceed two (Constantin *et al*., 2024). The air spring selected for this work has a main chamber volume of approximately 5.4 L. Therefore, the relationship between the volume of the auxiliary chamber and the stiffness of the air spring was explored by selecting auxiliary chamber volumes of 4, 6, 8, and 10 L.

Selection of the connecting pipelines

To minimize the obstruction to air flow caused by the connecting pipeline and to accommodate the installation position of the air spring on the vehicle, a pipeline length of 800 mm was selected for this simulation. Additionally, pipeline diameters of 8, 10, 12, 16, 18, and 20 mm were chosen to investigate their relationship with the stiffness of the air spring.

Extraction of research parameters

After initializing the loading pressure for the ASWAC, a dynamic mesh was utilized to apply a sinusoidal resonant frequency with an amplitude of ±10 mm to the airbag section. The frequency values were the same as those used in the dynamic characteristic analysis of the main chamber, namely 30, 23, 14, 6, and 2 Hz. Concurrently, the surface pressure on the moving part of the airbag mesh surface was recorded when the sinusoidal resonant frequency was applied, and a fitting function was used to obtain the stiffness value of the ASWAC at the design height. Combining different loading frequencies, a total of 250 simulation experiments were conducted, with each simulation lasting approximately 7 h, amounting to a total of 1750 h.

To facilitate further exploration of the relationship between the stiffness of the ASWAC and its internal gas, a reference point inside the connecting pipeline was established. This allowed the measurement of the internal gas flow velocity during the operation of the air spring, with the flow direction from the main chamber to the auxiliary chamber designated as the positive direction. The reference point was positioned in the middle of the connecting pipeline (Figure 5).

RESULTS AND DISCUSSION

Impact of the connecting pipeline diameter (CPD) on the dynamic characteristics of air springs under different initial internal pressure (IIP)

By varying the CPD, the dynamic characteristic curves of the ASWAC at its design height for different CPDs were obtained under various IIPs (Figure 8). The stiffness of CPDs 8 and 10 mm was relatively high at 2 Hz, while the stiffness of CPDs 12, 16, 18, and 20 mm was lower at 2 Hz, with little difference among them. As the loading frequency increased, the stiffness of CPD 8 mm rose rapidly between 2 and 6 Hz but more slowly between 6 and 30 Hz, with the rising speed decreasing as the frequency increased. The stiffness of CPDs 10 and 12 mm increased rapidly between 2 and 14 Hz but more slowly between 14 and 30 Hz, with the rising speed gradually decreasing as the frequency increased. For CPDs 16, 18, and 20 mm, the stiffness increased from slow to fast and then slowed down again between 2 and 30 Hz, with slower increases between 2–6 Hz and 23–30 Hz and faster increases between 6 and 23 Hz.

The stiffness value of CPD 8 mm was the highest at all IIP levels for the respective loading frequencies when comparing 2 and 6 Hz. At 14 Hz, when the IIP was 0.1 and 0.15 MPa, the stiffness value of CPD 8 mm was the highest. However, as the IIP increased to 0.2 and 0.25 MPa, the stiffness values of CPDs 10 and 12 mm surpassed those of 8 mm. At 23 Hz, the stiffness value of CPD 16 mm became the highest. At 30 Hz, the stiffness values increased as CPD decreased.

The flow velocity diagrams at reference points for different CPDs of the ASWAC at its design height (Figure 9) showed that, across different IIPs, the flow velocities of CPDs

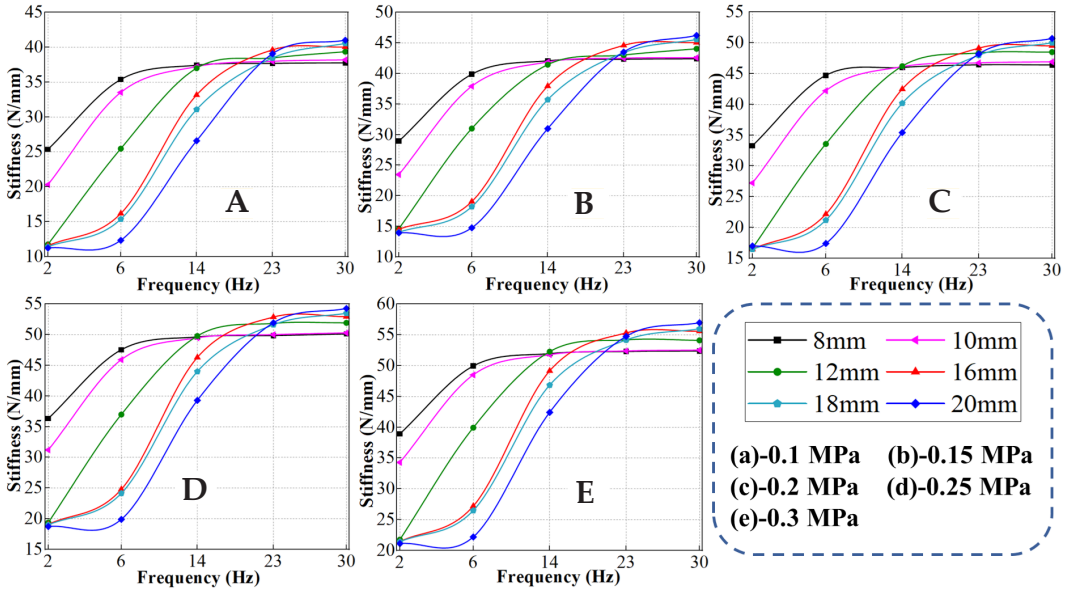

Figure 8. Influence of the connecting pipeline diameter (CPD) under different initial internal pressures (IIP) on the dynamic characteristics of air springs.

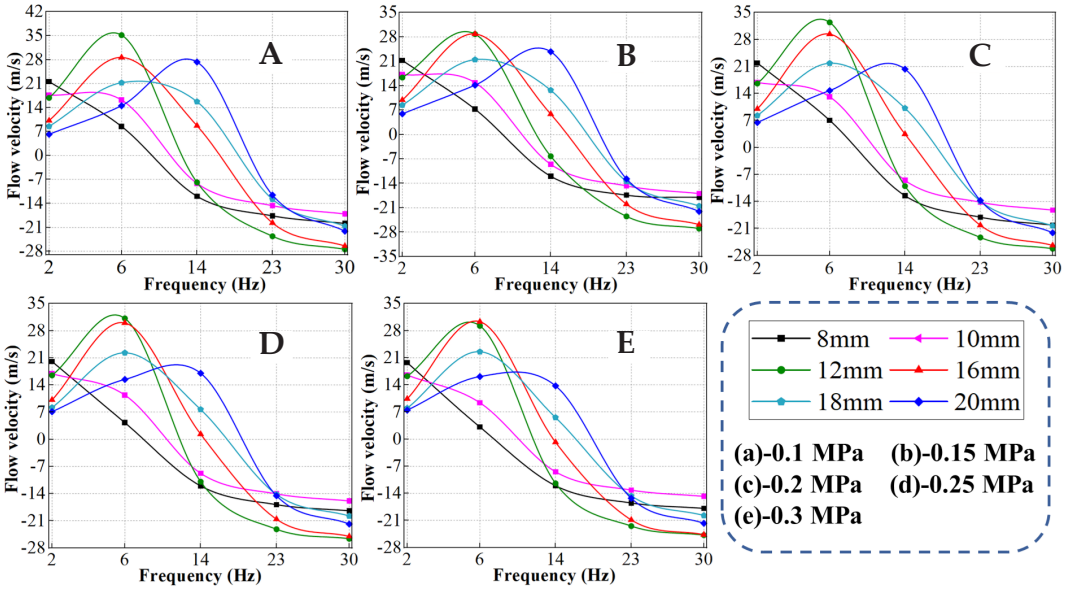

Figure 9. Influence of the connecting pipeline diameter (CPD) on flow velocity inside pipelines under different initial internal pressures (IIP).

8 and 10 mm exhibited a downward trend between 2 and 30 Hz. For CPDs 12, 16, and 18 mm, the flow velocities increased between 2 and 6 Hz and decreased between 6 and 30 Hz. The flow velocity of CPD 20 mm increased between 2 and 14 Hz and decreased between 14 and 30 Hz. At lower loading frequencies, as the frequency increased, the reference point velocity of CPD 8 mm decreased, indicating that internal air choking occurred within CPD 8 mm in this frequency range. As CPD increased, the decrease in reference point velocity shifted to higher frequencies, suggesting that increasing CPD facilitated the additional air chamber's operation at more frequencies. However, excessively increasing the CPD can weaken its damping effect on vibration elimination and increase the difficulty of the vehicle's piping layout.

Under all IIPs, CPDs of 8, 10, and 12 mm exhibited a trend of slow change in both stiffness values and reference point velocity values between the frequencies of 14 and 30 Hz (Figures 8 and 9). Similarly, CPDs of 16, 18, and 20 mm also showed a similar phenomenon between the frequencies of 23 and 30 Hz. It can be concluded that as the loading frequency increases to a certain value, the internal fluid velocity of the CPD will reach a limit value, which determines the maximum stiffness of the air spring.

The influence of the connecting pipeline diameter (CPD) on the dynamic characteristics of air springs at different loading frequencies

The dynamic characteristic curves of ASWAC at the design height for different CPDs were evaluated under various loading frequencies (Figure 10). At a loading frequency of 2 Hz, stiffness increased with increasing IIP. The stiffness of CPD 8 mm was the

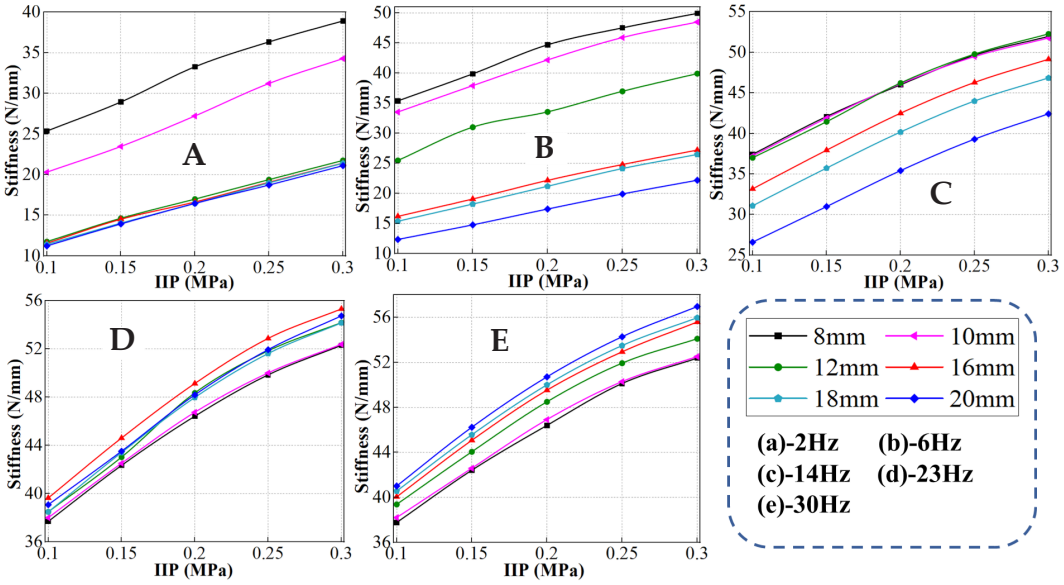

Figure 10. Influence of the connecting pipeline diameter (CPD) on the dynamic characteristics of air springs under different loading frequencies.

highest among all CPDs at all IIPs. At 6 Hz, stiffness exhibited a linear growth trend with increasing IIP. At the same IIP, stiffness decreased as CPD increased. At 14 Hz, stiffness increased with increasing IIP. At the same IIP, the stiffness values of 16, 18, and 20 mm decreased as CPD increased. At 23 Hz, stiffness increased with increasing IIP for all CPDs. At this frequency, the stiffness of 16 mm was the highest among all CPDs at all IIPs. At 30 Hz, stiffness increased with increasing IIP for all CPDs. Compared with 23 Hz, the stiffness values further increased, and the stiffness of 20 mm became the highest among all CPDs at all IIPs. At the same IIP, stiffness increased with increasing CPD.

The overall analysis (Figure 10) revealed that as the loading frequency increased, the stiffness value of CPD 8 mm began to shift, transitioning from being the maximum value at lower IIPs to becoming the minimum value. At a loading frequency of 6 Hz, under the same IIP, the stiffness values of CPD decreased in the order of 8, 10, 12, 16, 18, and 20 mm. However, at a loading frequency of 30 Hz, the stiffness values of CPD increased in the reverse order (20, 18, 16, 12, 10, and 8 mm). This trend was opposite compared to that at a loading frequency of 6 Hz. Overall, under the same IIP, as the loading frequency increased, stiffness decreased while the trend of increasing CPD reversed, establishing a rule that stiffness increases with higher CPD.

The velocity profiles at the reference points for different CPDs at the design height of ASWAC under varying loading frequencies were calculated (Figure 11). At the same IIP, velocity decreased with increasing CPD. In comparison (Figures 10a and 11a), at 2 Hz, CPD 8 mm experienced severe choking, while CPD 10 mm showed mild

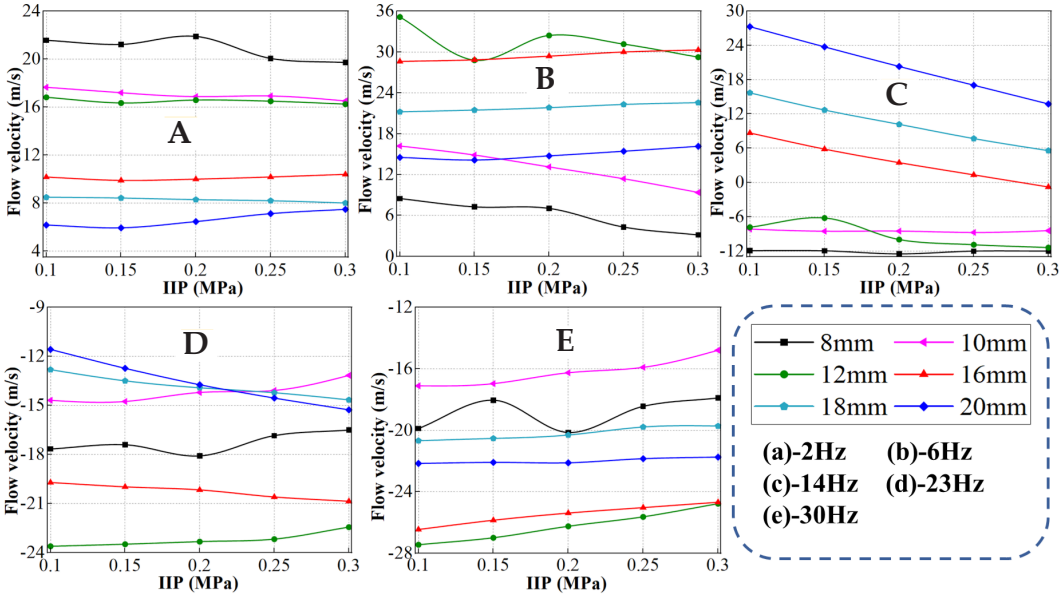

Figure 11. Influence of the connecting pipeline diameter (CPD) on flow velocity inside the pipeline under different loading frequencies.

choking. At 6 Hz, the velocities of CPDs 16, 18, and 20 mm remained stable across different IIPs, whereas CPD 12 mm fluctuated significantly. The velocities of CPD 8 and 10 mm decreased with increasing IIP, and CPD 8 mm reached the lowest positive value. Furthermore, stiffness differences emerged among CPD 12, 16, 18, and 20 mm, indicating that choking occurred in different CPDs as the loading frequency increased (Figures 10b and 11b).

At 14 Hz, the velocities of CPDs 8, 10, and 12 mm first became negative, with CPD 12 mm fluctuating significantly. The velocities of CPDs 16, 18, and 20 mm decreased with increasing IIP, and CPD 16 mm became negative at 0.3 MPa. At the same IIP, the velocities and stiffness values of CPDs 8, 10, and 12 mm were similar, indicating severe choking and reverse flow in these CPDs at 14 Hz (Figures 10c and 11c). The other CPDs showed stiffness differences; however, comparison of the two figures indicated partial choking in their pipelines. At 23 Hz, the velocities of all CPDs became negative, indicating severe choking in all pipelines. The stiffness values of different CPDs were similar across various IIPs, and the regulatory effect of the additional air chamber diminished, corresponding to severe choking at this loading frequency (Figures 10d and 11d).

At 30 Hz, severe choking occurred in all pipelines, with greater reverse flow velocities. The velocities of CPD 8 and 10 mm exceeded those of CPD 20 mm, and CPD 12 mm tended to exceed CPD 16 mm. Smaller CPDs, such as 8 and 10 mm, inhibited the increase in the absolute velocity, resulting in reduced stiffness (Figures 10e and 11e).

Larger CPDs, including 12, 16, 18, and 20 mm, exhibited higher stiffness due to greater absolute velocities. Overall analysis showed that as frequency increased, choking in pipelines of different diameters gradually worsened, particularly in smaller diameters (Figure 11). This indicated that different CPD sizes exerted varying effects on the damping regulation of the additional air chamber. Larger CPDs allowed the additional air chamber to influence stiffness over a wider frequency range.

Influence of auxiliary chamber volume (ACV) on the dynamic characteristics of air springs under different initial internal pressure (IIP)

By adjusting the ACV, the dynamic characteristic curves of ASWAC at the design height were obtained for different ACVs under varying IIPs (Figure 12). For ACVs of 4, 6, and 8 L, stiffness decreased with increasing frequency between 2 and 6 Hz, whereas between 14 and 30 Hz, stiffness increased with frequency. For the 10 L ACV, stiffness increased with frequency across the entire range from 2 to 30 Hz. Across all IIPs, within the frequency range of 2 to 6 Hz, stiffness decreased with increasing ACV at a given frequency. In contrast, between 14 and 30 Hz, stiffness increased with increasing ACV at a given frequency, showing the opposite trend compared to the 2–6 Hz range. This indicated that the influence of ACV on air spring stiffness was largely independent of IIP.

The flow velocity diagrams at the reference point for different ACVs of the ASWAC were obtained at the design height under various IIPs (Figure 13). Across different IIPs, between 2 and 14 Hz, the flow velocity increased with frequency. Between 14

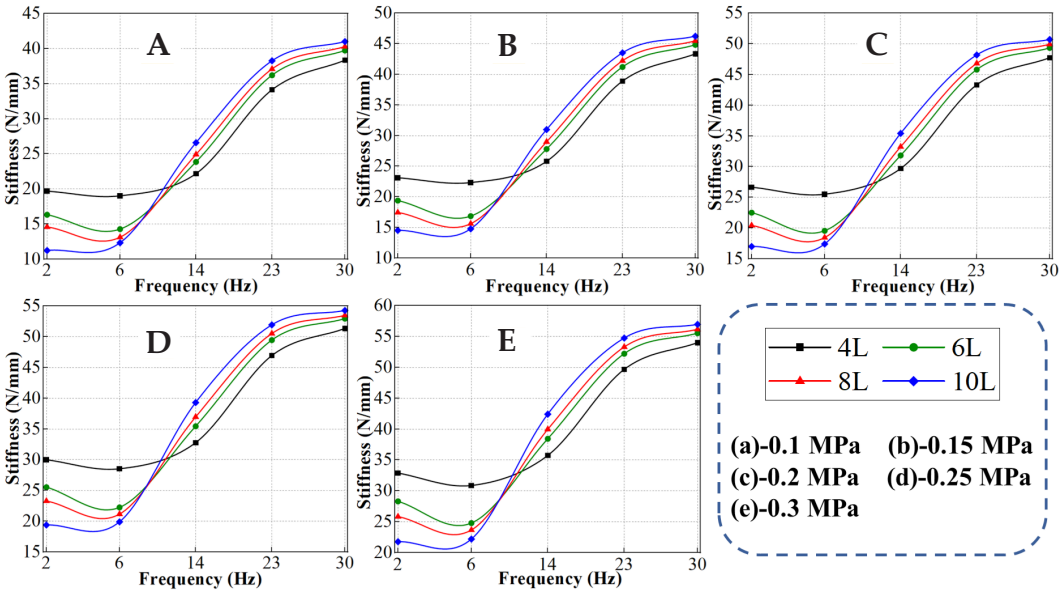

Figure 12. Influence of the auxiliary chamber volume (ACV) under different initial internal pressures (IIP) on the dynamic characteristics of air springs.

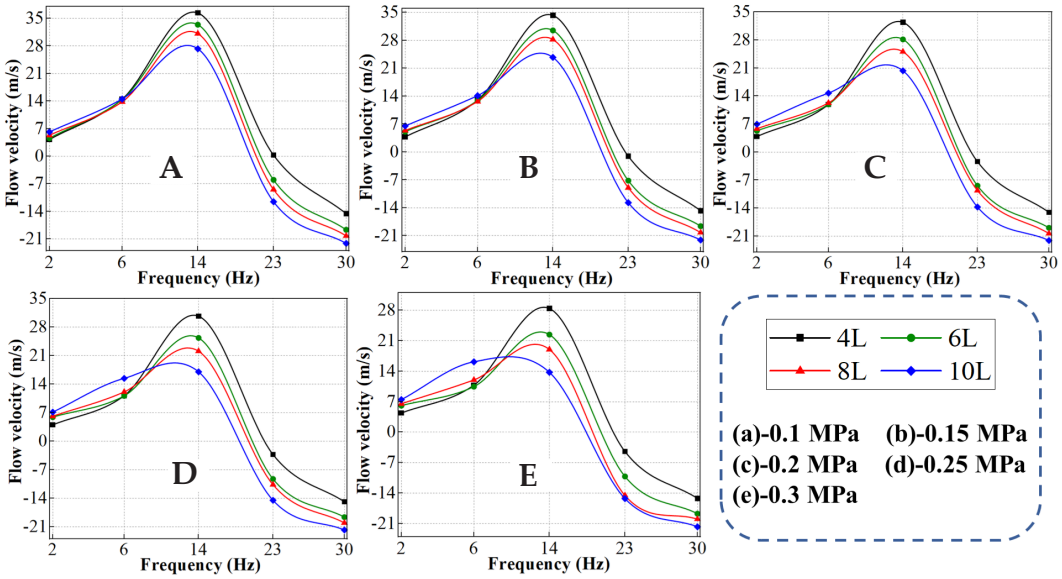

Figure 13. Influence of the auxiliary chamber volume (ACV) on flow velocity inside pipes under different initial internal pressures (IIP).

and 30 Hz, the flow velocity at the reference point decreased with frequency. Under different IIPs, within the frequency range of 14 to 30 Hz, at the same frequency, the flow velocity at the reference point decreased with increasing ACV. Between 14 and 23 Hz, the flow velocity became negative, indicating the occurrence of choking within the pipeline at this point.

Within the frequency ranges of 2–6 and 23–30 Hz, the change in flow velocity at the reference point was relatively slow, corresponding to the slower variation in stiffness within these ranges (Figures 12 and 13). Between 6 and 23 Hz, the flow velocity changed more rapidly, and the stiffness values also varied more significantly within this frequency range.

Influence of the auxiliary chamber volume (ACV) on the dynamic characteristics of air springs under different loading frequencies

The dynamic characteristic curves for different ACVs of the ASWAC at the design height under various loading frequencies were obtained (Figure 14). Across different loading frequencies, stiffness increased with increasing IIP. At higher loading frequencies, the growth rate of stiffness gradually slowed as IIP increased. At loading frequencies of 2 and 6 Hz, stiffness decreased with increasing ACV at the same IIP. However, at loading frequencies of 14, 23, and 30 Hz, stiffness increased with increasing ACV at the same IIP. This finding indicated that as loading frequency increased, the trend shifted from stiffness decreasing with ACV to stiffness increasing with ACV at the same IIP.

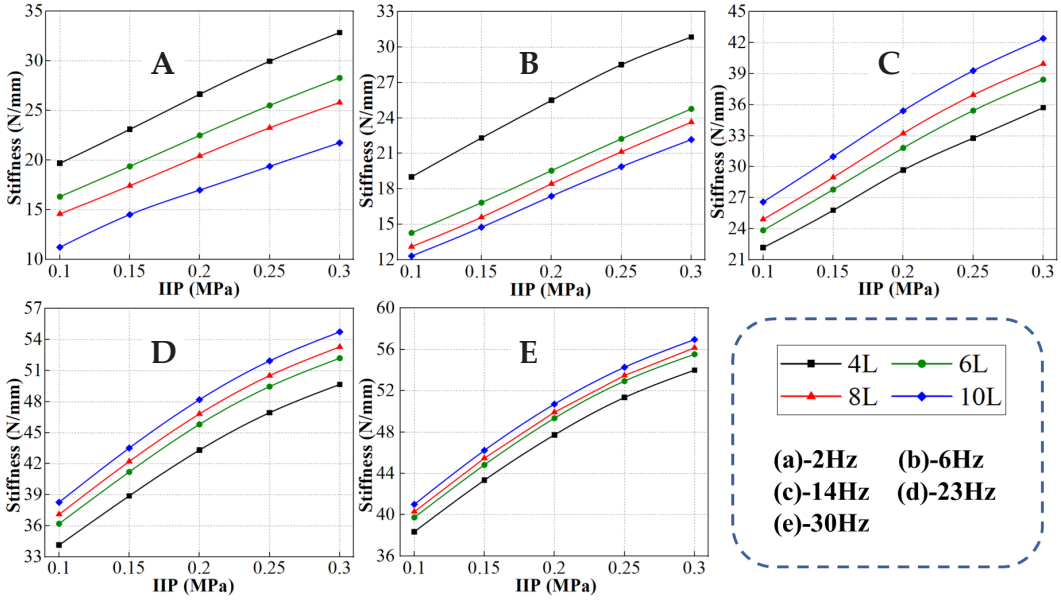

Figure 14. Influence of the auxiliary chamber volume (ACV) on the dynamic characteristics of air springs under different loading frequencies.

The reference point flow velocity diagrams for different ACVs of the ASWAC at the design height under various loading frequencies were obtained (Figure 15). At a loading frequency of 2 Hz and relatively low IIP, choking had already occurred in

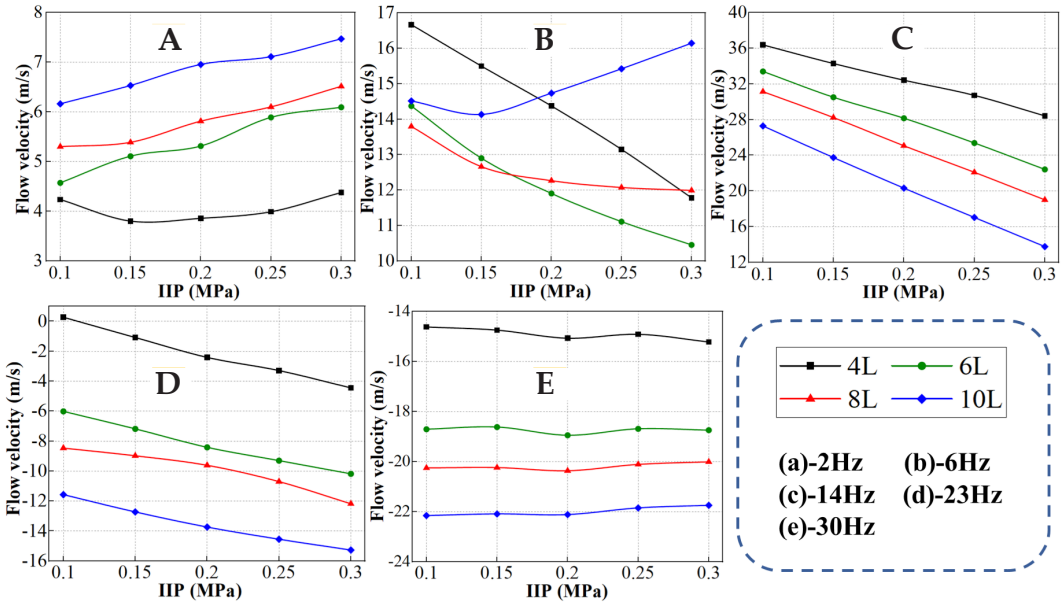

Figure 15. The influence of ACV on flow velocity inside the pipeline under different loading frequencies.

the pipeline of ACV 4 L (Figures 14a and 15a). As IIP increased, the reference point flow velocity continued to increase. At 6 Hz, the flow velocities at the reference point of ACVs 4, 6, and 8 L decreased with increasing IIP, whereas the velocity of ACV 10 L first decreased slightly and then increased with IIP. The decrease in flow velocity at the reference point was most pronounced for ACV 4 L, corresponding to a stiffness value significantly higher than those of the other additional air chambers at this frequency (Figures 14b and 15b).

At 14 Hz, the flow velocities at the reference point of all ACVs decreased with increasing IIP. At the same IIP, the flow velocity decreased with increasing ACV, showing a trend opposite to that observed at 2 Hz. As loading frequency increased to 14 Hz, both stiffness and velocity exhibited trends opposite to those at 2 Hz (Figures 14c and 15c). This indicated that between 2 and 14 Hz, the flow velocity at the reference point reflected the changes in stiffness. At 23 Hz, the flow velocities of all ACVs decreased slightly with increasing IIP. As the variation in flow velocity at the reference point decreased, the differences in stiffness among different ACVs at the same IIP also decreased (Figures 14d and 15d). This result indicated that the influence of ACV on stiffness gradually diminished with increasing IIP. At 30 Hz, the flow velocities at the reference point of all ACVs remained essentially unchanged with variations in IIP. The differences in stiffness among different ACVs at the same IIP became less pronounced (Figures 14e and 15e). At 30 Hz, the influence of ACV on stiffness was minimal.

CONCLUSIONS

Under the same initial internal pressure (IIP), the influence of different connecting pipeline diameters (CPDs) on the dynamic characteristics of the air spring followed the same pattern, with the frequency at which stiffness tended to flatten shifting to higher values as CPD increased. With increasing CPD, the auxiliary chamber influenced stiffness over a wider frequency range. At lower loading frequencies, smaller CPDs exerted a greater influence on stiffness, whereas larger CPDs had a smaller effect. As frequency increased, larger CPDs gradually exerted a stronger influence on stiffness. Between 6 and 30 Hz, at the same IIP, the pattern of stiffness decreasing with diameter gradually shifted to stiffness increasing with diameter.

Under all IIPs, the influence of different auxiliary chamber volumes (ACVs) on the dynamic characteristics of the air spring followed the same pattern. Between 2 and 6 Hz, stiffness decreased with increasing ACV for all IIPs, whereas between 14 and 30 Hz, the opposite trend was observed. At all loading frequencies, particularly at 2 Hz, stiffness decreased with increasing ACV under different IIPs. As loading frequency increased, this trend gradually reversed. Because air springs are subjected to substantial longitudinal loads during operation, this study considered only the influence of longitudinal loads on their static and dynamic characteristics. Future research could investigate and analyze the effects of transverse loads.

ACKNOWLEDGEMENTS

This work was supported by Structural Design and Characteristic Analysis of Automobile Air Spring Shock Absorber (No. H232269).

REFERENCES

Atindana VA, Xu X, Nyedeb AN, Quaisie JK, Nkrumah JK, Assam SP. 2023. The evolution of vehicle pneumatic vibration isolation: A systematic review. Shock and Vibration 2023: 1716615. https://doi.org/10.1155/2023/1716615

Berg M. 2000. A three-dimensional airspring model with friction and orifice damping. Vehicle System Dynamics 33: 528−539. https://doi.org/10.1080/00423114.1999.12063109

Chen C, Hu RR, Huang L. 2011. Study on characteristics of cylindrical air spring. Advanced Materials Research 308–310: 1992–1996. https://doi.org/10.4028/www.scientific.net/amr.308-310.1992

Constantin L, Titurus B, Rendall TCS, de Courcy JJ, Cooper JE. 2024. Experimental analysis of liquid vertical slosh damping at vacuum and atmospheric pressures. Journal of Sound and Vibration 574: 118228. https://doi.org/10.1016/j.jsv.2023.118228

Karachinskii SI, Timofeev OA. 2023. Operation parameters of a gas-dynamic pressure source with explosive initiation. Combustion, Explosion, and Shock Waves 59 (2): 224–228. https://doi.org/10.1134/s0010508223020132

Karpenko M, Stosiak M, Šukevičius Š, Skačkauskas P, Urbanowicz K, Deptuła A. 2023. Hydrodynamic processes in angular fitting connections of a transport machine's hydraulic drive. Machines 11 (3): 355. https://doi.org/10.3390/machines11030355

Kong C, Liu G, Li Y, Yang M, Liao Y, Xia J, Wang Y, Long G. 2025. Multifactor analysis of static and dynamic characteristics of membrane air springs for small passenger cars. Journal of Computational and Nonlinear Dynamics 20 (10): 101005. https://doi.org/10.1115/1.4068976

Kong C, Xia J, Yang M, Li Y, Liao Y. 2024. Analysis of static and dynamic characteristics of membrane air springs for small passenger cars. Journal of the Brazilian Society of Mechanical Sciences and Engineering 46 (12): 682. https://doi.org/10.1007/s40430-024-05244-8

Liu H, Lee JC. 2011. Model development of automotive air spring based on experimental research. *In* 2011 Third International Conference on Measuring Technology and Mechatronics Automation. Institute of Electrical and Electronics Engineers: Shanghai, China. https://doi.org/10.1109/icmtma.2011.433

Mao L, Wei C, Zeng S, Cai M. 2023. Heat transfer mechanism of cold-water pipe in ocean thermal energy conversion system. Energy 269: 126857. https://doi.org/10.1016/j.energy.2023.126857

Mehmood K, Zhang B, Jalal FE, Wan W. 2023. Transient flow analysis for pumping system comprising pressure vessel using unsteady friction model. International Journal of Mechanical Sciences 244: 108093. https://doi.10.1016/j.ijmecsci.2022.108093

Mendia-García I, Gil-Negrete N, Nieto F, Facchinetti A, Bruni S. 2022. Analysis of the axial and transversal stiffness of an air spring suspension of a railway vehicle: mathematical modelling and experiments. International Journal of Rail Transportation 12 (1): 56−75. https://doi.org/10.1080/23248378.2022.2136276

Papkov V, Shadymov N, Pashchenko D. 2023. CFD-modelling of fluid flow in Ansys fluent using python-based code for automation of repeating calculations. International Journal of Modern Physics C 34 (9): 2350114. https://doi.org/10.1142/s0129183123501140

Piller M, Nobile E, Hanratty TJ. 2002. DNS study of turbulent transport at low Prandtl numbers in a channel flow. Journal of Fluid Mechanics 458: 419–441. https://doi.org/10.1017/s0022112001007704Quaglia G, Sorli M. 2001. Air suspension dimensionless analysis and design procedure. Vehicle System Dynamics 35 (6): 443–475. https://doi.org/10.1076/vesd.35.6.443.2040

Toyofuku K, Yamada C, Kagawa T, Fujita T. 1999. Study on dynamic characteristic analysis of air spring with auxiliary chamber. JSAE Review 20 (3): 349–355. https://doi.org/10.1016/s0389-4304(99)00032-6

Van LV, Tung NT. 2023. Application of air suspension system on multi-purpose forest fire fighting vehicle for reducing dynamic load. Journal of Vibration Engineering and Technologies 12 (6): 7219–7230. https://doi.org/10.1007/s42417-023-01069-2

Williams RA. 1997. Automotive active suspensions Part 1: basic principles. Proceedings of the Institution of Mechanical Engineers Part D: Journal of Automobile Engineering 211 (6): 415–426. https://doi.org/10.1243/0954407971526551

Wissink JG. 2003. DNS of separating, low Reynolds number flow in a turbine cascade with incoming wakes. International Journal of Heat and Fluid Flow 24 (4): 626–635. https://doi.org/10.1016/s0142-727x(03)00056-0

Wong P, Deng M, Zhao J, Ghadikolaei MA, Wang H. 2024. Model reference backstepping control for semi-active air suspension systems with parameter uncertainty. Proceedings of the Institution of Mechanical Engineers, Part D: Journal of Automobile Engineering 238 (9): 2650–2659. https://doi.org/10.1177/09544070231173168

Zhang G, Shen G, Can S. 2005. Study on dynamic airspring model with connecting pipe. Journal of the China Railway Society 4: 36–41.

Zhang Z, Wang J, Wu W, Huang C. 2020. Semi-active control of air suspension with auxiliary chamber subject to parameter uncertainties and time-delay. International Journal of Robust and Nonlinear Control 30 (17): 7130–7149. https://doi.org/10.1002/rnc.5169

Zheng E, Fan Y, Zhu R, Zhu Y, Xian J. 2016. Prediction of the vibration characteristics for wheeled tractor with suspended driver seat including air spring and MR damper. Journal of Mechanical Science and Technology 30 (9): 4143–4156. https://doi.org/10.1007/s12206-016-0826-x

Zhu S, Wang J, Zhang Y. 2008. Research on theoretical calculation model for dynamic stiffness of air spring with auxiliary chamber. *In* 2008 IEEE Vehicle Power and Propulsion Conference. Institute of Electrical and Electronics Engineers: Harbin, China. https://doi.org/10.1109/vppc.2008.4677717

Agrociencia

A SUSTAINABLE FUTURE FOR AQUACULTURE: A GLOBAL OVERVIEW WITH A FOCUS ON MEXICO'S POTENTIAL

Karla Jareth **Pérez-Viveros**[1], Javier **Castro-Rosas**[1], José Roberto **Villagómez-Ibarra**[1], Arturo **Cadena-Ramírez**[2], Carlos Alberto **Gómez-Aldapa**[1*]

[1]Universidad Autónoma del Estado de Hidalgo. Instituto de Ciencias Basicas e Ingenieria, Área Academica de Química. Carretera Pachuca-Tulancingo km 4.5, Colonia Carboneras, Mineral de la Reforma, Hidalgo, Mexico. C. P. 42184.
[2]Universidad Politécnica de Pachuca. Posgrado en Biotecnología. Carretera Pachuca-Ciudad Sahagún km 20, Ex-Hacienda de Santa Bárbara, Zempoala, Hidalgo, Mexico. C. P. 43830.
* Author for correspondence: cgomeza@uaeh.edu.mx

Citation: Pérez-Viveros KJ, Castro-Rosas J, Villagómez-Ibarra JR, Cadena-Ramírez A, Gómez-Aldapa CA. 2026. A sustainable future for aquaculture: a global overview with a focus on Mexico's potential. **Agrociencia** 60(2): 195-208. https://doi.org/ 10.47163/agrociencia.v60i2.3117

Editor in Chief:
Dr. Fernando C. Gómez Merino

Received: September 21, 2025.
Approved: March 13, 2026.
Published in Agrociencia: March 30, 2026.

ABSTRACT

Currently, aquaculture is a worldwide development activity, with an overall volume of more than 110.2 million Mg live weight and a value of approximately 243 billion USD, contributing more than 60 % of the combined production of aquatic organisms. Among major economic activities, aquaculture has grown more rapidly both internationally and domestically. Asia represents the region with the most extensive development in the cultivation of most species, with China as the dominant producer. However, in terms of growth, some countries in Africa and Latin America, such as Egypt, Nigeria, Chile, and Mexico, are emerging on the world stage. Mexican aquaculture grew by around 70 % from 2013 to 2021, and further growth is expected in the coming years. Despite its importance and growth for human livelihood, aquaculture involves significant water consumption, and its degradation represents a major threat to the future of humanity. Therefore, it is essential to establish clear notions of water quality and sustainable management, monitor social and economic variables, and intensify research on alternatives for water treatment and use control. The present work provides an overview of Mexican aquaculture in the global context, including its importance, concepts related to sustainable management and its alternatives, as well as the development of the industry.

Key words: aquatic ecosystems, pisciculture, water pollution, water resources.

INTRODUCTION

Aquaculture is the economic, social, and cultural activity that consists of the breeding and cultivation of aquatic organisms. Breeding requires human intervention to increase and ensure the production of species with high demand, such as shrimp, catfish, tilapia, and trout (FAO, 1998; Justino *et al*., 2016; Ottinger *et al*., 2016). Populations must be fed and protected from predators in a controlled environment, and their growth must be managed effectively.

Practices differ across regions according to environmental conditions and production systems. In Vietnam, fish are raised using freshwater in paddy fields, while in Ecuador

saltwater shrimp are produced in ponds. In Norway and Scotland, cages are used along the coasts for salmon production (Bergheim, 2012; Phuong and Oanh, 2010; Hamilton and Stankwitz, 2012). The most important cultured organisms are freshwater species, which require less water and have lower maintenance costs, including tilapia and carp (Yuan *et al*., 2017).

From a food systems perspective, aquaculture represents a viable alternative for the global food supply. Capture fisheries and aquaculture both contribute to food security and form an integral part of national economies. This activity supports national food security, generates foreign currency, creates employment opportunities in vulnerable areas, and helps alleviate poverty (Tacon and Metian, 2015, 2017). In addition, aquaculture products are rich in animal protein, contributing to the growth and stability of the food system as one of the healthiest food sources. Fish is among the most widely produced food products and represents one of the most important sources of animal protein, accounting for about 17 % of global animal protein consumption. In less developed countries, this proportion may exceed 50 % (Béné *et al*., 2015).

GLOBAL AQUACULTURE PRODUCTION AND TRENDS

Aquaculture has been practiced in a low-technology manner for at least two centuries; however, intensive farming systems comparable to the production of terrestrial animals are much more recent, developing mainly after 1950 (Campbell and Pauly, 2013). In 2016, worldwide production of aquatic organisms totaled around 170.9 million Mg, with a value of approximately 250 billion USD (FAO, 2018; OECD, 2020). Of this amount, just over 110.2 million Mg came from aquaculture, representing about 64 % of the total production (World Bank Group, 2023). These data show that aquaculture is a major contributor to global food security, a trend expected to continue (Little *et al*., 2018; Ottinger *et al*., 2016).

Since 2011, production of aquatic organisms from capture fisheries has remained relatively stable, averaging close to 93 million Mg per year. In contrast, aquaculture production increased by about 48 million Mg during the same period, representing growth of approximately 78 % (World Bank Group, 2013; FAO, 2018). The Asian continent has made the most significant advances in aquaculture development, with China leading production at nearly 64 million Mg in 2021. Other major producing countries include Indonesia, India, Vietnam, Bangladesh, the Philippines, Korea, Egypt, Norway, and Japan, each producing around one million Mg (World Bank Group, 2023). Among the main groups contributing to aquaculture production, fish account for 54.091 million Mg (49.08 %), crustaceans for 7.862 million Mg (7.13 %), mollusks for 17.139 million Mg (15.55 %), and aquatic plants for 30.139 million Mg (27.35 %). Other organisms, including frogs and invertebrates, contribute approximately 939 thousand Mg (0.85 %) to total production (FAO, 2018).

Of the combined global production of approximately 171 million Mg of aquatic organisms from fisheries and aquaculture, about 88 % is used for direct human

consumption. The remaining portion is processed into fishmeal and fish oil for applications such as livestock feed, aquaculture feed, industrial products, and pharmaceutical uses (Gjedrem *et al*., 2012; FAO, 2018). The dependence of aquaculture and terrestrial animal production on fishmeal represents an important sustainability concern. In 2021, fishmeal production totaled about 24 million Mg, of which around 5 million Mg were used for non-food purposes. Consequently, the development of alternative protein sources for aquaculture feeds and other animal production systems has become increasingly necessary (Hua *et al*., 2019).

Fishmeal remains a key input in aquaculture feed formulations (Olsen and Hasan, 2012) and is one of the most expensive commercial protein ingredients because of its complex composition of proteins, fatty acids, minerals, and vitamins, as well as its balanced profile of essential amino acids (Hardy, 2010). However, the growing demand for aquaculture products has intensified efforts to develop alternative feed ingredients that maintain fish health and nutritional quality. Research in this area often focuses on locally available resources adapted to regional production systems and species requirements. Feed typically represents about 60 % of operating costs within the aquaculture production chain (Han *et al*., 2016; Hardy, 2010; Olsen and Hasan, 2012).

ALTERNATIVE PROTEIN SOURCES FOR AQUACULTURE FEED

Studies on the use of fish silage and shrimp waste indicate that these preparations can replace up to 75 % of fishmeal while maintaining beneficial effects on fry and providing a profitable alternative (Goddard and Perret, 2005; Madage *et al*., 2015). However, silage is prone to fermentation due to the lack of preservatives, which can affect its quality. Feed acidity has also been associated with poor fish acceptance, as it may suppress appetite. The use of fish meal produced from *Gambusia affinis* or *Atherina boyeri* has allowed the replacement of up to 50 % of commercially used fishmeal without affecting feed efficiency, and this substitution has been supported by economic analyses (Abdelghany, 2003; Gümüş, 2010).

Use of terrestrial animal proteins

Substituting fishmeal with terrestrial animal proteins has been explored using by-products such as food residues, blood, feathers, meat, and bone (Hernández *et al*., 2010; Hu *et al*., 2013). However, these proteins often present inadequate amino acid profiles, containing low levels of essential amino acids such as lysine, isoleucine, and methionine that are required by aquatic species (Liaqat *et al*., 2017). When these deficiencies are corrected through supplementation, such alternative protein sources can replace up to 75 % of fishmeal and remain cost-effective. Nevertheless, their efficiency is still debated because of the need for additional supplements (Hua *et al*., 2019).

Use of vegetable proteins

Oil plants

Among plant protein sources, soybean meal stands out due to its high protein content and relatively complete amino acid profile. However, it shows deficiencies in methionine, lysine, and cysteine. Soybean meal also contains antinutritional factors such as trypsin inhibitors, antivitamins, and lectins like phytohemagglutinin (Bai *et al*., 2015). These compounds can be reduced or eliminated through heat treatment. With proper processing, soybean meal has shown good performance in partial substitutions of fishmeal of up to 75 %. The success of substitution depends on the species, growth stage, and minimum nutritional requirements, as well as mineral availability in soybean meal.

Cottonseed meal is another alternative widely used in tropical and subtropical regions because of its high protein content and low cost (Sun *et al*., 2015; Teves and Ragaza, 2016). However, protein content and quality vary depending on seed management and processing methods, ranging from 26–54 %. In addition, cottonseed meal has relatively low levels of cysteine and lysine, although substitution efficiencies from 50 % to complete assimilation in aquatic species have been reported (Nehete *et al*., 2013).

Aquatic plants

Among aquatic plants, duckweed has been highlighted as a potential plant protein source, with crude protein levels reaching up to 45 %. It also presents a suitable amino acid and mineral profile and has been used as the sole nutrient source in some production systems. Nevertheless, optimal performance is generally achieved with substitution rates around 50 %, allowing good growth without adverse effects while remaining economically viable. Other aquatic plants, including ferns, have also demonstrated positive results when combined with duckweed, particularly during the fry stage (Nakphet *et al*., 2016; Hasan, 2017).

Legumes

Legumes are commonly used as partial substitutes for cereals in aquaculture feed. For example, *Leucaena* can contribute up to 30 % of the protein in feed mixtures. Beans and corn are also used as alternative ingredients, although many legumes present variable amino acid profiles (Laining and Kristanto, 2015). They are often deficient in essential amino acids such as arginine, isoleucine, methionine, and threonine. Additionally, antinutritional compounds such as mimosine, a non-protein amino acid that can be toxic, must be considered. Some plant ingredients, including cassava and corn, have shown favorable results during the fry stage, with substitution levels of up to 25 and 100 %, respectively, producing satisfactory growth. However, the presence of phytic acid in these plants can reduce mineral bioavailability, particularly when feed formulations are already deficient in one or more minerals (de Silva, 2012).

Use of unicellular organisms

Microorganisms such as algae, fungi, bacteria, cyanobacteria, and yeasts are gaining attention as alternative protein sources in semi-intensive and intensive aquaculture feeding systems because they can simplify production and reduce costs (Maisashvili *et al*., 2015; Wang *et al*., 2019). These microorganisms can utilize carbon sources such as wheat or rice bran, helping optimize production systems with relatively inexpensive inputs. Unicellular proteins therefore represent a promising group of microbial resources that promote growth while also providing environmental benefits, as some bacteria contribute to reducing ammonia concentrations in aquaculture systems (Guedes *et al*., 2015).

GLOBAL RISKS AND CHALLENGES

Monitoring in aquaculture production systems

Monitoring in aquaculture facilities should provide the information needed to support decision-making based on reference data, production levels, area limits, and environmental impacts. Accurate and periodic monitoring at sectional scales is required to achieve this (Mulema and García, 2019; Simbeye *et al*., 2014). However, implementing such monitoring, particularly through cartography-based methods, remains challenging due to the high cost and limited availability of appropriate systems, as well as insufficient financing, infrastructure, and trained personnel (Ferreira *et al*., 2020).

To address these limitations, the Food and Agriculture Organization has promoted initiatives focused especially on developing regions. One proposed approach is the development of cost-effective technologies capable of generating inventories of cultivable species and supporting management systems. These technologies could enable sustainable management and assist licensing processes by identifying unregistered or illegal facilities. They can also provide information for site selection and for evaluating farm evolution in relation to surrounding ecosystems, helping prevent environmental damage (Soininen *et al*., 2019). In this context, global positioning systems are essential for recording the location of aquaculture facilities and facilitating the integration of geographic information systems and spatial analyses (Mulema and García, 2019; Ferreira *et al*., 2020).

Social challenges in aquaculture

Low-quality employment is frequently associated with low productivity, and its causes vary depending on local contexts. In aquaculture, producers often face challenges such as limited access to formal education, which restricts the availability of services and hinders the adoption of advanced technologies and access to demanding markets (Carlarne and Depledge, 2019; Ngajilo and Jeebhay, 2019). In addition, inadequate fish handling and poor capture, processing, and storage facilities contribute to high post-capture losses, reducing overall production yields (Song and Soliman, 2019).

In Mexico, families lacking alternative employment opportunities often accept low wages and poor working conditions within aquaculture operations. Continuous industry expansion may also lead to overexploitation of resources, environmental degradation, and risks to the livelihoods of communities dependent on aquaculture. Addressing the shortage of decent work requires improving access to education and training, adopting new technologies, and enhancing fish handling, capture, processing, and storage infrastructure. These measures can increase productivity while supporting the sustainability of the sector and the communities that depend on it (Espinosa-Romero *et al*., 2017).

Workers in the aquaculture and fisheries sectors often belong to vulnerable social groups and face hazardous working conditions. Although these activities represent an essential source of income for low-income populations, social protection mechanisms are frequently limited or absent (Watterson, 2018). In many countries, workers rely on informal or minimal protection, and integration into formal social security systems remains difficult. As a result, workers and their families face environmental, social, physical, and economic risks, often intensified by factors such as migration, sexually transmitted diseases, gender violence, and substance abuse (Ahmed and Thompson, 2019).

Beyond resource overexploitation, the occupation itself is considered highly dangerous. Each year, approximately 24 000 workers experience illness, injury, or death due to long working hours and fatigue. Insufficient enforcement of occupational safety regulations further increases these risks. Strengthening social protection through improved access to healthcare, education, training programs, and occupational health and safety regulations is therefore essential. Such measures help protect workers' rights while supporting the long-term sustainability of the aquaculture sector and the well-being of dependent communities (Ahmed and Thompson, 2019; Soininen *et al*., 2019).

Climate change

Climate change represents a major global challenge, requiring aquaculture systems to develop adaptive strategies capable of addressing its impacts, variability, and associated risks. Key factors include warming of water bodies, sea-level rise, ocean acidification, and changes in weather patterns that may result in extreme events (Falconer *et al*., 2020). Climate change poses significant risks to aquaculture systems. Increased atmospheric CO_2 levels and the resulting acidification of water bodies can affect the physiology of many species, influencing growth, reproduction, and product quality.

At the same time, global warming may create certain opportunities, such as increased growth rates and expanded geographic ranges for some cultured species. Research on sensitive fish species across life stages (from embryo to adulthood) has shown that temperature variation influences growth, disease susceptibility, spawning time, and mortality rates at different developmental stages (Dubey *et al*., 2017). Metabolic changes

associated with these environmental shifts may also generate significant economic impacts. Adaptation will likely require modifications to aquaculture infrastructure and the development of more specific and nutritionally adequate feed formulations (Bhuiyan *et al*., 2018; Steeves and Filgueira, 2019).

Species vulnerability

Assessing the vulnerability of species and environmental systems in aquaculture often involves classifying farms according to geographic location (continental, coastal, or arid tropical environments) as well as production density and intensity (Navas *et al*., 2011). Even within the same region, farms may differ in technological capacity and production systems, which can increase vulnerability for producers, particularly regarding supply limitations. Reducing these vulnerabilities requires the adoption of improved local practices and advanced technologies (Islam *et al*., 2019). Potential strategies include the use of new biological strains, such as catfish varieties adapted to salinity conditions, and improvements in harvesting methods to ensure product quality. Additional technological approaches may involve water-recycling systems and innovations that enhance fish health and feed efficiency (Rickard *et al*., 2020; Yogev *et al*., 2020).

Sustainability through organization

Many fishers and fish farmers operate small-scale systems without formal contracts, which limits organization within the sector and reduces opportunities for policy development. Dependence on intermediaries within the value chain further affects producers, as these actors often control market access and influence the economic viability of primary production (Valenti *et al*., 2018). Addressing these issues requires context-specific interventions that strengthen communication and coordination among stakeholders (Davies *et al*., 2019). Developing simple, sustainable, and inclusive value chains, particularly at small scales, can help prevent sector overcapacity and reduce economic, environmental, and social disruptions. Currently, an important concern within the production chain involves the generation of by-products and the continued reliance on fishmeal and fish oil, which may place additional pressure on wild fish populations and other aquatic species (Carlarne and Depledge, 2019; Dubey *et al*., 2017).

AQUACULTURE IN MEXICO

Water has played a crucial role in human settlement and societal development throughout history. Its uses range from domestic consumption to livestock watering, irrigation, aquaculture, power generation, navigation, and recreation. In aquaculture, water availability is essential, and Mexico's altitudinal profile creates a wide diversity of climatic conditions and ecosystems that support the development of the aquaculture sector (Oyarzabal, 2000). However, the successful expansion of the industry also

depends on the efficient application of technologies and on processes of innovation, modernization, and productive reconversion (FAO, 2013). In Mexico, fish farming was formally established at the end of the 19th century when the Ministry of Development initiated the construction of a fish nursery in Ocoyoacac, State of Mexico, using a batch of 500 000 rainbow trout (*Oncorhynchus mykiss*) fry imported from the United States.

Regional development of Mexican aquaculture

Mexico is divided into five regions as part of the "Diagnosis and Regional Planning of Fisheries and Aquaculture" initiative, designed to promote sustainable and integrated development of this economically and socially important sector. Region I, the Pacific North, includes Baja California, Baja California Sur, Sonora, Sinaloa, and Nayarit. In 2021, this region produced 195 705.71 Mg of live weight, with Sonora and Sinaloa each contributing about 39 % of the total production. Region II, the Central and South Pacific Zone, comprises Chiapas, Jalisco, Colima, Michoacán, Oaxaca, and Guerrero. In 2021, this region generated 34 599.87 Mg in live weight, with Jalisco leading production with 37 %.

Region III, the Northern Gulf of Mexico Zone, includes Veracruz and Tamaulipas. Veracruz dominated production in this region, accounting for 86 % of the total 3182.55 Mg produced. Region IV, known as the Gulf of Southern Mexico and Caribbean Sea region, includes Quintana Roo, Yucatán, Tabasco, and Campeche. Aquaculture production in this region reached 14 718.68 Mg of live weight, with Tabasco contributing 82 % of the total. Region V corresponds to the landlocked states, which do not have coastal aquaculture systems and rely mainly on inland water production. This region produced 1406.8 Mg of live weight, with the State of Mexico contributing 34 % of the total production.

In 2021, aquaculture production in Mexico reached 249 613.71 Mg. A notable limitation of the industry is its strong dependence on shrimp and mojarras, mainly produced through crossbreeding systems. To ensure sustainable use of marine, brackish, and inland water resources, diversification of cultured species is necessary. Other species considered in Mexican aquaculture include freshwater fish such as robalo, bass, and catfish; marine fish such as snapper, sea bream, red snapper, sea bass, horse mackerel, and tuna; mollusks such as clams, abalone, and snails; freshwater crustaceans such as freshwater lobster and shrimp; and other groups including ornamental fish (CONAPESCA, 2020).

During the 1990s, social, political, economic, and environmental factors contributed to the expansion of aquaculture activity in Mexico. Legal reforms and federal government support programs strengthened value chains by promoting more structured projects and improving the availability of socio-economic and environmental data. Despite these advances, the aquaculture sector still faces challenges in achieving full sustainability. Greater investment in science and technology is required, together with the promotion of a culture that values the balance between economic development and environmental protection. Although value chains have improved, bureaucratic

barriers continue to limit stronger collaboration among producers, researchers, and government institutions.

Risks associated with aquaculture in Mexico

Like any productive sector, aquaculture in Mexico faces several risks that may affect its sustainability and profitability.

Disease outbreaks. Aquaculture facilities are vulnerable to disease outbreaks that can cause major production losses and affect the health and welfare of fish and shellfish. Diseases can spread rapidly through water, particularly in systems with high stocking densities, and can be difficult to control.

Environmental impacts. Improper management of aquaculture systems may generate negative environmental effects. Overcrowding, excessive feed use, and waste discharge can cause eutrophication and water quality degradation, affecting surrounding ecosystems and reducing production efficiency. Certain practices may also affect wild fish populations and natural habitats.

Economic risks. Aquaculture requires substantial investments in infrastructure, technology, and labor. Fluctuations in market demand, price volatility, and production risks, such as disease outbreaks or extreme weather events, can generate significant financial losses for producers and companies.

Regulatory compliance. Aquaculture activities in Mexico are subject to national and international regulations related to food safety, environmental protection, and animal welfare. Failure to comply with these regulations may result in penalties, production restrictions, or reputational damage.

Climate change. Climate change represents an additional risk for aquaculture production, including changes in temperature, precipitation patterns, sea-level rise, and the occurrence of extreme weather events.

To reduce these risks, aquaculture producers can implement best management practices such as regular monitoring and water quality testing, biosecurity protocols, and environmental impact assessments. In addition, diversification of production systems and increased investment in research and development can improve resilience and adaptability to changing environmental and market conditions.

CONCLUSIONS

Aquaculture is a sector characterized by constant change and growing demand. Although aquaculture production in Mexico has progressed steadily, national demand for seafood continues to increase. These trends require optimization across the value

chain and the adoption of more efficient practices, including technological innovation in equipment and feed products adapted to different socio-economic contexts and cultured species. Such innovations can promote sustainable practices and balanced growth in the industry.

Mexico has several advantages that could position it among the leading countries in global aquaculture production, particularly in the cultivation of freshwater and shrimp species. Favorable climatic conditions in many regions support the production of species of commercial interest, including native species with characteristics suitable for aquaculture. These conditions provide an opportunity to expand production and supply seafood to major consumer markets. To support the growth and sustainability of the aquaculture industry, the federal administration should establish legislation that recognizes aquaculture as an activity independent from fisheries. State governments should adopt similar frameworks and implement long-term policies to ensure the continued development of the sector beyond individual government administrations.

REFERENCES

Abdelghany AE. 2003. Partial and complete replacement of fish meal with gambusia meal in diets for red tilapia '*Oreochromis niloticus* × *O. mossambicus*.' Aquaculture Nutrition 9 (3): 145–154. https://doi.org/10.1046/j.1365-2095.2003.00234.x

Ahmed N, Thompson S. 2019. The blue dimensions of aquaculture: A global synthesis. Science of The Total Environment 652: 851–861. https://doi.org/10.1016/j.scitotenv.2018.10.163

Bai SC, Katya K, Yun H. 2015. Additives in aquafeed. *In* Feed and Feeding Practices in Aquaculture. Woodhead Publishing: Sawston, UK, pp: 171–202. https://doi.org/10.1016/b978-0-08-100506-4.00007-6

Béné C, Barange M, Subasinghe R, Pinstrup-Anderson P, Merino G, Hemre GI, Williams M. 2015. Feedig 9 billion by 2050 – Putting fish back on the menu. Food Security 7 (2): 261–274. https://doi.org/10.1007/s12571-015-0427-z

Bergheim A. 2012. Recent growth trend and challenges in the Norwegian aquaculture industry. Latin American Journal of Aquatic Research 40 (3): 800–807.

Bhuiyan MA, Jabeen M, Zaman K, Khan A, Ahmad J, Hishan SS. 2018. The impact of climate change and energy resources on biodiversity loss: Evidence from a panel of selected Asian countries. Renewable Energy 117: 324–340. https://doi.org/10.1016/j.renene.2017.10.054

Campbell B, Pauly D. 2013. Mariculture: A global analysis of production trends since 1950. Marine Policy 39: 94–100. https://doi.org/10.1016/j.marpol.2012.10.009

Carlarne C, Depledge MH. 2019. Climate change, environmental health, and human rights. *In* Encyclopedia of Environmental Health (Second edition). Elsevier: Amsterdam, Netherlands, pp: 653–660. https://doi.org/10.1016/b978-0-12-409548-9.11689-6

CONAPESCA (Comisión Nacional de Acuacultura y Pesca). 2020. Acuasesor. Gobierno de México. Secretaría de Agricultura y Desarrollo Rural. Comisión Nacional de Acuacultura y Pesca. Ciudad de México, México. https://acuasesor.conapesca.gob.mx/index.php (Retrieved: June 2020).

Davies IP, Carranza V, Froehlich HE, Gentry RR, Kareiva P, Halpern BS. 2019. Governance of marine aquaculture: Pitfalls, potential, and pathways forward. Marine Policy 104: 29–36. https://doi.org/10.1016/j.marpol.2019.02.054

de Silva SS. 2012. Aquaculture: A newly emergent food production sector—and perspectives of its impacts on biodiversity and conservation. Biodiversity and Conservation 21 (12): 3187–3220. https://doi.org/10.1007/s10531-012-0360-9

Dubey SK, Trivedi RK, Chand BK, Mandal B, Rout SK. 2017. Farmers' perceptions of climate change, impacts on freshwater aquaculture and adaptation strategies in climatic change hotspots: A case of the Indian Sundarban delta. Environmental Development 21: 38–51. https://doi.org/10.1016/j.envdev.2016.12.002

Espinosa-Romero MJ, Torre J, Zepeda JA, Solana FJV, Fulton S. 2017. Civil society contributions to the implementation of the small-scale fisheries guidelines in Mexico. *In* Jentoft S, Chuenpagdee R, Barragán-Paladines M, Franz N. (eds.), The Small-Scale Fisheries Guidelines. Springer: Cham, Switzerland. https://doi.org/10.1007/978-3-319-55074-9_20

Falconer L, Hjøllo SS, Telfer TC, McAdam BJ, Hermansen Ø, Ytteborg E. 2020. The importance of calibrating climate change projections to local conditions at aquaculture sites. Aquaculture 514: 734487. https://doi.org/10.1016/j.aquaculture.2019.734487

FAO (Food and Agriculture Organization of the United Nations). 1998. Rural aquaculture: Overview and framework for country reviews (XF1999084549). Bangkok, Thailand. https://www.fao.org/4/x6941e/x6941e00.htm#Contents (Retrieved: June 2025).

FAO (Food and Agriculture Organization of the United Nations). 2013. National aquaculture sector overview, Mexico. Mexico City, Mexico. https://www.fao.org/fishery/en/countrysector/naso_mexico (Retrieved: August 2025).

FAO (Food and Agriculture Organization of the United Nations). 2018. The state of world fisheries and aquaculture 2018 – Meeting the sustainable development goals. Rome, Italy. https://openknowledge.fao.org/handle/20.500.14283/i9540en (Retrieved: August 2025).

Ferreira RG, Ferreira JG, Boogert FJ, Corner RA, Nunes JP, Grant J, Johansen J, Dewey WF. 2020. A multimetric investor index for aquaculture: Application to the European Union and Norway. Aquaculture 516: 734600. https://doi.org/10.1016/j.aquaculture.2019.734600

Gjedrem T, Robinson N, Rye M. 2012. The importance of selective breeding in aquaculture to meet future demands for animal protein: A review. Aquaculture 350–353: 117–129. https://doi.org/10.1016/j.aquaculture.2012.04.008

Goddard JS, Perret JSM. 2005. Co-drying fish silage for use in aquafeeds. Animal Feed Science and Technology 118 (3–4): 337–342. https://doi.org/10.1016/j.anifeedsci.2004.11.004

Guedes AC, Sousa-Pinto I, Malcata FX. 2015. Application of microalgae protein to aquafeed. *In* Handbook of Marine Microalgae. Academic Press: Cambridge, MA, USA, pp: 93–125. https://doi.org/10.1016/b978-0-12-800776-1.00008-x

Gümüş E. 2010. Fatty acid composition of fry mirror carp (*Cyprinus carpio*) fed graded levels of sand smelt (*Atherina boyeri*) meal. Asian-Australasian Journal of Animal Sciences 24 (2): 264–271. https://doi.org/10.5713/ajas.2011.10223

Hamilton SE, Stankwitz C. 2012. Examining the relationship between international aid and mangrove deforestation in coastal Ecuador from 1970 to 2006. Journal of Land Use Science 7 (2): 177–202. https://doi.org/10.1080/1747423x.2010.550694

Han D, Shan X, Zhang W, Chen Y, Wang Q, Li Z, Zhang G, Xu P, Li J, Xie S, *et al*. 2016. A revisit to fishmeal usage and associated consequences in Chinese aquaculture. Reviews in Aquaculture 10 (2): 493–507. https://doi.org/10.1111/raq.12183

Hardy RW. 2010. Utilization of plant proteins in fish diets: Effects of global demand and supplies of fishmeal. Aquaculture Research 41 (5): 770–776. https://doi.org/10.1111/j.1365-2109.2009.02349.x

Hasan MR. 2017. Feeding global aquaculture growth. FAO Aquaculture Newsletter 56 (2). Rome, Italy.

Hernández C, Olvera-Novoa MA, Hardy RW, Hermosillo A, Reyes C, González B. 2010. Complete replacement of fish meal by porcine and poultry by-product meals in practical diets for fingerling Nile tilapia *Oreochromis niloticus*: Digestibility and growth performance. Aquaculture Nutrition 16 (1): 44–53. https://doi.org/10.1111/j.1365-2095.2008.00639.x

Hu L, Yun B, Xue M, Wang J, Wu X, Zheng Y, Han F. 2013. Effects of fish meal quality and fish meal substitution by animal protein blend on growth performance, flesh quality and liver histology of Japanese seabass (*Lateolabrax japonicus*). Aquaculture 372–375, 52–61. https://doi.org/10.1016/j.aquaculture.2012.10.025

Hua K, Cobcroft JM, Cole A, Condon K, Jerry DR, Mangott A, Praeger C, Vucko MJ, Zeng C, Zenger K, Strugnell JM. 2019. The future of aquatic protein: Implications for protein sources in aquaculture diets. One Earth 1 (3): 316–329. https://doi.org/10.1016/j.oneear.2019.10.018

Islam MM, Barman A, Kundu GK, Kabir MA, Paul B. 2019. Vulnerability of inland and coastal aquaculture to climate change: Evidence from a developing country. Aquaculture and Fisheries 4 (5): 183–189. https://doi.org/10.1016/j.aaf.2019.02.007

Justino CI, Duarte KR, Freitas AC, Panteleitchouk TS, Duarte AC, Rocha-Santos TA. 2016. Contaminants in aquaculture: Overview of analytical techniques for their determination. TrAC Trends in Analytical Chemistry 80: 293–310. https://doi.org/10.1016/j.trac.2015.07.014

Laining A, Kristanto AH. 2015. Aquafeed development and utilization of alternative dietary ingredients in aquaculture feed formulations in Indonesia. *In* Catacutan MR, Coloso MR, Acosta BO. (eds.), Development and Use of Alternative Dietary Ingredients or Fish Meal Substitutes in Aquaculture Feed Formulation. Nay Pyi Taw, Myanmar, pp: 3–13).

Liaqat I, Mukhtar B, Malik M, Shah SH, Azzam A, Slahuddin. 2017. Lysine supplementation in fish feed. International Journal of Applied Biology and Forensics 1 (2): 26–31.

Little DC, Young JA, Zhang W, Newton RW, Al Mamun A, Murray FJ. 2018. Sustainable intensification of aquaculture value chains between Asia and Europe: A framework for understanding impacts and challenges. Aquaculture 493: 338–354. https://doi.org/10.1016/j.aquaculture.2017.12.033

Madage SSK, Medis WUD, Sultanbawa Y. 2015. Fish silage as replacement of fishmeal in red tilapia feeds. Journal of Applied Aquaculture 27 (2): 95–106. https://doi.org/10.1080/10454438.2015.1005483

Maisashvili A, Bryant H, Richardson J, Anderson D, Wickersham T, Drewery M. 2015. The values of whole algae and lipid extracted algae meal for aquaculture. Algal Research 9: 133–142. https://doi.org/10.1016/j.algal.2015.03.006

Mulema SA, García AC. 2019. Monitoring of an aquatic environment in aquaculture using a MEWMA chart. Aquaculture 504: 275–280. https://doi.org/10.1016/j.aquaculture.2019.01.019

Nakphet S, Ritchie RJ, Kiriratnikom S. 2016. Aquatic plants for bioremediation in red hybrid tilapia (*Oreochromis niloticus* × *Oreochromis mossambicus*) recirculating aquaculture. Aquaculture International 25 (2): 619–633. https://doi.org/10.1007/s10499-016-0060-7

Navas JM, Telfer TC, Ross LG. 2011. Spatial modeling of environmental vulnerability of marine finfish aquaculture using GIS-based neuro-fuzzy techniques. Marine Pollution Bulletin 62 (8): 1786–1799. https://doi.org/10.1016/j.marpolbul.2011.05.019

Nehete J, Narkhede M, Bhambar R, Gawali S. 2013. Natural proteins: Sources, isolation, characterization and applications. Pharmacognosy Reviews 7 (14): 107. https://doi.org/10.4103/0973-7847.120508

Ngajilo D, Jeebhay MF. 2019. Occupational injuries and diseases in aquaculture – A review of literature. Aquaculture 507: 40–55. https://doi.org/10.1016/j.aquaculture.2019.03.053

OECD (Organisation for Economic Co-operation and Development). 2020. Aquaculture production. OECD Data Explorer. Paris, France. https://data-explorer.oecd.org/ (Retrieved: March 2026).

Olsen RL, Hasan MR. 2012. A limited supply of fishmeal: Impact on future increases in global aquaculture production. Trends in Food Science and Technology 27 (2): 120–128. https://doi.org/10.1016/j.tifs.2012.06.003

Ottinger M, Clauss K, Kuenzer C. 2016. Aquaculture: Relevance, distribution, impacts and spatial assessments – A review. Ocean and Coastal Management 119: 244–266. https://doi.org/10.1016/j.ocecoaman.2015.10.015

Oyarzabal F. 2000. Comentarios a las leyes e instituciones que reglamentan las aguas superficiales de México. Natural Resources Journal 22 (4): 999–1005.

Phuong NT, Oanh DTH. 2010. Striped catfish aquaculture in Vietnam: A decade of unprecedented development. *In* de Silva SS, Davy FB. (eds.), Success Stories in Asian Aquaculture. Springer: Dordrecht, Germany. https://doi.org/10.1007/978-90-481-3087-0_7

Rickard LN, Britwum K, Noblet CL, Evans KS. 2020. Factory-made or farm fresh? Measuring U.S. support for aquaculture as a food technology. Marine Policy 115: 103858. https://doi.org/10.1016/j.marpol.2020.103858

Simbeye DS, Zhao J, Yang S. 2014. Design and deployment of wireless sensor networks for aquaculture monitoring and control based on virtual instruments. Computers and Electronics in Agriculture 102: 31–42. https://doi.org/10.1016/j.compag.2014.01.004

Soininen N, Belinskij A, Similä J, Kortet R. 2019. Too important to fail? Evaluating legal adaptive capacity for increasing coastal and marine aquaculture production in EU-Finland. Marine Policy 110: 103498. https://doi.org/10.1016/j.marpol.2019.04.002

Song AM, Soliman A. 2019. Situating human rights in the context of fishing rights – Contributions and contradictions. Marine Policy 103: 19–26. https://doi.org/10.1016/j.marpol.2019.02.017

Steeves L, Filgueira R. 2019. Stakeholder perceptions of climate change in the context of bivalve aquaculture. Marine Policy 103: 121–129. https://doi.org/10.1016/j.marpol.2019.02.024

Sun H, Tang J, Yao X, Wu Y, Wang X, Liu Y, Lou B. 2015. Partial substitution of fish meal with fermented cottonseed meal in juvenile black sea bream (*Acanthopagrus schlegelii*) diets. Aquaculture 446: 30–36. https://doi.org/10.1016/j.aquaculture.2015.04.020

Tacon AGJ, Metian M. 2015. Feed matters: Satisfying the feed demand of aquaculture. Reviews in Fisheries Science and Aquaculture 23 (1): 1–10. https://doi.org/10.1080/23308249.2014.987209

Tacon AGJ, Metian M. 2017. Food matters: Fish, income, and food supply—A comparative analysis. Reviews in Fisheries Science and Aquaculture 26 (1): 15–28. https://doi.org/10.1080/23308249.2017.1328659

Teves JFC, Ragaza JA. 2016. The quest for indigenous aquafeed ingredients: A review. Reviews in Aquaculture 8 (2): 154–171. https://doi.org/10.1111/raq.12089

Valenti WC, Kimpara JM, Preto BL, Moraes-Valenti P. 2018. Indicators of sustainability to assess aquaculture systems. Ecological Indicators 88: 402–413. https://doi.org/10.1016/j.ecolind.2017.12.068

Wang A, Ran C, Wang Y, Zhang Z, Ding Q, Yang Y, Olsen RE, Ringø E, Bindelle J, Zhou Z. 2019. Use of probiotics in aquaculture of China—A review of the past decade. Fish and Shellfish Immunology 86: 734–755. https://doi.org/10.1016/j.fsi.2018.12.026

Watterson A. 2018. Aquaculture/occupational safety: Towards healthy work. International Collective in Support of Fishworkers: Amsterdam, Netherlands.

World Bank Group. 2013. Fish to 2030: Prospects for fisheries and aquaculture. Agriculture and environmental services discussion paper no. 3. Washington, DC, USA. https://doi.org/10.1596/17579

World Bank Group. 2023. Aquaculture production. Washington, DC, USA. https://data.worldbank.org/indicator/ER.FSH.AQUA.MT (Retrieved: June 2025).

Yogev U, Barnes A, Giladi I, Gross A. 2020. Potential environmental impact resulting from biased fish sampling in intensive aquaculture operations. Science of The Total Environment 707: 135630. https://doi.org/10.1016/j.scitotenv.2019.135630

Yuan Y, Yuan Y, Dai Y, Gong Y. 2017. Economic profitability of tilapia farming in China. Aquaculture International 25 (3): 1253–1264. https://doi.org/10.1007/s10499-017-0111-8

Agrociencia

FERTILIZATION OF NATIVE MAIZE INTERCROPPED WITH HUSK TOMATO IN PEASANT FARMING PLOTS: YIELD, INCOME, AND FOOD SECURITY

Rocio **Albino-Garduño**[1], Horacio **Santiago-Mejía**[1*], Eduardo **Muñoz-Ruíz**[1], Antonio **Turrent-Fernández**[2], José Isabel **Cortés-Flores**[3]

[1]Universidad Intercultural del Estado de México. División de Desarrollo Sustentable. Libramiento Francisco Villa S/N, Colonia Centro, San Felipe del Progreso, State of Mexico, Mexico. C. P. 50640.
[2]Instituto Nacional de Investigaciones Forestales, Agrícolas y Pecuarias. Campo Experimental Valle de México. Carretera Los Reyes-Texcoco km 13.5, Coatlinchán, Texcoco, State of Mexico, Mexico. C. P. 56250.
[3]Colegio de Postgraduados Campus Montecillo. Carretera México-Texcoco km 36.5, Montecillo, Texcoco, State of Mexico, Mexico. C. P. 56264.
* Author for correspondence: horacio.santiago@uiem.edu.mx

Citation: Albino-Garduño R, Santiago-Mejía H, Muñoz-Ruíz E, Turrent-Fernández A, Cortés-Flores JI. 2026. Fertilization of native maize intercropped with husk tomato in peasant farming plots: Yield, income, and food security. **Agrociencia** 60(2): 209-225. https://doi.org/ 10.47163/agrociencia.v60i2.3214

Editor in Chief:
Dr. Fernando C. Gómez Merino

Received: September 24, 2025.
Approved: February 23, 2026.
Published in Agrociencia: March 05, 2026.

ABSTRACT

The objective of this study was to explore the effect of mineral fertilization and mineral fertilization with cattle manure on income, yields, and food baskets generated by intercropping maize (*Zea mays* L.) and husk tomato (*Physalis ixocarpa* Brot. ex Horm.) in three locations in the State of Mexico. Three experimental plots were established with farming families from El Ejido, Santa Rosa de Lima, and San Mateo in 2015. Using a split-plot design, two large plots were tested, one without manure and the other with precomposted cattle manure (10 Mg ha^{-1}). In a small plot, nine nitrogen (N) and phosphorus (P) combination treatments were tested at five levels. Husk tomato, grain, and maize stover yields were evaluated. Net income (in MXN), the maize food security index, and the basic food basket were estimated. In all three locations, husk tomato, grain, and maize stover yields were higher with mineral fertilization plus manure compared to mineral fertilization alone. The highest net incomes from the maize-husk tomato intercropping system in El Ejido (27 498 MXN), Santa Rosa (37 436 MXN), and San Mateo (58 081 MXN) were obtained with 140-85, 140-35, and 150-40 kg of N-P_2O_5 and 10 Mg of manure ha^{-1}, respectively. These incomes can cover two to five basic food baskets for the three communities, as well as the family's corn consumption in El Ejido and San Mateo.

Keywords: *Zea mays* L., *Physalis ixocarpa* Brot. ex Horm., milpa, mazahua, MIAF.

INTRODUCTION

Maize (*Zea mays* L.) is the most widely cultivated crop in the State of Mexico. In 2015, the state produced 2 036 339 Mg of maize grain with an average yield of 3.82 Mg ha^{-1} (SIAP, 2023). For farming families in the northwest of the state, maize holds significant cultural, nutritional, and symbolic value. The Mazahua people inhabit this region and

predominantly cultivate native rainfed maize in monoculture on plots of less than 1 ha as a supplementary activity due to its low profitability, while practicing some traditional ceremonies (Monroy-López *et al*., 2018). Furthermore, the husk tomato (*Physalis ixocarpa* Brot. ex Horm.) is one of the component species of the traditional Mexican milpa and predominates in monoculture and for commercial purposes. In the State of Mexico, husk tomato production in 2015 was estimated at 44 156 Mg, with an average yield of 16 Mg ha^{-1} (SIAP, 2023).

Research has shown the productive, economic, and nutritional potential of native maize intercropped with bush beans (*Phaseolus vulgaris* L.) when using various doses and sources of fertilization within the Milpa Intercropped with Fruit Trees (MIAF) system and has been studied under different conditions in Mixe (Ruiz-Mendoza *et al*., 2012), Mazatec (Santiago-Mejía *et al*., 2008), and Chiapas (Cadena-Iñiguez *et al*., 2018) peasant farming systems. However, there is limited information about the conditions of Mazahua peasant farming and the cultivation of husk tomatoes.

Nitrogen (N), phosphorus (P), and potassium (K) are essential elements for crop growth, development, and production and can be supplied through mineral fertilizers or organic sources (Battisti *et al*., 2023). The use of synthetic chemical fertilizers is the preferred option to meet the immediate nutritional needs of crops; however, they have high production costs and an environmental impact when used excessively (McLeod *et al*., 2020). Combining organic and mineral fertilizers can be an effective way to improve the availability of yield-limiting nutrients (Roohi *et al*., 2022; Zhang *et al*., 2022). Laub *et al*. (2023), at four experimental sites in Kenya, observed the positive effect of fertilization with mineral nitrogen (120 kg ha^{-1}) combined with manure (4 Mg ha $year^{-1}$) on maize yield over 16 years. The increase in the yield of intercropped crops when using manure has been attributed to the improvement of soil structure and the increase in pH, porosity, water retention capacity, and the supply of macro- and micronutrients (Roohi *et al*., 2022).

The technical recommendation for maize monoculture in the Atlacomulco region is 115-46-30 kg ha^{-1} of N-P-K, respectively (ICAMEX, 2023). This fertilization ratio was developed at an experimental center specializing in maize hybrids. In the study region, farmers apply fertilizers based on sources and doses determined by collective experience. In the nearby localities of Fresno Nichi, San Juan Coajomulco, and San Pedro el Alto, maize monoculture is fertilized with 119-77-3080, 162-60-1810, and 158-15-4940 kg ha^{-1} of N-P-manure (Albino-Garduño *et al*., 2021). Roohi *et al*. (2022) recommend that each site should utilize a tailored combination of inputs, which should be assessed for effectiveness.

A challenge for sustainable agricultural production is to make the most of the resources available to farming families to generate sufficient food and income; therefore, it is important to understand the optimal combination of production inputs. In Mexico, studies have been conducted on the economic optimization of maize hybrids (Barrios-Ayala *et al*., 2008; Albino-Garduño *et al*., 2016) and native maize varieties (Padilla-Fidencio *et al*., 2022). Although peasant farming primarily produces for

self-consumption, it is important to identify the combination of inputs and planting arrangements to ensure sufficient maize for family consumption and higher income from the sale of surplus intercropped crops. Some indicators evaluated for production in the diversified agroecosystem include crop yields, family maize supply, relative land efficiency, net income, minimum wages, and the cost of basic food baskets (Mahmud *et al*., 2018; Li *et al*., 2020; Padilla-Fidencio *et al*., 2022).

The benefits of polyculture production can be limited without proper fertilization and agronomic management (Roohi *et al*., 2022). Intercropping takes advantage of the complementarity of species to achieve sustainable intensification, increasing yield per unit of land with reduced production inputs (Xu *et al*., 2020). The production of native husk tomato and maize in intercropped systems on smallholder farms in the State of Mexico has been studied very little, and information on this production method is unavailable. Therefore, the importance of conducting research on small farms is highlighted to obtain technical recommendations appropriate to local conditions.

The objective of this research was to study the effect of mineral fertilization and cattle manure on the yield, net income, food baskets, and family food supply of native maize, intercropped with husk tomato, in three different soils of the Mazahua region of the State of Mexico. The planting design in this study is similar to that of annual crops in MIAF systems, so the results could contribute to their adaptation to this system.

MATERIALS AND METHODS

Experimental site

The study was conducted on three farm plots in municipalities of the Mazahua region in the State of Mexico: 1) El Ejido, in San Felipe del Progreso; 2) Santa Rosa de Lima, in El Oro; and 3) San Mateo, in Ixtlahuaca (Figure 1). The plots were established with three farming families interested in collaboration, who participated in the community outreach program of the Intercultural University of the State of Mexico. The experimental plots were representative of each location in terms of size, slope, soil type, and management practices. The climate in all three sites is temperate sub-humid with summer rains.

The plot in El Ejido belongs to the Muñoz-Ruíz family and features Fluvisol soil with a slope greater than 20 %. It is situated at an altitude of 2563 m and receives 1235 mm of annual rainfall, with an average temperature of 14 °C (in 2015). In Santa Rosa de Lima, the plot was established with the Segundo-Rojas family, on Andosol soil with a slope greater than 20 %, at an altitude of 2822 m, with 1001 mm of annual rainfall and an average temperature of 15 °C. In San Mateo, work was carried out on the plot of the Lucas-Álvarez family, on Planosol soil with a slope of less than 20 %, at an altitude of 2532 m, 882 mm of annual precipitation, and an average temperature of 10 °C. All plots use tillage methods with animal traction (CONAGUA, 2023; INEGI, 2023).

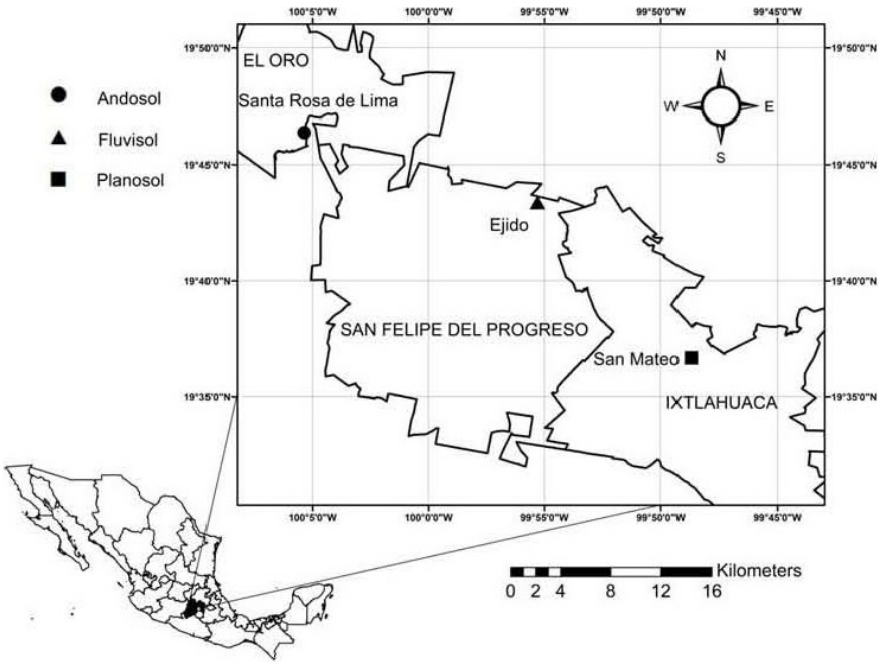

Figure 1. Location of the experimental plots in the northwest of the State of Mexico, Mexico.

Experimental design

A split-plot design was used (Table 1) with two large-plot treatments and nine small-plot subtreatments, which were tested in a maize-husk tomato intercropping system with two rows of each species (Figure 2A). The large-plot treatments were 1) fertilization with 10 Mg ha^{-1} of cattle manure and 2) no manure. The nine subtreatments were generated in a central composite design (Volke *et al*., 2005) with the combination of N and P factors (Table 1).

Each large plot was treated with the central dose and no potassium (120-80-0 kg ha^{-1} of N-P_2O_5-K_2O) to determine the effect of this element. Husk tomatoes received the same fertilization treatments as maize. Subtreatments were randomly assigned to each replicate. The experimental unit (8 m^2) consisted of two rows, each 0.8 m wide by 5 m long, in each of the three replicates. The usable plot area was 7 m^2, with plants outside the boundaries of each experimental unit not being harvested.

Crop management

Fallowing and furrowing were done using animal traction (Figure 2B). The furrows were 0.8 m wide. Sowing was done manually with a shovel, as is customary for families. During the second week of April 2015, in each location, native white conical maize seed from each collaborating farming family was used. The planting density for maize and husk tomato was 30 000 and 15 625 plants per 0.4 ha, respectively.

Table 1. List of fertilization treatments in the intercropping of native maize (*Zea mays* L.) and husk tomato (*Physalis ixocarpa* Brot. ex Horm.) in three peasant plots in the State of Mexico.

Large plot	Small plot			
Cattle manure	Coded levels		Dose* (kg ha^{-1})	
(Mg ha^{-1})	N	P	N	P_2O_5
10	-1	-1	90	50
10	+1	-1	150	50
10	-1	+1	90	110
10	+1	+1	150	110
10	-2	0	60	80
10	+2	0	180	80
10	0	-2	120	20
10	0	+2	120	140
10	0	0	120	80
0	-1	-1	90	50
0	+1	-1	150	50
0	-1	+1	90	110
0	+1	+1	150	110
0	-2	0	60	80
0	+2	0	180	80
0	0	-2	120	20
0	0	+2	120	140
0	0	0	120	80

*In all treatments of the experimental matrix, 40 kg ha^{-1} of K_2O were used.

Figure 2. A: Plantation arrangement in El Ejido, in the municipality of San Felipe del Progreso, State of Mexico; B: agricultural work with animal traction in Santa Rosa de Lima, in the municipality of El Oro, State of Mexico.

Husk tomatoes were sown in seedbeds and transplanted between 56 and 62 days after sowing (DDS) maize. At maize sowing and husk tomato transplanting, 1/3 of the nitrogen (N) and all of the phosphorus (P) and potassium (K) were applied. The remaining N was applied to the maize at the first weeding and to husk tomatoes at the second weeding of maize at 80 DDS. The mineral fertilizers used were triple superphosphate ($Ca(NH_2PO_4)_2 \cdot H_2O$), urea ($CO(NH_2)_2$), and potassium chloride (KCl). The manure used had been decomposing outdoors for six months and was moistened two months before planting, covered with black plastic, and mixed once a week. Manure was applied during maize planting across the entire plot, including the area where the husk tomatoes were later transplanted. Weed control was done manually. The husk tomato harvest took place between 118 and 148 days after sowing (DDS) maize (first to last week of August), and the maize harvest between 220 and 226 DDS.

Variables evaluated

Grain and stubble yield

To assess grain yield, all ears of maize from each plot were harvested, counted, weighed, and shelled manually. Ears, kernels, and cobs were weighed separately on a digital scale (Torrey). Grain moisture was determined using a John Deere portable moisture meter (SW5300, Ill). To determine stubble yield, all plants in each experimental unit were counted, cut, and weighed on the same day as the ear harvest. Stubble weight at harvest was obtained using a digital hanging scale (Torrey). Stubble biomass was calculated after dehydration in a drying oven (LUMISTELL HTP-42), with three samples per replicate. Grain yield was estimated at 14 % moisture.

Husk tomato yield

The husk tomato harvest was done in four cuttings. The weight of the fruit was recorded in each plot and the yield was estimated.

Maize Food Security Index (MFSI)

It was calculated according to López-González *et al.* (2018) using the following equation:

$$MFSI = \frac{(R)(SS)}{(NMF)(196.4)}$$

where R is the maize yield (kg 0.5 ha^{-1}) estimated using the regression equation (detailed in the statistical analysis); SS is the planted area (ha); NMF is the number of members of the producing family, considering five as the average; and 196.4 is the per capita maize consumption (kg). MFSI values <1 indicate the absence of food security, while MFSI >1 reflects its presence.

Basic food basket (BFB)

This represents the number of people who could afford their basic food basket with the income generated from the crops. It was calculated using the following formula:

$$BFB = \frac{NI}{11\,256.24}$$

where *NI* is the net income generated from the intercropping, and 11 256.24 corresponds to the cost of the annual basic food basket per person (in MXN) in 2015 (CONEVAL, 2023).

Statistical analysis

A split-plot analysis of variance was performed using the SAS program (SAS Institute, Cary, NC, USA) as well as a multiple comparisons test of means for interactions between treatments and subtreatments, using the following model:

$$Y_{ijk} = \mu + B_i + T_j + \varepsilon_{ij} + S_k + TS_{jk} + e_{ijk}$$

where Y_{ijk} is the response variable, μ is the overall mean effect, B_i is the effect of the *i*-th block, T_j is the effect of the *j*-th treatment, ε_{ij} is the large plot error, S_k is the effect of the *k*-th treatment, *TSjk* is the interaction effect of the *j*-th treatment with the *k*-th treatment, and e_{ijk} is the small plot error (Castillo, 2011).

Regression models were fitted for maize grain yield and husk tomato fruit yield as a function of N, P, manure, and location. The regression procedure (stepwise, SLE = 0.2; SLS = 0.1) included significant effects ($p \leq 0.05$) for each dependent variable. Auxiliary variables with values of 0 and 1 were used in the overall yield equation: a_1 for the manure factor and s_1 and s_2 for locations. The assignments were: $a_1 = 0$ for mineral fertilization without manure and $a_1 = 1$ for mineral fertilization with cattle manure; $s_1 = 0$, $s_2 = 0$ for El Ejido; $s_1 = 1$, $s_2 = 0$ for Santa Rosa; and $s_1 = 0$, $s_2 = 1$ for Ixtlahuaca. Graphs were created in SigmaPlot (version 15) with the significant effects identified in the regression equation for each location.

Net income

The economic analysis was performed using the discrete method (Martínez-Garza and Martínez-Damián, 1996). An economic optimization program was developed in SAS using the regression equation, which determined the maximum net income (NI) and the corresponding combination of nitrogen (N), phosphorus (P), and manure. Applying the model, the combination of N and P that estimated the highest income (in MXN) within the evaluated range was identified, between 60–180 kg of N ha^{-1} and 20–140 kg of P ha^{-1}, in increments of five units, with and without sheep manure. The formula used was:

$$NI = IT - CT$$

where *IT* is the total revenue obtained by multiplying the yields of husk tomato and maize (grain and stubble) by their selling prices, and *CT* is the total cost, which corresponds to the sum of fixed and variable costs. For the calculation of total revenue, the following prices per Mg were considered, which include transportation, shelling, baling, and harvesting: 2290 MXN for maize grain, 1860 MXN for stubble, and 5010 MXN for husk tomato.

Fixed production costs were MXN 14 300.39 ha^{-1}, broken down as follows: MXN 1120 for land rent, MXN 3700 for land preparation (fallow, harrowing, furrowing, and weeding), MXN 6038.40 for labor (planting, replanting, weeding, manual weeding, fertilization, transplanting, and husk tomato staking), and MXN 3441.99 for tools and supplies (hoe, weeder, shovel, mower, staking materials, seeds, seedlings, and potassium). Variable costs were calculated using the following prices per kilogram: MXN 13.51 for N, MXN 18.32 for P_2O_5, and MXN 0.3166 for pre-composted manure. All prices and costs correspond to 2015.

RESULTS AND DISCUSSION

Effect of fertilization on the yield of intercropped maize and husk tomato

There was a significant effect (Table 2) of the study factors N, P, and manure, both individually and in interaction. The combination of mineral fertilizers with manure increased the grain and stover yield of intercropped maize and husk tomato compared to treatments with mineral fertilization alone (Figure 3). This positive effect was corroborated in the regression equations, where the manure factor increased yield (0.97 and 2.17 Mg 0.5 ha^{-1} of maize and husk tomato, respectively) (Table 3) compared to mineral fertilization alone at the three experimental sites.

The increased yield of maize intercropped with other crops and with the application of mineral and organic fertilizers has also been demonstrated in recent studies (Fan *et al*., 2020; Roohi *et al*., 2022; Laub *et al*., 2023). Roohi *et al*. (2022), in their study of maize intercropped with cowpea in Pakistan, attribute this phenomenon to the slow-release fertilization pattern (N-P-K combined with enriched compost), which could promote adequate nutrient supply. Laub *et al*. (2023), in their maize intercropping study in sub-Saharan Africa on tropical soils, also argue that the synchronization of nitrogen release from manure with plant demand may explain the high yield when applied to the crops.

The positive effect of combining mineral fertilizers with manure on husk tomato yield aligns with the findings of Aguiñaga-Bravo *et al*. (2020) in a Leptosol soil in Conkal, Yucatán. In their study involving two varieties of *Physalis* sp. grown in monoculture, the authors recommended the use of cattle manure at a rate of 20.85 Mg

Table 2. Analysis of variance of husk tomato (*Physalis ixocarpa* Brot. ex Horm.) yield and maize grain and stubble yield (*Zea mays* L.) in response to N and P_2O_5 doses, with and without manure, in three experimental sites.

Source of variation (Treatments*)	Degrees of freedom	Maize				Husk tomato	
		Grain		Stubble			
		MS	FC	MS	FC	MS	FC
				El Ejido			
Block	2	0.0641	1.39	0.0056	0.16	0.1446	8.33**
Large plot (LP)	1	13.4970	292.11***	23.1555	637.36***	32.2449	1857.66***
Error in large plot (*a*)	2	0.0480	1.04	0.1492		0.0508	
Small plot (SP)	8	0.9400	20.35***	1.3500	37.16***	3.2723	188.53***
LP × SP	8	2.5666	55.55***	1.5684	43.17***	1.6889	97.30***
Error in small plot (*b*)	32	1.4785		1.1625		0.5554	
Total	53						
				Santa Rosa de Lima			
Block	2	0.0033	1.28	0.0002	0.20	0.1785	3.16*
LP	1	8.7137	3341.68***	3.8747	3289.46***	28.0786	497.75***
Error *a*	2	0.0013		0.0002		0.003	
SP	8	0.5638	216.23***	0.5337	85.05***	4.4332	78.59***
LP × SP	8	0.2215	84.96***	0.2512	213.28***	0.8071	14.31***
Error *b*	32	0.0834		0.0376		1.8051	
Total	53						
				San Mateo			
Block	2	0.0879	4.69*	0.0014	0.07	0.1566	0.81
LP	1	1.4314	76.38 ***	0.5075	26.09***	89.6319	462.53***
Error *a*	2	0.0030		0.0038		0.6171	
SP	8	0.3404	18.16***	1.0266	52.79***	14.4744	74.69***
LP × SP	8	0.1075	18.16***	0.1672	8.60***	13.6840	74.69***
Error *b*	32	0.5997		0.6223		6.2011	
Total	53			53		53	

*Large plot: 0 and 10 Mg of manure ha^{-1}; small plot: five levels of two factors (60–180 kg N ha^{-1} and 20–140 kg P_2O_5 ha^{-1}).
*, **, *** Significant differences at $p \leq 0.05$, 0.01, and 0.001, respectively. MS: mean squares; FC: calculated F.

ha^{-1} combined with mineral fertilizer (10-75-50 N-P-K). This combination enhanced nitrogen accumulation in the plants and increased the levels of fats, total phenols, and essential minerals (Cu, Fe, P, Ca, and K) compared to fertilization methods that did not include cattle manure. Higher husk tomato yields have been observed with organic fertilization (10.66 Mg ha^{-1}) when the soil has 34.85 g dm^{-3} of organic matter and the manure contains 2.65 % N (Ariati *et al*., 2017).

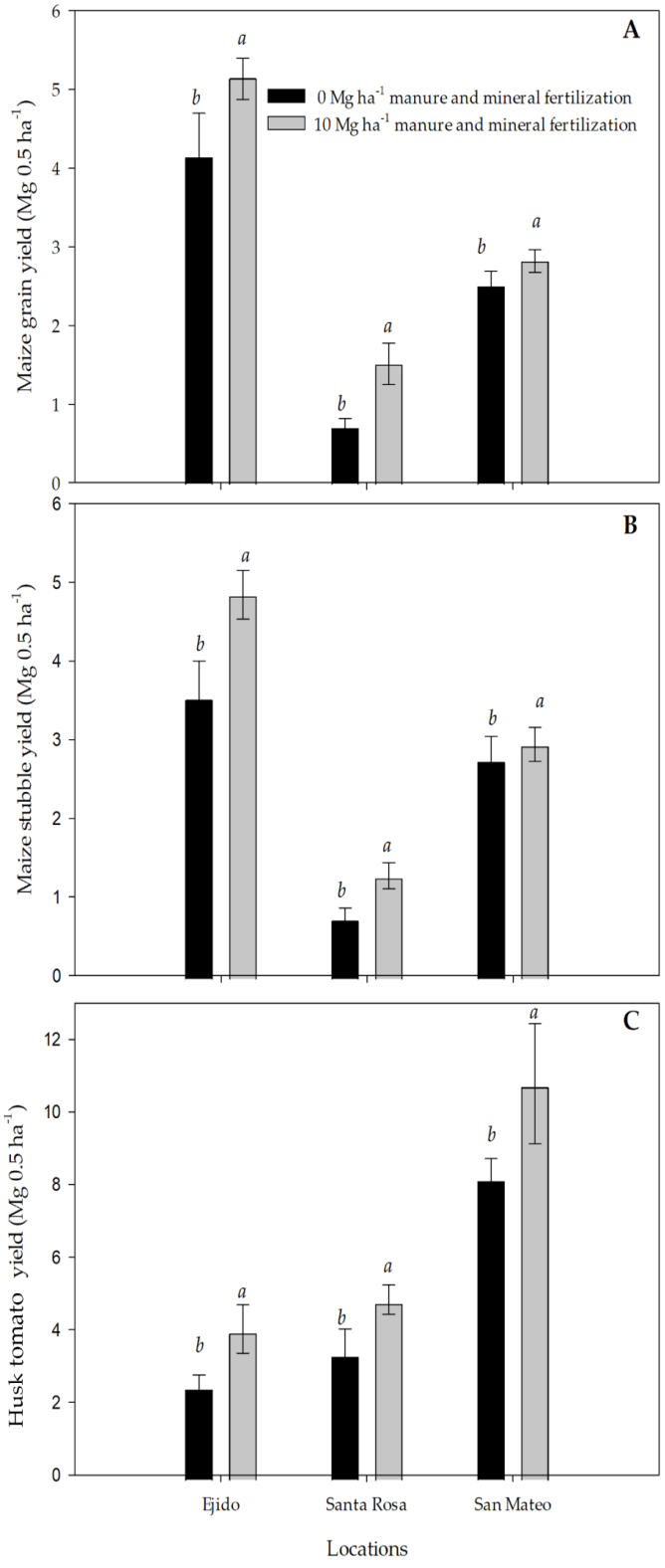

Figure 3. Effect of cattle manure combined with mineral fertilization on the yield of A) grain, B) maize stover (*Zea mays* L.), and C) husk tomato (*Physalis ixocarpa* Brot. ex Horm.) in three locations in the State of Mexico. Yields correspond to 0.5 ha of maize and 0.5 ha of husk tomato intercropped within 1 ha. The plotted values represent the mean of the small plot in its subtreatments ± standard error. Different letters between bars within each location indicate significant differences ($p \leq 0.05$, Tukey-Kramer).

Table 3. General yield equations for maize (*Zea mays* L., grain and stubble) and husk tomato (*Physalis ixocarpa* Brot. ex Horm.), integrating locations and large plot treatments.

Variable	Equation	R^2
$\hat{Y}M =$	$4.2998^{***} + 0.9704a_1{}^{***} - 0.4872N^{***} - 3.2785s_1{}^{**} - 1.6437s_2{}^{***} - 0.1149N_2{}^{**} + 0.6081a_1N^{***} + 0.0831a_1N_2{}^{*} - 0.0719a_1P_2{}^{*} + 0.4589s_1N^{**} + 0.1176s_1a_1P^{*} - 0.1239s_1P_2{}^{*} + 0.6087s_2N^{***} - 0.6597s_2a_1{}^{***} - 0.6387s_2a_1N^{***} - 0.2153s_2NP^{**} - 0.4367a_1s_1N^{***} - 0.1256a_1s_1N_2{}^{**}$	0.93
$\hat{Y}R =$	$3.5315^{***} + 1.1664a_1{}^{***} - 0.2191N^{***} + 0.0752P^{*} - 2.7991s_1{}^{***} - 0.6412s_2{}^{***} + 0.1074a_1N_2{}^{*} + 0.2593s_1N^{**} - 0.7739s_1a_1{}^{***} + 0.2061s_2N^{**} + 0.1610s^2P^{*} - 1.1159s_2a_1{}^{***} - 0.1076s_2N_2{}^{*}$	0.91
$\hat{Y}T =$	$3.0978^{***} + 2.1713a_1{}^{***} + 3.8424s_2{}^{***} - 0.1242N_2{}^{*} - 0.2657P_2{}^{*} + 0.5575a_1N^{**} + 0.19070a_1P^{*} - 0.2380a_1N_2{}^{*} - 0.3492a_1P_2{}^{*} + 3.5964s_1a_1{}^{***} - 0.5408s_1a_1N^{***} - 1.0617s_1NP^{***} + 0.5686s_1P_2{}^{***} - 0.1547s_2P - 1.4235s_2a_1P^{***} + 0.6876s_2N_2{}^{***} + 0.6043s_2P_2{}^{***} + 0.3749a_1s_1N_2{}^{**} - 0.4621a_1s_1P^{**} + 0.6268a_1s_1P_2 - 0.8634a_1s_2N^{***} + 0.9715a_1s_2N_2{}^{***} - 2.2843a_1s_2NP^{***}$	0.95

$\hat{Y}_M$: estimated maize yield (Mg 0.5 ha^{-1}); $\hat{Y}_R$: estimated maize stover yield (Mg 0.5 ha^{-1}); $\hat{Y}_T$: estimated husk tomato yield (fresh weight, Mg 0.5 ha^{-1}). *, **, *** Terms significant at $p \leq 0.05$, 0.01, and 0.001, respectively. Terms with a_1 represent the additional effect of manure; terms without a_1 correspond to mineral fertilization. Terms without s_1 or s_2 refer to El Ejido locality; those including only s_1, to Santa Rosa; and those including only s_2, to San Mateo.

Agronomic response, income, food basket, and supply

El Ejido

The analysis of the treatment × subtreatment interaction by crop showed that, in El Ejido, the highest yield of maize grain (5.86 ± 0.37 Mg 0.5 ha^{-1}) and stubble (5.72 ± 0.47 Mg 0.5 ha^{-1}) and husk tomato (6.19 ± 0.48 Mg 0.5 ha^{-1}) was obtained at the doses 180-80-40, 60-80-40, and 120-80-40 kg of N-P_2O_5-K_2O + 10 Mg of manure ha^{-1}, respectively. The economic optimization of intercropped maize and husk tomato as a polyculture system indicated that the highest economic income was achieved with a fertilization regimen of 140-85-40 kg of N-P_2O_5 and K_2O, along with 10 Mg of manure ha^{-1} (Table 4). With the income generated from this combination of inputs, the basic food basket for two people and the maize consumption of a family of five could be supplied.

Table 4. Maximum net income (NI), basic food basket (BFB) and maize food security index (MFSI) generated in the intercropping of maize (*Zea mays* L.) with husk tomato (*Physalis ixocarpa* Brot. ex Horm.), with their respective level of fertilization and yield, in three communities of the State of Mexico.

Location	N	P	Manure	Mgy	Msy	Hty	NI	BFB	MFSI
	(kg ha^{-1})		(Mg ha^{-1})	(Mg ha^{-1})			(MXN)		
El Ejido	140	85	10	5.33	4.61	5.49	27 498	2.4	5.42
	85	70	0	4.71	3.77	2.92	15 715	1.4	4.79
Santa Rosa	140	35	10	0.98	0.73	10.94	37 436	3.3	0.99
	150	40	0	1.64	0.99	5.52	16 320	1.4	1.67
San Mateo	150	40	10	2.25	1.65	13.96	58 081	5.2	2.29
	160	50	0	3.75	2.81	8.92	41 241	3.7	3.81

N: nitrogen; P: P_2O_5; Mgy: maize grain yield; Msy: maize stover yield; Hty: husk tomato yield.

Among the factors evaluated that correspond to the combination of mineral fertilizer doses with manure, nitrogen (N) and potassium (K) had an effect on crop yield. In this location, a positive response in maize grain yield (Figure 4A) was observed in response to the combined factors of nitrogen × manure fertilization. In other words, when native white maize was fertilized with 10 Mg ha^{-1} of cattle manure, the increment of the nitrogen dose (60, 120, 180 kg of N ha^{-1}) increased grain yield at constant phosphorus (P) and potassium (K) doses (80–40 kg of P-K ha^{-1}). Manure provides nitrogen to maize crops even beyond the year of application, as it releases around 30 % of the total N in the first year (Laub *et al*., 2023). Therefore, conducting long-term studies to better understand the effects of nitrogen would be advisable.

In El Ejido, a positive effect on maize grain yield was identified with increased potassium (K) at the same nitrogen (N) and phosphorus (P) levels (Figure 4B). Other studies with maize have also observed increased grain yield with increased K at the same N levels (Zhang *et al*., 2023). Benkova *et al*. (2023) argue that applying compost to maize crops in Fluvisols increases available N and K. The increase in starch and protein content in the grain is attributed to the increased potassium (at the same N levels) (Zhang *et al*., 2022).

Santa Rosa de Lima

In this plot, the maximum net income (37 436 MXN) was estimated for the maize-husk tomato intercropping system using 140-35-40 kg of N-P_2O_5-K_2O + 10 Mg of manure ha^{-1}. The addition of manure with the mineral fertilization resulted in an additional amount of MXN 21 116 compared to the application of 150-40-00 kg of N-P_2O_5-K_2O ha^{-1} (Table 4). In this location, the net income generated was sufficient to purchase the basic food basket for 1–3 people in the rural area with the current level of inputs. The maximum income achieved with the use of manure is attributed to the high tomato yield estimated under these conditions.

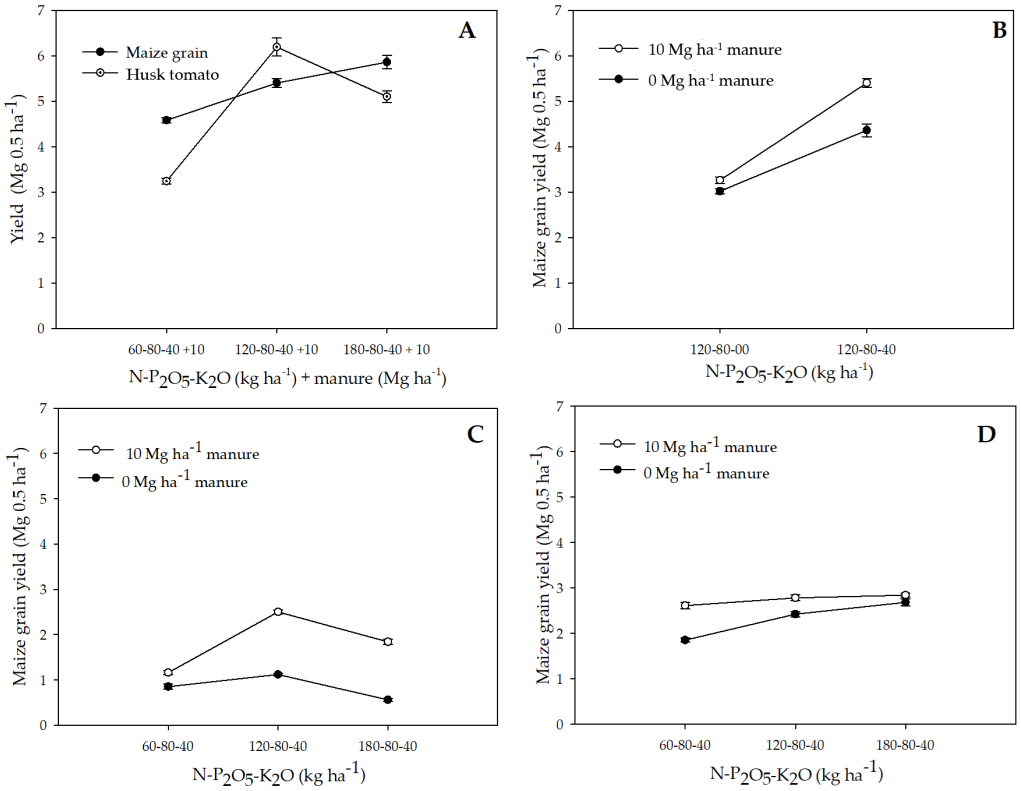

Figure 4. A: Effect of nitrogen on the yield of husk tomato (*Physalis ixocarpa* Brot. ex Horm.) and maize grain (*Zea mays* L.) with fertilization at 80-40 + 10 000 kg of P_2O_5-K_2O + cattle manure in El Ejido; B: effect of potassium on maize grain yield with and without the addition of cattle manure in El Ejido; C: nitrogen on maize grain yield with and without manure application in fertilization in Santa Rosa de Lima; D: maize grain yield, intercropped with husk tomato, at three levels of nitrogen fertilization, with and without manure in San Mateo. The values plotted are the average of six samples ± standard error.

Santa Rosa de Lima has Andosol soils characterized by their strong phosphorus fixation caused by active aluminum, iron, and their amorphous clay mineralogy (allophane). The presence of short-range amorphous compounds combined with a high organic matter content gives the Andosol a variable load (Shoji *et al*., 1993). Low nitrogen use efficiency has been observed in these soils (Bekele *et al*., 2022), and it is difficult to predict nitrogen fluxes (Deng *et al*., 2015). This explains why the regression equation (Table 3) indicated a negative effect of nitrogen in Santa Rosa.

Graphical analysis (Figure 4C) showed that increasing the application rate from 120 to 180 kg of N ha^{-1} decreased yield, regardless of the addition of manure with the mineral fertilizer. In Andosols of Ethiopia, intensive manure application in maize has been reported to reduce N use efficiency and promote NO_3^--N leaching and N_2O

volatilization (Deng *et al*., 2015). These results provide an initial understanding of the effect of fertilization on crops; however, further evaluation is needed over several growing seasons, taking into account the year factor.

San Mateo

In this location, the highest estimated net income from the maize-husk tomato intercropping system was obtained with 150-40-10 kg of N-P_2O_5-K_2O + 10 Mg of manure ha^{-1} (Table 4). The highest net incomes were achieved when mineral fertilization was combined with manure. The economic optimum (58 081 MXN) provides enough for five basic food baskets and more than twice the amount of maize required for family consumption. The profits from the maize-husk tomato intercropping system in San Mateo (Table 4) are attributed to the soil type, year, variety, and climate (Zhang *et al*., 2022), which are suitable for husk tomato, which provides the highest income.

In San Mateo, nitrogen (N) showed a significant effect on the regression equation for maize grain yield (Table 3). Graphical analysis of the data shows that yield increases with the applied N dose, with or without manure (Figure 4D). The study by Tofa *et al*. (2022) also showed a progressive response of maize grain yield to N application.

CONCLUSIONS

Combined fertilization (pre-composted cattle manure plus mineral NPK) resulted in increased crop yields for native maize intercropped with husk tomatoes compared to mineral fertilization alone. Additionally, net income from the intercropped system was higher with combined fertilization than with mineral fertilization alone. The native maize-husk tomato intercropping system is capable of providing sufficient food for 1–5 people and covers family maize consumption needs, with the exception of Santa Rosa de Lima.

ACKNOWLEDGEMENTS

The authors wish to thank the collaboration provided by the Muñoz-Ruíz, Segundo-Rojas, and Lucas-Álvarez families.

REFERENCES

Aguiñaga-Bravo A, Medina-Dzul K, Garruña-Hernández R, Latournerie-Moreno L, Ruíz-Sánchez E. 2020. Efecto de abonos orgánicos sobre el rendimiento, valor nutritivo y capacidad antioxidante de tomate verde (*Physalis ixocarpa*). Acta Universitaria 30: 1–14. https://doi.org/10.15174/au.2020.2475

Albino-Garduño R, Santiago-Mejía H, Avendaño-Gómez A, González-Álvarez L, Cruz-Reyes R. 2021. Conocimiento campesino sobre fertilización del maíz en comunidades mazahua (Jñatjo) de México. Agricultura Sociedad y Desarrollo 18 (2): 305–320. https://doi.org/10.22231/asyd.v18i2.1002

Albino-Garduño R, Turrent-Fernández A, Cortés-Flores JI, González-Estrada A, Mendoza-Castillo M, Volke-Haller VH, Santiago-Mejía H. 2016. Optimización económica de N, P, K y densidades de plantación en maíz y frijol intercalados. Revista Mexicana de Ciencias Agrícolas 7(5): 993–1004.

Ariati AC, Oliveira MC, Loss EMS, Gomes I, Pacheco V, Negri RC. 2017. Mineral and organic fertilizer in two *Physalis* species. African Journal of Agricultural Research 12 (2): 104–110. https://doi.org/10.5897/ajar2016.11717

Barrios-Ayala A, Turrent-Fernández A, Ariza-Flores R, Otero-Sánchez M, Michel-Aceves A. 2008. Interacción genotipos x prácticas de manejo en el rendimiento de grano de híbridos de maíz. Agricultura Técnica en México 34 (1): 85–90.

Battisti M, Moretti B, Blandino M, Grignani C, Zavattaro L. 2023. Maize response to nitrogen and phosphorus starter fertilisation in mineral-fertilised or manured systems. The Crop Journal 11 (3): 922–932. https://doi.org/10.1016/j.cj.2022.09.010

Bekele I, Lulie B, Habte M, Boke S, Hailu G, Mariam EH, Ahmed JS, Abera W, Sileshi GW. 2022. Response of maize yield to nitrogen, phosphorus, potassium and sulphur rates on Andosols and Nitisols in Ethiopia. Experimental Agriculture 58 (11): 1–17. https://doi.org/10.1017/S0014479722000035

Benkova M, Nenova L, Simeonova T, Harizanova M, Atanassova I. 2023. Effect of organic amendments on soil characteristics and maize biomass in a greenhouse experiment. Bulgarian Journal of Agricultural Science 29 (1): 55–61.

Cadena-Iñiguez P, Camas-Gómez R, López-Báez W, López-Gómez HC, González-Cifuentes JH. 2018. El MIAF, una alternativa viable para laderas en áreas marginadas del sureste de México: caso de estudio en Chiapas. Revista Mexicana de Ciencias Agrícolas 9 (7): 1351–1361. https://doi.org/10.29312/remexca.v9i7.1670

Castillo MLE. 2011. Introducción al SAS para Windows (Tercera edición). Universidad Autónoma Chapingo: Chapingo, México. 295 p.

CONAGUA (Comisión Nacional del Agua). 2023. Proyecto de base de datos climatológicos. Información estadística climatológica. Gobierno de México. Secretaría de Medio Ambiente y Recursos Naturales. Comisión Nacional del Agua. Servicio Metereológico Nacional. Ciudad de México, México. https://smn.conagua.gob.mx/es/climatologia/informacion-climatologica/informacion-estadistica-climatologica (Retrieved: November 2025).

CONEVAL (Consejo Nacional de Evaluación de la Política de Desarrollo Social). 2023. Línea de pobreza extrema por ingresos rural a precios de 2015, canasta alimentaria-rural. Ciudad de México, México. https://www.coneval.org.mx/Medicion/MP/Paginas/Lineas-de-Pobreza-por-Ingresos.aspx (Retrieved: November 2025).

Deng M, Bellingrath-Kimura SD, Zeng L, Hojito M, Zhang T, Yoh M. 2015. Evaluation of N environmental risks on Andosols from an intensive dairy farming watershed using DNDC. Science of the Total Environment 512: 659–671. https://doi.org/10.1016/j.scitotenv.2015.01.047

Fan Y, Wang Z, Liao D, Raza MA, Wang B, Zhang J, Chen J, Feng L, Wu X, Liu C, Yang W. 2020. Uptake and utilization of nitrogen, phosphorus and potassium as related to yield advantage in maize-soybean intercropping under different row configurations. Nature Scientific Reports 10 (1): 9504. https://doi.org/10.1038/s41598-020-66459-y

ICAMEX (Instituto de Investigación y Capacitación Agropecuaria, Acuícola y Forestal). 2023. Maíz de temporal Valles Altos del Estado de México. Gobierno del Estado de México. Instituto de Investigación y Capacitación Agropecuaria, Acuícola y Forestal. Metepec, México. https://icamex.edomex.gob.mx/maiz (Retrieved: November 2025).

INEGI (Instituto Nacional de Estadística y Geografía). 2023. Mapa digital de México. Ciudad de México, México. https://gaia.inegi.org.mx/mdm6/ (Retrieved: July 2023).

Laub M, Corbeels M, Mathu Ndungu S, Mucheru-Muna MW, Mugendi D, Necpalova M, van de Broek M, Waswa W, Vanlauwe B, Six J. 2023. Combining manure with mineral N fertilizer maintains maize yields: Evidence from four long-term experiments in Kenya. Field Crops Research 291: 108788. https://doi.org/10.1016/j.fcr.2022.108788

Li C, Hoffland E, Kuyper TW, Yu Y, Zhang C, Li H, Van DW. 2020. Syndromes of production in intercropping impact yield gains. Nature Plants 6 (6): 653–660. https://doi.org/10.1038/s41477-020-0680-9

López-González JL, Damián-Huato MA, Álvarez-Gaxiola JF, Méndez-Espinosa JA, Rappo-Miguez SE, Paredes-Sánchez JA. 2018. Maíz (*Zea mays* L.) y seguridad alimentaria en el municipio de Calpan, Puebla-México. Agroproductividad 11 (1): 37–43.

Mahmud S, Alam M, Rahman M, Amin M, Hassan M. 2018. Productivity and economics of maize-squash intercropping at different planting systems. Journal of Bangladesh Agricultural University 16 (1): 23–26. https://doi.org/10.3329/jbau.v16i1.36476

Martínez-Garza A, Martínez-Damián MA. 1996. Diseño de experimentos con fertilizantes. Sociedad Mexicana de la Ciencia del Suelo. Chapingo, México. 151 p.

McLeod MK, Sufardi S, Harden S. 2020. Soil fertility constraints and management to increase crop yields in the dryland farming systems of Aceh, Indonesia. Soil Research 59 (1): 68–82. https://doi.org/10.1071/sr19324

Monroy-López L, Albino-Garduño R, González-Pablo L, Santiago-Mejía H, Pedraza-Durán I. 2018. Manejo generacional de la milpa en la comunidad mazahua de Palmillas, Estado de México. Iberoforum. Revista de Ciencias Sociales 13 (25): 94–113.

Padilla-Fidencio V, Albino-Garduño R, Santiago-Mejía H, Turrent-Fernández A, Ronquillo-Cedillo I, González Pablo L. 2022. Intensification of milpa in the State of Mexico: Net incomes, food security and land equivalent ratio. Agrociencia 56 (4): 727–751. https://doi.org/10.47163/agrociencia.v56i4.2453

Roohi M, Arif MS, Guillaume T, Yasmeen T, Riaz M, Shakoor A, Farooq TH, Shahzad SM, Bragazza L. 2022. Role of fertilization regime on soil carbon sequestration and crop yield in a maize-cowpea intercropping system on low fertility soils. Geoderma 428: 116152. https://doi.org/10.1016/j.geoderma.2022.116152

Ruiz-Mendoza AD, Jiménez-Sánchez L, Figueroa-Rodríguez OL, Morales-Guerra M. 2012. Adopción del sistema milpa intercalada en árboles frutales por cinco municipios mixes del estado de Oaxaca. Revista Mexicana de Ciencias Agrícolas 3 (8): 1605–1621.

Santiago-Mejía E, Cortés-Flores JI, Turrent-Fernández A, Hernández-Romero E, Jaen-Contreras D. 2008. Calidad del fruto del duraznero en el sistema milpa intercalada con árboles frutales en laderas. Agricultura Técnica en México 34 (2): 159–166.

Shoji S, Nanzyo M, Dahlgren RA. 1993. Volcanic ash soils. Elsevier: San Diego, CA, USA. 277 p.

SIAP (Servicio de Información Agroalimentaria y Pesquera). 2023. Anuario estadístico de la producción agrícola. Gobierno de México. Servicio de Información Agroalimentaria y Pesquera. Ciudad de México, México. https://www.agricultura.gob.mx/datos-abiertos/siap (Retrieved: November 2025).

Tofa AI, Kamara AY, Babaji BA, Aliyu KT, Ademulegun TD, Bebeley JF. 2022. Maize yield as affected by the interaction of fertilizer nitrogen and phosphorus in the Guinea savanna of Nigeria. Heliyon 8 (11): e11587. https://doi.org/10.1016/j.heliyon.2022.e11587

Volke HV, Turrent FA, Castillo M. 2005. Diseños de tratamientos y estimación de funciones de respuesta en la investigación agrícola. Colegio de Postgraduados: Montecillo, México. 68 p.

Xu Z, Li C, Zhang C, Yu Y, van der Werf W, Zhang F. 2020. Intercropping maize and soybean increases efficiency of land and fertilizer nitrogen use; A meta-analysis. Field Crops Research 246 (1): 107661. https://doi.org/10.1016/j.fcr.2019.107661

Zhang M, Hu Y, Han W, Chen J, Lai J, Wang Y. 2023. Potassium nutrition of maize: Uptake, transport, utilization, and role in stress tolerance. The Crop Journal 11 (4): 1048–1058. https://doi.org/10.1016/j.cj.2023.02.009

Zhang Q, Li G, Lu W, Lu D. 2022. Interactive effects of nitrogen and potassium on grain yield and quality of waxy maize. Plants 11 (19): 2528. https://doi.org/10.3390/plants11192528

Agrociencia

EVALUATION OF THREE OIL EXTRACTION PROCESSES FOR HASS VARIETY AVOCADO (*Persea americana* Mill.)

Tito Emilio **Ariza-Ortega**[1], José Alberto **Ariza-Ortega**[2], Joel **Díaz-Reyes**[3*], María Elena **Ramos-Cassellis**[4], Ma. Dolores **Castañeda-Antonio**[5], José de Jesús **Manríquez-Torres**[6], Eva María **Molina-Trinidad**[7]

[1] Instituto Mexicano del Seguro Social. Unidad de Medicina Familiar Número 57. Heroica Puebla de Zaragoza, Puebla, México. C. P. 72560.
[2] Universidad Autónoma del Estado de Hidalgo. Instituto de Ciencias de la Salud, Área Académica de Nutrición, Centro de Investigación Interdisciplinario. Carretera Pachuca-Actopan Camino a Tilcuautla s/n, San Agustín Tlaxiaca, Hidalgo, México. C. P. 42160.
[3] Instituto Politécnico Nacional. Centro de Investigación en Biotecnología Aplicada. Ex-Hacienda San Juan Molino, Carretera Estatal Santa Inés Tecuexcomac-Tepetitla km 1.5, Tepetitla, Tlaxcala, México. C. P. 90700.
[4] Benemérita Universidad Autónoma de Puebla. Facultad de Ingeniería Química. Ciudad Universitaria, Heroica Puebla de Zaragoza, Puebla, México. C. P. 72570.
[5] Benemérita Universidad Autónoma de Puebla. Instituto de Ciencias, Centro en Investigaciones en Ciencias Microbiológicas. Ciudad Universitaria, Heroica Puebla de Zaragoza, Puebla, México. C. P. 72592.
[6] Universidad Autónoma de Baja California, Facultad de Medicina y Psicología. Parque Internacional Industrial Tijuana, Universidad, Tijuana, Baja California, México. C. P. 22390.
[7] Universidad Autónoma del Estado de Hidalgo, Instituto de Ciencias de la Salud, Área Académica de Medicina, Centro de Investigación Interdisciplinario. Carretera Pachuca-Actopan Camino a Tilcuautla s/n, San Agustín Tlaxiaca, Hidalgo, México. C. P. 42160.
* Author for correspondence: joel_diaz_reyes@hotmail.com

Citation: Ariza-Ortega TE, Ariza-Ortega JA, Díaz-Reyes J, Ramos-Cassellis ME, Castañeda-Antonio MD, Manríquez-Torres JJ, Molina-Trinidad EM. 2026. Evaluation of three oil extraction processes for Hass variety avocado (*Persea americana* Mill.). **Agrociencia** 60(2): 226-238. https://doi.org/ 10.47163/agrociencia.v60i2.3398

Editor in Chief:
Dr. Fernando C. Gómez Merino

Received: May 03, 2025.
Approved: January 29, 2026.
Published in Agrociencia: February 13, 2026.

ABSTRACT

The pulp of avocados has a high oil concentration that is usually extracted with hexane, a nonpolar solvent that affects yield and poses health and environmental hazards. This problem requires the exploration of alternative extraction techniques, such as centrifugation. In this work, three avocado oil extraction methods were evaluated for Hass avocado (*Persea americana* Mill.) using proton (^{1}H) and carbon (^{13}C) nuclear magnetic resonance (NMR) spectroscopy to assess oil quality. One kilogram of avocado was purchased in 2023 at the Zapata market in Puebla City, Mexico. A controlled experimental design was used, with triplicate replications. Avocado pulp (250 g) was dehydrated at 70 °C for 24 h in a convection oven and then homogenized to a particle size of 250 μm. Oil extraction was performed using three methods with 1 g of dehydrated pulp: 1) Soxhlet extraction with hexane at 60 °C for 4 h, 2) maceration with hexane at 25 °C for 24 h, and 3) centrifugation at 11 000 rpm (15 557 × gravity) at 40 °C for 10 min. Oil quality was evaluated using ^{1}H-NMR and ^{13}C-NMR, with acquisition times of 2049 and 4.5 s, respectively. The highest yield (78 %) was obtained using the first method. However, the second and third methods showed minimal oxidation of their double bonds and lower generation of free fatty acids due to their lower processing temperatures. The third method was the most

effective, as the oil retained its characteristic sensory properties and did not require further refinement.

Keywords: Avocado oil, fatty acids, ^{1}H-NMR and ^{13}C-NMR spectroscopy, traditional extraction.

INTRODUCTION

The avocado (*Persea americana* Mill.) belongs to the Lauraceae family, which includes 45 genera and approximately 2850 species. The Hass variety is the most widely consumed worldwide, with Mexico being the primary producer, exporter, and consumer (FAO, 2024). This fruit consists of three components: shell (15 %), seed (20 %), and pulp (65 %) (García-Vargas *et al*., 2020), with oleic fatty acid predominating in the pulp (43.65–63.73 %), similar to extra virgin olive oil (Barros *et al*., 2016). The extraction process of avocado oil determines the quantity and quality of its bioactive components, facilitating its diversification into various products, including food, cosmetics, and pharmaceuticals (Flores *et al*., 2019).

One of the most common extraction methods is solvent extraction, typically using hexane or n-hexane. Due to its chemical properties, hexane interacts effectively with oils, enhancing extraction efficiency and yield (Badui, 2019). After extraction, the solvent is separated from the oil by distillation and recovered for reuse, yielding crude oil (Rosenthal *et al*., 1996). However, in the oil industry, approximately 350 thousand Mg of hexane are lost annually, contributing to increased atmospheric pollution (European Commission, 2003).

Crude oil can undergo a refining process that includes sample conditioning, degumming, neutralization, bleaching, and deodorization (Cravotto *et al*., 2022). During deodorization (180–220 °C), temperatures exceed the boiling point of hexane (68.7 °C), eliminating the characteristic odor of the solvent and yielding refined oil (Badui, 2019). However, in refined oils obtained by solvent extraction, hexane levels above the permissible limit (0.005 mg kg^{-1}) have been reported, such as in olive and canola oils, with concentrations of 0.4 and 0.233 (European Commission, 2003). If not eliminated from the body, results in its metabolism to 2,5-hexanedione, which causes neurotoxicity (Ruiz-García *et al*., 2020).

On the other hand, despite concerns about residues, there is no conclusive evidence that trace amounts of residual hexane chemically react with lipids or significantly modify their structure, as hexane is a nonpolar aliphatic hydrocarbon and largely chemically unreactive; moreover, it is almost completely eliminated during refining due to its high volatility (Cravotto *et al*., 2022). However, several studies have shown that hexane extraction can alter the composition of minor compounds, such as tocopherols, sterols, volatile compounds, and phospholipids, which are key determinants of oxidative stability and nutritional quality of the oil. For example, Junyusen *et al*. (2022) reported significant differences in phytochemical and antioxidant contents when comparing solvent-extracted oils with those obtained by cold pressing. These variations directly affect oxidative stability and shelf life. Although residual hexane itself does not

typically chemically alter triglycerides, the solvent-based extraction process and its associated thermal conditions can indirectly influence oil composition and stability (Cravotto *et al*., 2022; Junyusen *et al*., 2022).

Due to the above, alternatives to solvent-based oil extraction are being explored, including solvent-free methods such as centrifugation (Pérez-Saucedo *et al*., 2021), which has emerged as a viable alternative for extracting edible vegetable oils, particularly from matrices such as avocado or olive pulp. This technique separates the oil phase using centrifugal forces without the need for organic solvents like hexane, substantially reducing risks to human health and environmental impact (Zuin *et al*., 2018). Unlike conventional solvent extraction, centrifugation leaves no toxic residues and requires minimal thermal energy, which helps preserve heat-labile compounds such as tocopherols, carotenoids, and phenolic compounds (Mahato *et al*., 2019). This method significantly improves the preservation of bioactive compounds that are crucial for both the oxidative stability and nutritional value of the oil (Gil-Martín *et al*., 2022).

For oils obtained from pulp, such as avocado oil, centrifugation has shown yields that are comparable to or higher than those achieved by mechanical pressing, while preserving a stable fatty acid profile and consistent physicochemical properties. Studies have demonstrated that avocado oil extracted by centrifugation retains good sensory quality and high concentrations of antioxidant compounds, indicating that product integrity is not compromised (Pérez-Saucedo *et al*., 2021). At the industrial scale, this technique has also enhanced the efficiency of olive oil extraction by increasing oil recovery and reducing losses in byproducts such as olive pomace (Ranalli and Martinelli, 1995). In addition to its technical advantages, centrifugation supports cleaner and more continuous processing aligned with green processing principles. From an environmental perspective, it eliminates the need for organic solvents and reduces the generation of polluting effluents, contributing to more sustainable biorefinery designs that enable the efficient recovery of valuable compounds, including oils, proteins, and polyphenols, without producing hazardous byproducts (Zuin *et al*., 2018).

Centrifugation represents a clean, efficient, and safe technology capable of preserving the nutritional and functional quality of vegetable oils from pulp, with both economic and environmental benefits. Its industrial implementation continues to expand as process parameters are optimized and new strategies, such as aqueous and enzyme-assisted extraction, are integrated to further improve performance (Capaldi *et al*., 2024). Therefore, the objective of this work was to evaluate three methods for extracting avocado oil from the Hass variety using proton (^{1}H) and carbon (^{13}C) nuclear magnetic resonance (NMR) spectroscopy to determine its quality.

MATERIALS AND METHODS

The study was conducted in 2023 at the Centre for Research in Applied Biotechnology of the National Polytechnic Institute (CIBA-IPN, by its acronym in Spanish), located in

the municipality of Tepetitla de Lardizábal (19° 15′–19° 19′ N, 98° 20′–98° 25′ W; 2300 m altitude), Tlaxcala, Mexico. Avocado (*Persea americana* Mill. var. Hass) fruits were purchased at the Emiliano Zapata market in Puebla City, Mexico. Fruits were randomly selected based on commercial maturity criteria, including uniform dark green epicarp color with slight purplish tones, firmness between 15 and 25 N measured with a digital penetrometer (FT-327, Italy), individual weight between 180 and 250 g, and absence of mechanical damage or visible deterioration or fungal infection. Physiological maturity was confirmed according to NMX-FF-016-SCFI-2016 (DOF, 2017), which defines the physical and sensory characteristics of avocados at commercial maturity.

After selection, fruits were washed with distilled water and 0.1 % sodium hypochlorite solution, rinsed, and stored at 20 ± 2 °C and 65 % relative humidity for 24 h before processing to homogenize temperature and maturity conditions. The pulp was manually separated from the epicarp and seed, and 250 g of fresh pulp per fruit were homogenized for 2 min using an immersion blender (FPSTHB2600W-013, China). The pulp was spread on filter paper in stainless steel trays and dried in a convection oven (TE-H80, Mexico) at 70 °C for 24 h. Residual moisture content was determined gravimetrically by weighing the samples before and after drying (AOAC, 2019), with an average moisture loss of 65 ± 2 %. The dried pulp was then re-homogenized using the same blender to obtain a particle size of 250 μm.

Soxhlet extraction

Oil extraction was carried out using 1 g of dehydrated and homogenized avocado pulp. The sample was placed in a cellulose extraction thimble and inserted into a Soxhlet extractor. Analytical-grade hexane (Appcrom, Mexico) was used as the solvent, with 130 mL added to a round-bottom flask attached to the Soxhlet apparatus and equipped with a reflux condenser. The system was maintained at 60 °C for 4 h, facilitating the volatilization, condensation, and percolation of the solvent through the sample to solubilize the lipids in the pulp.

Once the solvent reached the overflow level in the extraction chamber, the contents were siphoned back into the round-bottom flask, initiating a new extraction cycle. This process was repeated continuously for the specified duration to ensure complete extraction of lipid compounds (AOAC, 2019). At the end of the procedure, the oil-solvent mixture was concentrated and purified by vacuum evaporation using a rotary evaporator (B-490, Mexico) at 50 °C and medium speed, coupled to a vacuum pump (V-700, Mexico). The recovered oil was stored in hermetically sealed amber bottles until further analysis.

Extraction by maceration

Avocado oil extraction by maceration was carried out using 1 g of dehydrated and homogenized avocado pulp placed in a 250 mL Erlenmeyer flask with an airtight stopper. Analytical-grade hexane (Appcrom, Mexico; 130 mL) was added, and the mixture was gently stirred in the dark for 24 h at 25 ± 1 °C to prevent photodegradation

of sensitive compounds and promote solvent diffusion throughout the matrix. Manual intermittent stirring was carried out every 6 h to improve extraction efficiency and phase equilibrium (AOAC, 2019).

After maceration, the mixture was gravity-filtered through Whatman No. 1 filter paper (11 μm pore size), previously conditioned with hexane to minimize sample loss by adsorption. The filtrate, containing the oil dissolved in the solvent, was concentrated by vacuum evaporation using a rotary evaporator (B-490, Mexico) at 50 °C, using a vacuum pump (V-700, Mexico), under the same conditions described for the Soxhlet method. The recovered oil was stored in hermetically sealed amber bottles.

Extraction by centrifugation

Oil extraction by centrifugation was based on the methodology proposed by Ariza-Ortega *et al*. (2011). One gram of dehydrated and homogenized avocado pulp was placed in a 15 mL Falcon tube and centrifuged in a refrigerated centrifuge (Hettich Rotina 380R, Andreas Hettich GmbH and Co. KG, Germany) at 11 000 rpm (15 557 × gravity) for 10 min at 40 °C. After centrifugation, three distinct phases were observed: an upper oily phase, an intermediate phase containing impurities, and a lower solid residue. The oily phase was carefully collected using a glass Pasteur pipette (Pyrex, USA), avoiding cross-contamination with the other layers. The recovered oil was stored in airtight amber bottles at 4 °C until further analysis.

Evaluation of avocado oil quality

The quality of the extracted oils was evaluated using ^{1}H and ^{13}C nuclear magnetic resonance (NMR) spectroscopy to identify characteristic proton and carbon signals associated with triacylglycerols and other lipid compounds. Analyses were performed using a Bruker Avance III 400 MHz spectrometer (Bruker BioSpin GmbH, Rheinstetten, Germany), operating at 400 MHz for ^{1}H and 100 MHz for ^{13}C. For each analysis, 10 μL of oil were dissolved in 0.6 mL of deuterated chloroform ($CDCl_3$, Sigma-Aldrich, USA) and transferred to 5 mm diameter glass NMR tubes.

Spectra for ^{1}H were obtained with the following instrumental parameters: 45° pulse, relaxation time of 1 s, acquisition time of 2.049 s, spectral width of 7997.6 Hz, and a line width of 0.2 Hz. A total of 64 scans were collected for each spectrum, with a total acquisition time of 3 min and 21 s per sample. Finally, ^{13}C spectra were obtained using the same equipment and sample preparation conditions, with a spectral width of 195 ppm, relaxation time of 7 s, and acquisition time of 4.5 s.

Experimental design

This study employed a controlled experimental design comparing three avocado oil extraction methods (Soxhlet, maceration, and centrifugation), with three independent replicates per treatment (experimental unit = 1 g of dehydrated avocado pulp), for a total of nine experimental units. Aliquots were randomly assigned to each treatment. Spectral data were processed using CRAFT software integrated into DELTA

version 5.3 (JEOL Resonance Inc., Tokyo, Japan). Peak integration was performed automatically and subsequently verified manually to identify characteristic chemical shifts associated with functional groups present in the oils. Results from the ^{1}H-NMR and ^{13}C-NMR analyses correspond to relative signal intensities of a descriptive nature, which are not comparable through statistical tests. Data were therefore interpreted through descriptive analysis and visual comparison of spectra, focusing on variations in chemical shifts and signal intensities characteristic of lipid compounds.

RESULTS AND DISCUSSION

Oil extraction

The highest extraction yield was obtained using hexane in the Soxhlet extractor (60 °C for 4 h), with an extraction rate of 78 %. This was followed by the maceration method (25 °C for 24 h), which achieved a yield of 58 %, and the centrifugation method, with a yield of 38.3 %. The Soxhlet method (78 %) exceeded values reported by Pérez-Saucedo *et al*. (2021) for Hass avocado oils from Tepic, Nayarit (66.57 %) and those described by Randrianarijaona *et al*. (2023) for avocado oils extracted in Madagascar (40.12 % by Soxhlet and 29.77 % by maceration). The increased oil yield achieved by Soxhlet extraction compared with maceration, and particularly centrifugation, is attributed to differences in physicochemical extraction mechanisms. In Soxhlet extraction, continuous renewal of hot hexane promotes disruption of the cellular matrix and maintains a constant solubility gradient, enabling near-exhaustive recovery of the lipid fraction (Flores *et al*., 2019; Eze *et al*., 2024).

The lower yield obtained by maceration (58 %) could be explained by the limited solvent diffusion within the solid matrix, associated with partial lipid encapsulation by proteins (≈1.9 g per 100 g) and carbohydrates (≈8.6 g per 100 g) present in the pulp (Flores *et al*., 2019; Liu *et al*., 2019). In contrast, centrifugation yielded 38.3 % under the conditions evaluated (11 000 rpm, 40 °C for 10 min), a value comparable to that reported by Pérez-Saucedo *et al*. (2021) (39 % at 10 000 rpm). Buenrostro and López-Munguía (1986) achieved up to 70 % extraction by combining centrifugation (12 300 × gravity) with α-amylase addition (1:5) at 65 °C, while Bizimana *et al*. (1993) reported yields of up to 78 % by increasing centrifugal force from 6000 to 12 300 × gravity. Similarly, Werman and Neeman (1987) obtained 65 % extraction by adding NaCl (5 %) and water to fresh pulp prior to centrifugation, which promoted the disruption of the water-oil emulsion. This effect has been attributed to increased membrane permeability and reduced interfacial tension between phases (Rosenthal *et al*., 1996).

Moreover, centrifugation relies on physical separation rather than chemical solubilization; therefore, only lipids released after initial mechanical disruption are recovered, leaving a substantial fraction retained within the plant matrix (Pérez-Saucedo *et al*., 2021). These observations are consistent with reports indicating that lipid recovery efficiency depends on the extent of cellular disruption, process

temperature, and the method's ability to renew the solvent or extraction medium (Jin *et al*., 2022). The avocado oils extracted using the three different methods (Figure 1) showed variations in color and clarity among the samples.

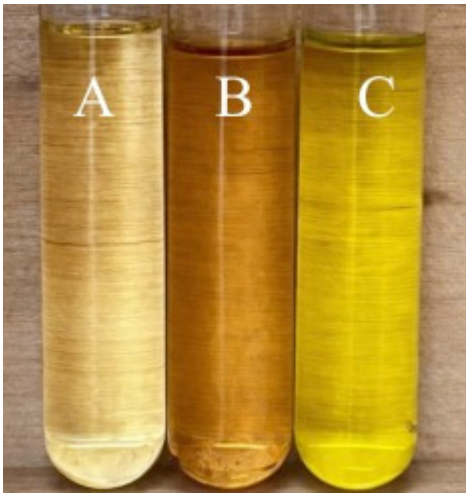

Figure 1. Avocado (*Persea americana* Mill.) oils obtained through three extraction methods. A: Soxhlet; B: maceration; C: centrifugation.

Evaluation of avocado oil quality

The three extraction methods exhibited similar spectral profiles (Figure 2), indicating that the chemical structure of Hass avocado oil was preserved regardless of the method used. However, differences were observed in signal intensities rather than in chemical shifts, suggesting variations in the relative concentrations of extracted triacylglycerols and unsaturated fatty acids (Table 1).

The ^{1}H NMR spectra revealed characteristic shifts at 5.29, 2.02, 2.76, 0.95, and 0.85 ppm, associated with allylic and methylene protons present in unsaturated fatty acid double bonds. These signals are consistent with those observed by Tang *et al*. (2021), who reported dominant peaks at 5.3 and 2.0 ppm for C=C and CH_2–CH=CH bonds in authentic avocado oils analyzed by high-resolution NMR. Such resonances are indicative of the presence of oleic (C18:1), linoleic (C18:2), and linolenic (C18:3) acids, the main components of avocado oil (Pérez-Saucedo *et al*., 2021).

In the ^{13}C NMR, the signals at 129.98, 129.67, 128.06, and 127.86 ppm correspond to the olefinic carbons (C=C) of unsaturated fatty acids, while the resonances at 31.88 ppm indicate saturated methylene carbons (–CH_2-) present in the acyl chains. These results are similar to those of Eze *et al*. (2024), who reported similar shifts in avocado oils, attributing them to the high proportion of monounsaturated fatty acids and the structural stability of the triacylglycerols. Furthermore, the signals at 174–176 ppm are assigned to carbonyls (C=O) of free fatty acids. Their low intensity in all three

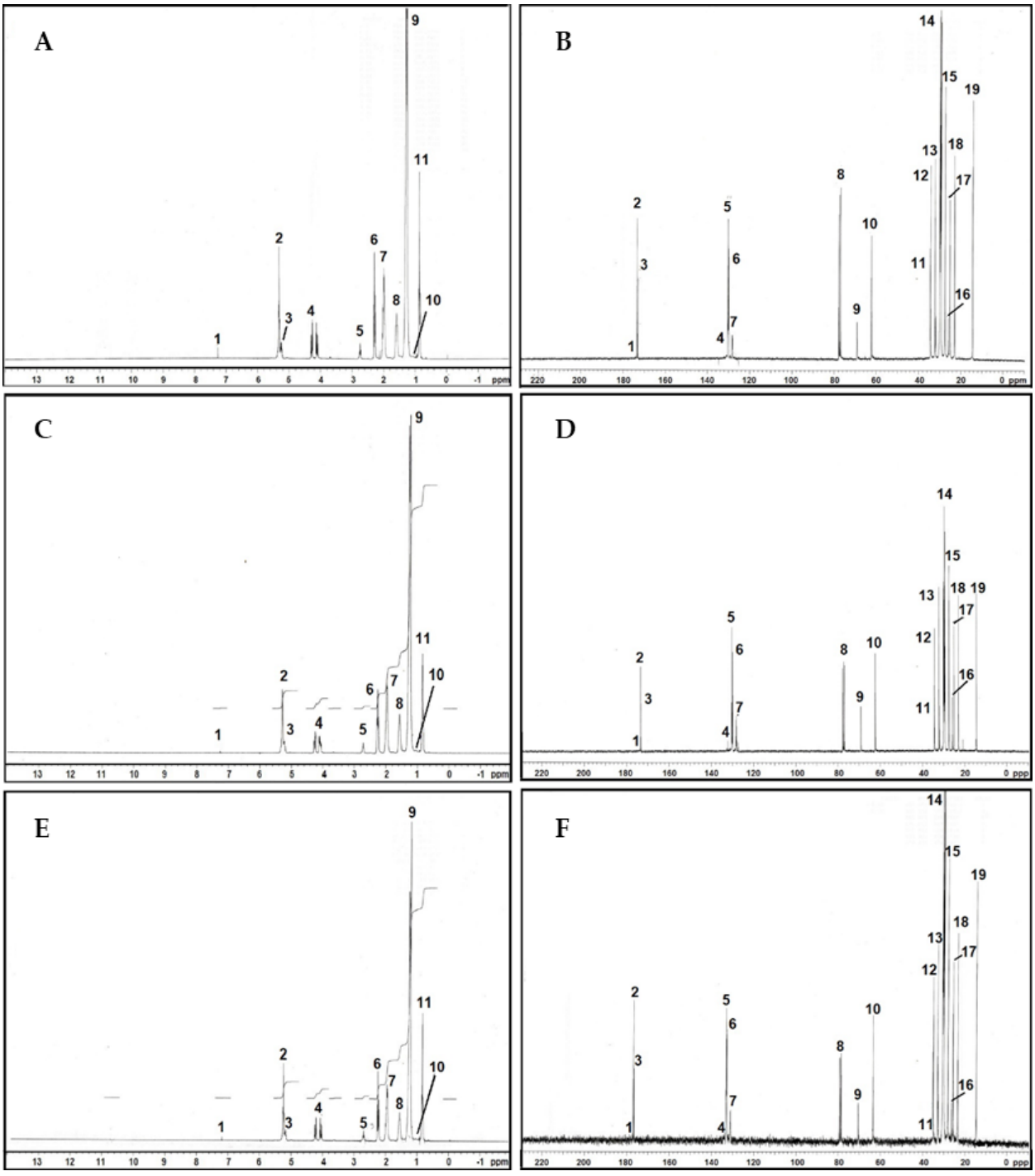

Figure 2. Spectrograms showing the identified signals and chemical shifts of Hass avocado (*Persea americana* Mill.) oils. Panels A, C, and E correspond to ^{1}H nuclear magnetic resonance (NMR) analyses, while panels B, D, and F correspond to ^{13}C-NMR analyses. A, B: Oils extracted via Soxhlet extraction at 60 °C for 4 h; C, D: Oils extracted through maceration at 25 °C for 24 h; E, F: Oils extracted using centrifugation at 11 000 rpm (15 557 × gravity) at 40 °C for 10 min.

Table 1. Chemical shifts (δ) and signals identified by 1H and 13C clear magnetic resonance (NMR) in Hass avocado (*Persea americana* Mill.) oils obtained by different extraction methods.

Sign	δ (ppm)	Functional group	SE Intensity	ME Intensity	CE Intensity	Compound
			Proton (^{1}H) NMR			
1	7.26	$CHCl_3$	High	Low	Medium	Chloroform (solvent)
2	5.29/2.02	$CH=CH/CH_2CH=CH$	High	Low	Medium	All unsaturated fatty acids
7			High	Medium	Low	
3	5.15/4.19	$CHOCOR/CH_2OCOR$	High	Medium	Medium	Glycerol (triacylglycerols)
4			High	Low	Medium	
5	2.76	$CH=CHCH_2CH=CH$	High	Low	Medium	Linoleic and linolenic
6	2.2/1.6/1.2	$CH_2COOH/CH_2CH_2COOH/(CH_2)n$	High	Low	Medium	Glycerol (triacylglycerols)
8			High	Medium	Low	
9			High	Medium	Medium	
10	0.95	$CH_2CH_2CH_2CH_3$	High	Low	Medium	Linoleic
11	0.85	$CH=CHCH_2CH_3$	High	Low	Medium	All unsaturated fatty acids except linolenic
			Carbon (^{13}C) NMR			
1	174–176	C-1	ND	ND	ND	Free fatty acids
2	173.26/172.81	C-1, sn-1,3/C-1, sn-2	High	Low	High	Triacylglycerols
3			High	Low	Medium	
4	129.98/129.67	C-10/C-9	Low	Medium	High	Oleic
5			High	High	High	
6	128.06/127.86	C-10/C-12	High	Low	Medium	Linoleic
7			Low	High	High	
8	77.01	$CDCl_3$	High	Low	Low	Solvent
9	68.92/62.18	CHO–, sn-2/CH_2O–, sn-1,3	Low	High	Medium	Triacylglycerols
10			High	Medium	High	
11	34.18/34.02	C-2, sn-2/C-2, sn-1,3	Medium	Low	High	All acyl chains
12			High	Low	High	
13	31.88	ω-3	Medium	Low	High	Saturates, ω-9 and ω-6
14	29.1–29.8	$(CH_2)n$	High	Low	High	All acyl chains
15	27.16	C-8–C-11/C-8–C-14	High	Low	High	Allyl position: oleic and linoleic, respectively
16	25.81	C-11/C-11–C-14	High	High	High	Allyl position: linoleic and linolenic, respectively
17	24.84, 22.65/14.15	C3, ω-2/ω-1(–CH_3)	Medium	Low	High	All acyl chains
18			Medium	Low	High	
19			Medium	Low	High	

SE: Soxhlet extraction (60 °C, 4 h); ME: maceration extraction (25 °C, 24 h); CE: centrifugation extraction (11 000 rpm, 40 °C, 10 min); ND: not detected.

extraction methods indicates minimal hydrolysis and good oil stability, which in turn results in a low free fatty acid content. This finding aligns with research conducted by Flores *et al*. (2019), as avocado oils with low acidity demonstrated reduced oxidative degradation and enhanced stability during storage.

The NMR results, together with fatty acid composition data, show that oil obtained by Soxhlet extraction had the highest signal intensities associated with aliphatic (0.85–2.8 ppm) and olefinic (5.3 ppm) groups, reflecting a higher concentration of triglycerides and unsaturated fatty acids. Oils obtained by maceration and centrifugation exhibited a similar spectral pattern but with lower intensities, indicating partial lipid extraction, consistent with reports of avocado oil extracted by Soxhlet extraction, maceration, and centrifugation (Table 2).

Table 2. Fatty acid percentages in Hass avocado (*Persea americana* Mill.) oil (Ariza-Ortega *et al*., 2011).

Name	Formula	Soxhlet extraction	Maceration extraction	Centrifugation extraction
Capric	C10:0	0.04	ND	0.02
Lauric	C12:0	0.02	ND	1.30
Myristic	C14:0	0.04	0.01	0.31
Palmitic	C16:0	13.70	17.00	17.06
Palmitoleic	C16:1	8.00	ND	7.10
Estearic	C18:0	5.50	5.10	6.90
Elaidic	C18:1t	0.10	0.10	0.10
Oleic	C18:1	59.10	60.60	58.70
Trans-linoleic acid	C18:2t	3.10	1.20	ND
Linoleic	C18:2	9.20	10.30	7.30
Linolenic	C18:3	0.04	0.10	0.06
Arachidic	C20:0	0.17	0.90	0.10
Eicosenoic	C20:1	0.17	ND	ND
Eicosadienoic	C20:2	0.73	ND	0.48

ND: Not detected.

The fatty acid percentages (Table 2) confirm that the oils obtained by the three methods primarily contain oleic (C18:1), palmitic (C16:0), and linoleic (C18:2) acids, with proportions of 58–61, 13–17, and 7–10 %, respectively. These values are consistent with those reported by Eze *et al*. (2024), who found that avocado oil exhibits a high oleic/palmitic ratio (>3.5), which indicates a healthy and oxidatively stable lipid profile.

According to Tang *et al*. (2021), the homogeneity of chemical shifts in genuine avocado oils can be used to verify their purity, since adulteration with soybean or sunflower oils alters the resonances in the 5.2–5.4 and 172–174 ppm regions. In this study, the spectra obtained by Soxhlet extraction, maceration, and centrifugation are similar to standard values, indicating that the oils are authentic and show no signs of contamination or significant degradation.

The low intensity of the carbonyl peaks (174–176 ppm) also indicates minimal oxidation and a low presence of free fatty acids, which coincides with reported acidity index values between 0.14 and 2.8 mg KOH g^{-1} (Ortiz-Moreno *et al*., 2003; Varzakas, 2021). According to Flores *et al*. (2019), this parameter confirms that high-quality avocado oil maintains its molecular integrity and antioxidant properties, even after moderate thermal processes such as those performed by the Soxhlet extractor.

Compared to other edible oils, such as that of *Dacryodes edulis* studied by Eze *et al*. (2024), avocado oil showed a higher proportion of monounsaturated fatty acids (C18:1) and a lower content of saturated fatty acids (C16:0, C18:0) (Table 2), which translates into better oxidative stability and a favorable nutritional profile. According to Flores *et al*. (2019), this composition makes it a functional oil with beneficial properties for cardiovascular health and potential applications in the cosmetic and pharmaceutical industries.

The spectral similarity among extraction methods suggests that thermal or mechanical conditions do not significantly modify the structure of triglycerides (Tang *et al*., 2021). However, comparative studies that include Soxhlet extraction have shown that this method tends to yield a more concentrated and stable lipid fraction (Flores *et al*., 2019; Eze *et al*., 2024). In contrast, research on centrifugation and cold extraction methods reports similar lipid profiles but lower signal intensity and reduced yield compared to solvent-based extraction, which is attributed to the partial recovery of triglycerides due to physical separation limitations (Pérez-Saucedo *et al*., 2021).

Studies using NMR techniques confirm that triglyceride signals remain consistent across extraction methods, although process parameters such as temperature, time, and centrifugal force influence yield and signal intensity (Tang *et al*., 2021; Jin *et al*., 2022). Therefore, increasing centrifugal force or improving phase separation efficiency may enhance both the recovery and the purity of the extracted oil.

CONCLUSIONS

Hass avocado oils obtained by Soxhlet extraction, maceration, and centrifugation have a stable molecular structure, with a predominance of triacylglycerols and monounsaturated fatty acids. The Soxhlet method yielded the highest yield and exhibited the most intense signals, indicating a higher concentration of lipid compounds. In contrast, maceration and centrifugation preserved oil quality, albeit with a slight decrease in spectral intensity.

REFERENCES

AOAC (Association of Official Analytical Chemists). 2019. Official methods of analysis of AOAC International (21st edition). Washington, DC, USA.

Ariza-Ortega JA, López-Valdez F, Coyotl-Huerta J, Ramos-Cassellis ME, Díaz-Reyes J, Martínez-Zavala A. 2011. Efecto de diferentes métodos de extracción sobre el perfil de ácidos grasos en el aceite de aguacate (*Persea americana* Mill. var. Hass). Revista Venezolana de Ciencia y Tecnología de Alimentos 2 (2): 263–276.

Badui DS. 2019. Lípidos. *In* Quintanar DE. (ed.), Química de Alimentos. Pearson: Ciudad de México, México, pp: 245–262.

Barros HDFQ, Coutinho JP, Grimaldi R, Godoy HT, Cabral FA. 2016. Simultaneous extraction of edible oil from avocado and capsanthin from red bell pepper using supercritical carbon dioxide as solvent. The Journal of Supercritical Fluids 107: 315–320. https://doi.org/10.1016/j.supflu.2015.09.025

Bizimana V, Breene WM, Csallany AS. 1993. Avocado oil extraction with appropriate technology for developing countries. Journal of the American Oil Chemists' Society 70 (8): 821–822. https://doi.org/10.1007/bf02542610

Buenrostro M, López-Munguía A. 1986. Enzymatic extraction of avocado oil. Biotechnology Letters 8 (7): 505–506. https://doi.org/10.1007/bf01025210

Capaldi G, Bassi F, Romano P. 2024. New trends in extraction-process intensification: Hybrid and green technologies. Journal of Food Engineering and Technology 78 (3): 215–228. https://doi.org/10.1016/j.indcrop.2023.117906

Cravotto C, Fabiano-Tixier AS, Claux O, Abert-Vian M, Tabasso S, Cravotto G, Chemat F. 2022. Towards substitution of hexane as extraction solvent of food products and ingredients with no regrets. Foods 11 (21): 3412. https://doi.org/10.3390/foods11213412

DOF (Diario Oficial de la Federación). 2017. NORMA Mexicana NMX-FF-016-SCFI-2016. Productos alimenticios no industrializados para uso humano. Fruta fresca. Aguacate (*Persea americana* Mill.). Especificaciones. Gobierno de México. Secretaría de Economía. Ciudad de México, México.

European Commission. 2003. *Integrated pollution prevention and control*. https://bureau-industrial-transformation.jrc.ec.europa.eu/sites/default/files/2020-03/superseded_mon_bref_0703.pdf

Eze JC, Nwadibia PC, Anyaogu DI, Abugu HO, Ejikeme PM. 2024. GC–MS, ^{1}H and ^{13}C NMR, and physiochemical properties of oils of *Dacryodes edulis* and *Persea americana*. Discover Chemistry 1 (1): 70. https://doi.org/10.1007/s44371-024-00072-0

FAO (Food and Agriculture Organization of the United Nations). 2024. The state of agricultural commodity markets 2024. Rome, Italy. https://doi.org/10.4060/cd2144en

Flores M, Saravia C, Vergara CE, Avila F, Valdés H, Ortiz-Viedma J. 2019. Avocado oil: Characteristics, properties, and applications. Molecules 24 (11): 2127. https://doi.org/10.3390/molecules24112172

García-Vargas MC, Contreras MM, Castro E. 2020. Avocado-derived biomass as a source of bioenergy and bioproducts. Applied Sciences 10 (22): 8195. https://doi.org/10.3390/app10228195

Gil-Martín E, Forbes-Hernández T, Romero A, Cianciosi D, Giampieri F, Battino M. 2022. Influence of the extraction method on the recovery of bioactive phenolic compounds from food industry by-products. Food Chemistry 378: 131918. https://doi.org/10.1016/j.foodchem.2021.131918

Jin H, Wang Y, Lv B, Zhang K, Zhu Z, Zhao D, Li C. 2022. Rapid detection of avocado oil adulteration using low-field nuclear magnetic resonance. Foods 11 (8): 1134. https://doi.org/10.3390/foods11081134

Junyusen T, Chatchavanthatri N, Liplap P, Junyusen P, Phan VM, Nawong S. 2022. Effects of extraction processes on the oxidative stability, bioactive phytochemicals, and antioxidant activity of crude rice bran oil. Foods 11 (8): 1143. https://doi.org/10.3390/foods11081143

Liu XX, Liu HM, Li J, Yan YY, Wang XD, Ma YX, Qin GY. 2019. Effects of various oil extraction methods on the structural and functional properties of starches isolated from tigernut

(*Cyperus esculentus*) tuber meals. Food Hydrocolloids 95 (2): 262–272. https://doi.org/10.1016/j.foodhyd.2019.04.044

Mahato N, Sinha M, Sharma K, Koteswararao R, Cho MH. 2019. Modern extraction and purification techniques for obtaining high purity food-grade bioactive compounds and value-added co-products from citrus wastes. Foods 8 (11): 523. https://doi.org/10.3390/foods8110523

Ortiz-Moreno AO, Dorantes L, Galíndez J, Guzmán RI. 2003. Effect of different extraction methods on fatty acids, volatile compounds, and physical and chemical properties of avocado (*Persea americana* Mill.) oil. Journal of Agricultural and Food Chemistry 51 (8): 2216–2221. https://doi.org/10.1021/jf0207934

Pérez-Saucedo MR, Jiménez-Ruiz EI, Rodríguez-Carpena JG, Ragazzo-Sánchez JA, Ulloa JA, Ramírez-Ramírez JC, Gastón-Peña CR, Bautista-Rosales PU. 2021. Properties of avocado oil extracted using centrifugation and ultrasound-assisted methods. Food Science and Biotechnology 30 (8): 1051–1061. https://doi.org/10.1007/s10068-021-00940-w

Ranalli A, Martinelli N. 1995. Integral centrifuges for olive oil extraction, at the third millenium threshold. Transformation yields. Grasas y Aceites 46 (4–5): 255–263. https://doi.org/10.3989/gya.1995.v46.i4-5.934

Randrianarijaona M, Rakotondramasy-Rabesiaka L, Ralambomanana D, Rabesiaka M. 2023. Study of the extraction of avocado oil *Persea americana* (Lauraceae) from fresh and dry pulp. International Journal of Advance Research and Innovative Ideas in Education 9 (3): 3962–3970

Rosenthal A, Pyle DL, Niranjan K. 1996. Aqueous and enzymatic processes for edible oil extraction. Enzyme and Microbial Technology 19 (6): 402–420. https://doi.org/10.1016/s0141-0229(96)80004-f

Ruiz-García L, Figueroa-Vega N, Malacara JM, Barrón-Vivanco B, Salamon F, Carrieri M, Jiménez-Garza O. 2020. Possible role of n-hexane as an endocrine disruptor in occupationally exposed women at reproductive age. Toxicology Letters 330: 73–79. https://doi.org/10.1016/j.toxlet.2020.04.022

Tang F, Green HS, Wang SC, Hatzakis E. 2021. Analysis and authentication of avocado oil using high-resolution NMR spectroscopy. Molecules 26 (2): 310. https://doi.org/10.3390/molecules26020310

Varzakas T. 2021. Extra Virgin Olive Oil (EVOO): Quality, safety, authenticity, and adulteration. Foods 10 (5): 995. https://doi.org/10.3390/foods10050995

Werman MJ, Neeman I. 1987. Avocado oil production and chemical characteristics. Journal of the American Oil Chemists' Society 64 (2): 229–232. https://doi.org/10.1007/BF02542007

Zuin VG, Ramin LZ. 2018. Green and sustainable separation of natural products from agro-industrial waste: Challenges, potentialities, and perspectives on emerging approaches. Topics in Current Chemistry 376 (1). https://doi.org/10.1007/s41061-017-0182-z

Agrociencia

CIRCULAR ECONOMY IN THE *Agave tequilana* Weber VALUE CHAIN

María Magdalena **Rojas-Rojas**[1], Karina **Valencia-Sandoval**[2*], Lucila **Godínez-Montoya**[3], José de Jesús **Brambila-Paz**[4]

[1]Universidad Autónoma Chapingo. Posgrado en Ciencia y Tecnología Agroalimentaria. Carretera México-Texcoco km 38.5, Texcoco, State of Mexico, Mexico, C. P. 56230.
[2]Universidad Autónoma del Estado de Hidalgo. Instituto de Ciencias Económico-Administrativas. Circuito La Concepción km 2.5, Colonia San Juan Tilcuautla, San Agustín Tlaxiaca, Hidalgo, Mexico. C. P. 42160.
[3]Universidad Autónoma del Estado de México. Centro Universitario UAEM Texcoco. Fraccionamiento El Tejocote, Texcoco, State of Mexico, Mexico, C. P. 56259.
[4]Colegio de Postgraduados. Posgrado en Socioeconomía, Estadística e Informática-Economía. Carretera México-Texcoco km 36.5, Montecillo, Texcoco, State of Mexico, Mexico. C. P. 56230.
* Author for correspondence: karina_valencia@uaeh.edu.mx

Citation: Rojas-Rojas MM, Valencia-Sandoval K, Godínez-Montoya L, Brambila-Paz JJ. 2026. Circular economy in the *Agave tequilana* Weber value chain. **Agrociencia** 60(2): 239-252. https://doi.org/ 10.47163/agrociencia.v60i2.3454

Editor in Chief: Dr. Fernando C. Gómez Merino

Received: July 07, 2025.
Approved: March 01, 2026.
Published in Agrociencia: March 20, 2026.

ABSTRACT

The blue variety of *Agave tequilana* Weber is a product of great economic and cultural importance in Mexico, although it faces fluctuations in the prices of agave and environmental challenges. In this study, diversification strategies were evaluated using investment portfolios in the agave value chain, aimed at the production of inulin, bioethanol, and biogas from residual biomass, as well as tequila, under a circular economy approach. The hypothesis proposed is that expanding into innovative products derived from the tequila agave enhances returns and mitigates risks throughout the sector's value chain. The biorefinery approach within a circular economy model makes it possible to use the entire agave plant, create high-value products, and reduce the risk of price fluctuation and the environmental impact. The diversification of products and the management of the residual biomass increased the production income and contributed to the dispersion of risk.

Keywords: Tequila agave, residual biomass, investment portfolios, biogas, agave inulin, bioethanol.

INTRODUCTION

Agave is a crop of agro-industrial importance due to its use in the production of foods, beverages, medications, construction material, and fibers. In 2023, tequila agave production in Mexico reached 2.125 thousand Mg, which represents a 30 % increase in regard to the previous year (SIAP, 2024a). The production was concentrated mostly in the states of Jalisco (59 %), Guanajuato (19 %), and Michoacán (12 %). These three states contributed 90 % of the domestic volume and registered production increments of 22.3, 20.4, and 187.1 %, respectively.

Agave production has become established as a highly lucrative activity due to its demand in international markets, associated with the recognition of tequila's designation of origin. This situation coincides with the growing trend in exports of this beverage, due to the increase in the preference of consumers in countries like the United States (SIAP, 2024a). In 2023, beverages derived from agave, including tequila, ranked second in export value at USD 4159 million, representing a 2 % increase compared to 2022. The main destinations were the United States (USD 3831 million), Japan (USD 78 million), and Spain (USD 69 million) (SIAP, 2024a). Tequila is currently sold in 141 countries, making it the second most significant agro-industrial product by value, following beer.

However, despite its economic importance and the growing rise in its consumption, the value chain for tequila faces environmental and social challenges. Among the main cyclic problems is the scarcity or oversupply of agave in the face of high demand, which causes volatility in the prices of the raw material (Herrera-Pérez *et al*., 2018). In addition, the increase in real prices of agave has boosted the expansion of its production, causing the displacement of less profitable crops such as maize and contributing to deforestation to expand the area under cultivation (Cruz-Ramírez *et al*., 2023a).

The productive processes of agave lead to a large amount of waste that, when disposed of in open areas, causes soil degradation. For every liter of tequila produced, between 10 and 12 L of vinasse and between 3.5 and 7 kg of bagasse are generated (Hoz-Zavala and Nava-Diguero, 2017). The tequila industry annually pollutes with over 4 billion L of vinasse, composed of organic acids, nitrogen, and sulfates, with a high organic matter content and high temperatures, which makes its treatment costly and difficult (CRT, 2019). Additionally, nearly 40 % of the weight of agave used as raw material corresponds to bagasse. Altogether, both waste products represent an economic, social, and environmental problem for the tequila sector.

Nevertheless, these residues have the potential to become valuable products through biorefineries, such as enzymes, biofuels, bioactive molecules, biomedications, construction materials, composts, paper, boards, substrates for vegetables, and feed for ruminants (Cardona-Alzate *et al*., 2023). Currently, these residues pose challenges for the agri-food system due to their contribution to greenhouse gas emissions, unpleasant odors, and potential health risks for people. However, new business models are emerging that adhere to the principles of circular economies. With the concept of biorefineries, this waste may become an opportunity to mitigate pollution and reduce the environmental footprint.

A biorefinery is a complex system designed to process biomass and obtain bioproducts that gradually replace oil by-products to satisfy the needs of different sectors, which requires the incorporation of technology and innovation (Cardona-Alzate *et al*., 2023). Likewise, it also allows the use of a single raw material to produce diverse products with multiple applications. Given the emphasis on the development of products with more added value, it is necessary to adapt and design financial instruments that

diversify the risk and increase profitability, such as investment portfolios (Rojas-Rojas *et al*., 2025b). These business models are characterized by their innovative nature, although they also involve greater risk due to price volatility, which is offset by a higher potential profitability (Brambila-Paz *et al*., 2019).

However, based on the above and despite the importance of research that integrates theoretical aspects of bio-economics, biorefineries, and investment portfolios that strengthen the empirical evidence on the topic, these types of studies continue to be limited. Among the most closely related studies are those by Brambila-Paz *et al*. (2013, 2019), focused on bio-economics, biorefineries, portfolios, and real options, as well as those by Carrillo-González and Ponce-Sánchez (2019) on circular economy, bio-economics, and biorefineries, among others.

In this sense, the aim of this investigation was to evaluate diversification mechanisms in the blue agave production process to obtain tequila, the use of waste generated in the process, and the convenience of adopting a biorefinery system for the production of inulin with the use of investment portfolios. As a hypothesis, it is proposed that the development of innovative products derived from tequila agave will increase the yield of the value chain of the sector and reduce its risk.

MATERIALS AND METHODS

The investment portfolio is a tool used for asset diversification, whose function it is to disperse risk for a specific profitability or maximize return at a given level of risk. This methodology was proposed by Markowitz (1952), who developed portfolio optimization techniques by combining different assets. The risk of a portfolio is measured through its volatility, which depends on the covariance or correlation among the returns of the assets. When the assets display correlated returns, the portfolio risk can be reduced by allocating adequate investment weights (Muñoz-González *et al*., 1992).

To propose a product diversification scheme in the agave value chain, the methodology proposed by Brambila-Paz *et al*. (2013) and Rojas-Rojas *et al*. (2025b) was applied, using the investment portfolio tool. Under the concept of biorefineries, the investor decides to invest in the production of tequila or inulin based on the availability of raw material. In the agave value chain, following the circular economy approach, the investor can diversify their production by using the waste generated in the processes. Estrada-Maya and Weber (2022) point out that the bagasse from the tequila production process can be used in the production of bioethanol and biogas through subsequent batch fermentations.

In this study, the design of investment portfolios was proposed, in which the investor has the option of developing a biorefinery and taking full advantage of the waste products of the tequila production process. Inulin, biogas, and bioethanol were considered differentiated products, whereas the traditional or commodity product was the tequila. The diversified portfolio includes the production of all the products

mentioned; the portfolio under a biorefinery scheme contemplates the production of inulin and/or tequila, and the traditional portfolio only considers the production of tequila.

An investor in the agave sector was assumed to have a certain amount of capital (Z), which is distributed in n assets. Each asset was assigned different investment weights $\alpha_1, \alpha_2, \ldots, \alpha_i$, in such a way that $Z\alpha_i$ represents the amount of capital invested in the i-th asset:

$$(\alpha_1 + \alpha_2 + \cdots + \alpha_i)Z = Z$$

Due to , $\alpha_1 + \alpha_2 + \ldots + \alpha_i = 1$, all investment weights are positive and comply with $0 \leq \alpha_i \leq 1$.

$\bar{R}_1, \bar{R}_2, \ldots, \bar{R}_n$ were considered to represent the returns obtained for each of the assets or products that make up the investment portfolio. The expected returns follow a normal distribution, therefore the expected profitability of the portfolio $E(\bar{R}_p)$ was modelled as a randomized variable with a normal distribution, mean $E(\bar{R}_p)$ and a constant variance (Muñoz-González *et al*., 1992):

$$E(\bar{R}_p) = \sum_{i=1}^{n} \alpha_i E(R_i)$$

In turn, the portfolio risk was estimated with the return variance. The return variance of a product's returns is defined as the weighted sum of the quadratic deviations of the gains in regard to its mean (Díaz-Carreño *et al*., 2007).

Markowitz (1952) points out that a portfolio with administrative risk must present a lower risk than the weighted sum of the individual risks, which is possible when the assets display a negative or very low covariance. The portfolio variance for n assets is described in the following equation:

$$VarP = \sum_{i=1}^{n} \sum_{j=1}^{n} \alpha_i \alpha_j Cov R_i R_j$$

where $VarP$ is the variance of the portfolio and α_i and α_j are the investment weights allocated to each asset. If $i = j$, $CovR_iR_j$ is the variance of each asset or product. If $i = j$, $CovR_iR_j$ represents the covariance of asset i with product j.

The standard deviation of portfolio *StDevP* represents the portfolio risk and is calculated as follows:

$$StDevP = \sqrt{VarP}$$

The risk and return of the portfolios analyzed were estimated using Microsoft Excel. Proxy annual variables were used from the 2000–2023 period. The statistical data for amounts (kg, L) and the value of the exports of each product (USD) were obtained from the National Statistics and Geography Institute (INEGI, 2024a). In particular, the prices of inulin (Pr_{1t}, USD kg^{-1}), tequila (Pr_{2t}, USD kg^{-1}), and ethanol (Pr_{3t}, USD kg^{-1}) were considered. For the biogas, the price of LP gas (Pr_{4t}, USD kg^{-1}) was used as a proxy variable, with information obtained from the Secretariat of Energy (SENER, 2015) and the Energy Regulating Commission (CRE, 2024). For subsequent calculations, the prices of Pr_{1t}, Pr_{2t}, Pr_{3t}, and Pr_{4t} were transformed into real prices using the National Index for Prices to Consumers (INPC), based on 2023 = 100, as published by INEGI (2024b).

To estimate the return of each asset or product, yield data were required as a measure of the production quantity (Q_i). An inulin yield of θ_1 = 4.87 kg was considered for every 48.9 kg of agave (Montañez-Soto *et al*., 2011). The tequila production coefficient was defined as θ_2 = 1 L of tequila per 7 kg of agave. The agave yield ($\theta_3 t$) was obtained from data reported by SIAP (2024b). Yields were calculated considering an ethanol yield of θ_4 = 2.9 % per kilogram of bagasse waste and a biogas yield of θ_5 = 4.5 % per kilogram of bagasse waste. (Estrada-Maya and Weber, 2022). Waste generation during tequila production was estimated assuming θ_6 = 2 kg of bagasse per liter of tequila and θ_7 = 10 L of vinasse per liter of tequila. The conversion factor for vinasse was defined as θ_8 = 0.06 kg of chemical oxygen demand (COD) per liter of vinasse. Methane generation through the anaerobic process was estimated using θ_9 = 0.35 m^3 of CH_4 per kilogram of COD. Both parameters were obtained according to del Real-Olvera and López-López (2012). Finally, a density of ϱ = 540 kg m^{-3} was assumed for LP gas.

The gross income (I_{it}), defined as the profit of the product or asset *i* in the year *t*, was estimated following the methodology by Rojas-Rojas *et al*. (2025b), which consists of multiplying the price of asset *i* in year *t* (Pr_{it}) by the amount produced of asset *i* (Q_{it}). In a biorefinery system, the value of I_{it} is based on the investment weights assigned to the production of inulin (α_1), tequila (α_2), or both activities (Table 1).

The yield of each asset (θ_i) and income (I_{it}) were determined for one hectare of tequila agave. For inulin, income was estimated as $I_{1t} = Pr_{1t}Q_{1t} = Pr_{1t}\theta_1\theta_{3t}\alpha_1$, where $Q_{1t} = \theta_1\theta_{3t}\alpha_1$. In the case of tequila, income was calculated as $I_{2t} = Pr_{2t}Q_{2t} = Pr_{2t}\theta_{3t}\theta_2\alpha_2$, where $Q_{2t} = \theta_{3t}\theta_2\alpha_2$.

To estimate the byproducts derived from bagasse, which are residues of the tequila production process (Q_{2t}), the amount of bagasse generated was first calculated:

$$Q_{bagazot} = Q_{2t}\theta_6$$

Table 1. Structure of investment weights of the analyzed portfolios.

Portfolio*	Investment weight		Portfolio*	Investment weight	
	Inulin (α_1)	Tequila (α_2)		Inulin (α_1)	Tequila (α_2)
P1	0 %	100 %	P8	70 %	30 %
P2	10 %	90 %	P9	80 %	20 %
P3	20 %	80 %	P10	90 %	10 %
P4	30 %	70 %	P11	100 %	0 %
P5	40 %	60 %	P12	50 %	50 %
P6	50 %	50 %	P13	0 %	100 %
P7	60 %	40 %			

*P1 corresponds to portfolios of tequila that use bagasse and vinasse for bioethanol and biogas. P2–P10 represent portfolios under a biorefinery scheme that produce inulin and tequila, with waste valorization. P11 only produces inulin; P12 produces inulin and tequila without the use of waste; and P13 produces exclusively tequila.

The income from ethanol was estimated as $I_{3t} = Pr_{3t}Q_{3t} = Pr_{3t}Q_{bagazot}\theta_4$, where $Q_{3t} = Q_{bagazot}\theta_4$. Similarly, the income from biogas derived from bagasse was calculated as $I_{4t} = Pr_{4t}Q_{4t} = Pr_{4t}Q_{bagazot}\theta_5$, where $Q_{4t} = Q_{bagazot}\theta_5$.
To estimate the biogas of the vinasses, which is also a waste product of the tequila production process (Q_{2t}), the amount of vinasse produced was estimated:

$$Q_{vinazast} = Q_{2t}\theta_7$$

The corresponding income was estimated as $I_{5t} = Pr_{4t}Q_{5t} = Pr_{4t}Q_{vinazast}\theta_8\theta_9\rho$, where $Q_{5t} = Q_{vinazast}\theta_8\theta_9\rho$.

From the above equations, the average income from asset *i* was calculated as a measure of profitability or return ($\bar{R}_i$), the variance of asset *i* as a measure of volatility (Var_i), and the standard deviation of asset *i* as a measure of risk ($desvest_i$):

$$\bar{R}_i = \sum_{t=1}^{n} I_{it}\, n^{-1}$$

$$Var_i = \sum_{t=1}^{n} (I_{it} - \bar{R}_i)^2\, n^{-1}$$

$$desvest_i = (Var_i)^{1/2}$$

where ($\bar{R}_i$) is the weighted profit of the product or asset i (i = 1, 2 ... 4), I_{it} is the weighted real gross income of product i in year t, and n is the number of observations.

The profitability or return of the portfolio (R_p) was obtained with the sum of the weighted profitability of the assets:

$$\bar{R}_p = \sum_{i=1}^{n} \bar{R}_i$$

The variance of the portfolio (*VarP*) was calculated with the matrix of variances (Var_i) and covariances ($CovR_iR_j$) of the assets that were included for each portfolio. The investment weights (α_i) were determined based on the weighted profitability ($\bar{R}_i$) in regard to the profitability or return of the portfolio ($\bar{R}_p$):

$$\begin{aligned} VarP = {} & \alpha_1^2 Var_1 + \alpha_2^2 Var_2 + \alpha_3^2 Var_3 + \alpha_4^2 Var_4 + \alpha_5^2 Var_5 + 2X_1X_2 CovR_1R_2 + 2\alpha_1\alpha_3 CovR_1R_3 \\ & + 2\alpha_1\alpha_4 CovR_1R_4 + 2\alpha_1\alpha_5 CovR_1R_5 + 2\alpha_2\alpha_3 CovR_2R_3 + 2\alpha_2\alpha_4 CovR_2R_4 \\ & + 2\alpha_2\alpha_5 CovR_2R_5 + 2\alpha_3\alpha_4 CovR_3R_4 + 2\alpha_3\alpha_5 CovR_3R_5 + 2\alpha_4\alpha_5 CovR_4R_5 \end{aligned}$$

With the estimations of $\bar{R}_i$, Var_i and $CovR_iR_j$ for each asset, the measure of risk (*StDevP*) and profitability ($\bar{R}_p$) of each portfolio was calculated following the methodology by Rojas-Rojas *et al*. (2025b) (Figure 1).

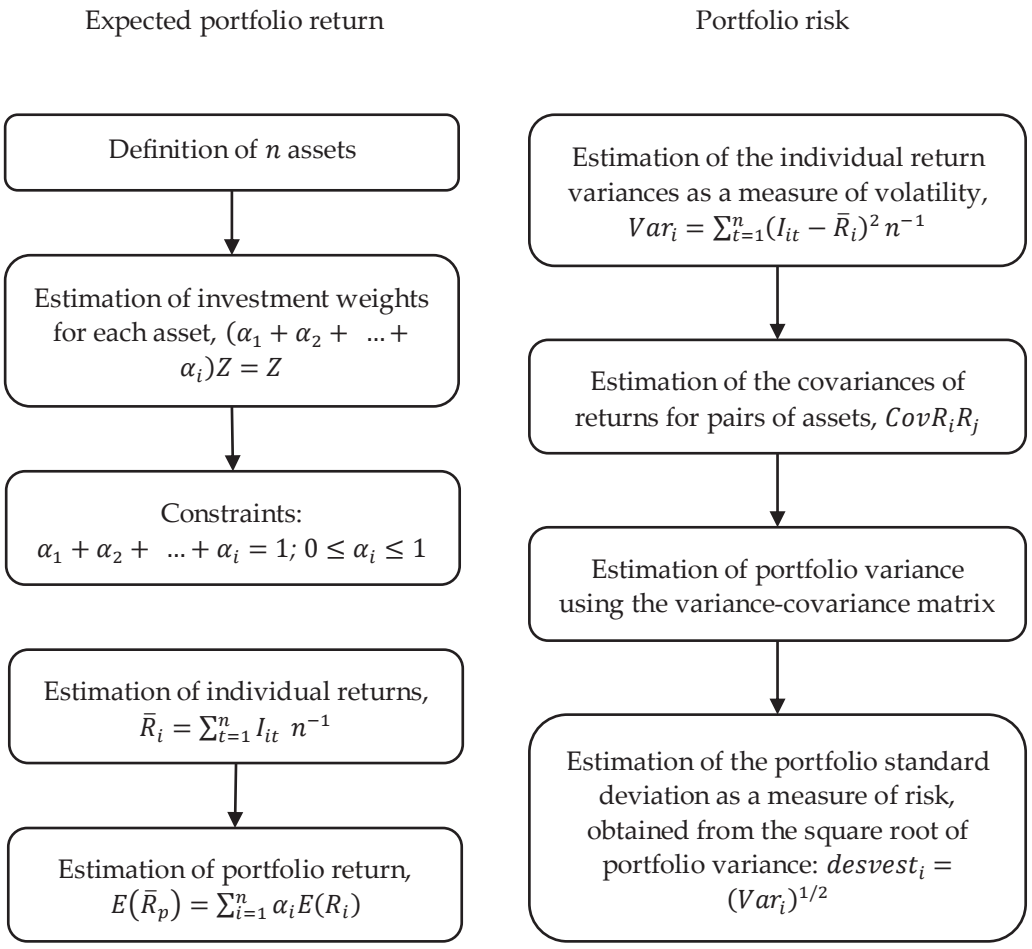

Figure 1. Estimation of the return on investment and risk of the traditional and the biorefinery portfolios.

RESULTS AND DISCUSSION

The tequila industry has proven to be highly productive and profitable due to its dynamism in the export market, mainly to the United States, where the presence of Mexican nationals has increased its consumption as a traditional beverage. As a result, the true price of tequila displayed an average annual increase of 4 % between 2000 and 2023, with a relatively low risk (Table 2).

However, in terms of profitability, the income per hectare of agave production as a raw material displayed a downward trend (-1 %), mainly due to the reduction in crop yield (-1.5 %) (SIAP, 2024b), despite the real price of agave having recorded a marginal growth in its average annual rate of 0.5 % between 2000 and 2023. This reduction in return is associated with the increasing demand for agave as an input for the production of tequila, which has led to soil overexploitation, nutrient depletion, and

Table 2. Return and risk analysis of prices for selected products (2000–2023).

Variable	Agave	Inulin	Tequila	Bioethanol	Biogas
Return	0.005	0.09	0.04	0.05	0.01
Volatility	0.19	2.05	0.02	2.52	0.01
Risk	0.43	1.43	0.13	1.59	0.10

the consequent adverse effects on plant health (Quezada-Chico *et al*., 2022). Likewise, the intensive use of agave has prevented plants from reaching an adequate maturity level, reducing the amount and quality of the raw material (Acosta-Salazar *et al*., 2021). Nevertheless, in the first half of 2024, the tequila agave value chain faced a raw material oversupply problem (Rojas-Rojas *et al*., 2021). Agave consumption for the production of tequila decreased by 25 % from January to July, 2024, in comparison with the same period of the previous year (CRT, 2024). As a consequence, the reduction in demand in the export market (-6 %) was reflected in an equivalent slowdown in the production. This situation led to an oversupply of agave in the first half of 2024 and anticipates a downward trend in the price of agave hearts in upcoming years (Cruz-Ramírez *et al*., 2023b; Díaz-Castellanos, 2023). In this scenario, the possibility of implementing a biorefinery system opens up to implement the use of the available raw material and generate products with a higher added value, such as inulin, while continuing to produce tequila. Inulin is a dietetic fiber with prebiotic effects that favors the reduction of blood cholesterol and the absorption of calcium in bones (Montañez-Soto *et al*., 2011).

On the other hand, to evaluate the normality of the individual returns, the Shapiro-Wilk test was used. Its decision criterion establishes that the null hypothesis (H_0) assumes a normal distribution of returns and is rejected when $p < 0.05$. In addition, a value of W close to 1 suggests normality in the distribution (Gujarati and Porter, 2010) (Table 3).

The results confirmed the normality of inulin and biogas. By contrast, bioethanol and tequila did not satisfy the normality criterion. Nevertheless, its W values were close to 1, which can be explained by the fact that, although the methodology assumes normality, the actual data do not reflect it, as they present fat tails or high peaks in the returns (Francis and Kim, 2013).

Table 3. Normality tests in the individual returns of the products selected.

Product	*p*-value	W
Inulin	0.0856	0.9275
Tequila	0.0140	0.8911
Bioethanol	0.0189	0.8973
Biogas	0.6198	0.9681

Portfolios were developed to utilize agave for the production of inulin and/or tequila. Tequila displayed a high return, as shown in portfolio P13, which has a return three times higher than portfolio P11, which only produces inulin. However, in light of scenarios of oversupply of agave and price volatility, an alternative is to allocate part of the raw material to the production of inulin. By diversifying production, such as in portfolio P12, the risk decreases (Table 4). These results are consistent with those reported by Valencia-Sandoval *et al*. (2020) through evaluation using real options.

Table 4. Risk and return on investment portfolios in the agave value chain.

Portfolio*	Investment weight		Portfolio risk (*StDevP*, $)	Portfolio variance (*VarP*, $²)	Portfolio return ($E(\bar{R}_p)$, $)	Portfolio return ($E(\bar{R}_p)$, USD)
	α_1	α_2				
P1	0 %	100 %	3 323 290.57	11 044 260 194 181.70	31 076 720.69	1 751 392.56
P2	10 %	90 %	2 983 294.61	8 900 046 736 753.88	28 041 219.40	1 580 320.63
P3	20 %	80 %	2 643 425.23	6 987 696 924 997.75	25 005 718.11	1 409 248.71
P4	30 %	70 %	2 303 734.99	5 307 194 898 730.34	21 970 216.83	1 238 176.79
P5	40 %	60 %	1 964 310.47	3 858 515 613 910.67	18 934 715.54	1 067 104.87
P6	50 %	50 %	1 625 305.26	2 641 617 197 272.32	15 899 214.25	896 032.94
P7	60 %	40 %	1 287 021.54	1 656 424 439 067.60	12 863 712.96	724 961.02
P8	70 %	30 %	950 152.52	902 789 818 683.79	9 828 211.67	553 889.10
P9	80 %	20 %	616 764.58	380 398 548 059.89	6 792 710.39	382 817.17
P10	90 %	10 %	297 988.43	88 797 103 976.98	3 757 209.10	211 745.25
P11	100 %	0 %	347 363.28	120 661 249 896.97	721 707.81	40 673.33
P12	50 %	50 %	192 966.10	37 235 916 569.12	1 425 687.23	80 347.54
P13	0 %	100 %	469 849.67	220 758 714 376.24	2 129 666.64	120 021.75

*P1 corresponds to portfolios of tequila that use bagasse and vinasse for bioethanol and biogas. P2–P10 represent portfolios under a biorefinery scheme that produce inulin and tequila, with waste valorization. P11 only produces inulin; P12 produces inulin and tequila without the use of waste; and P13 produces exclusively tequila. α_1 and α_2 represent the investment weights on inulin and tequila, respectively.

On the other hand, portfolios P1 to P10, designed to use the residual biomass such as vinasses and bagasse, represent a business opportunity and an alternative to mitigate the environmental problems of the sector. When comparing portfolio P1, which produces tequila and manages the waste to generate biogas and ethanol, with portfolio P13, which only produces tequila, profitability increased 14.5 times when the waste is used. Rodríguez-Hernández *et al*. (2016) found similar results, reporting cost-benefit ratios of 13.3 for *Agave angustifolia* and of 6.47 for *A. tequilana* in the production of bioethanol, although they pointed out that profitability depends on the price of agave and bioethanol in the market.

The management of waste in the tequila industry shows the generation of additional income (Figure 2). This can be observed in portfolio P6, corresponding to a biorefinery

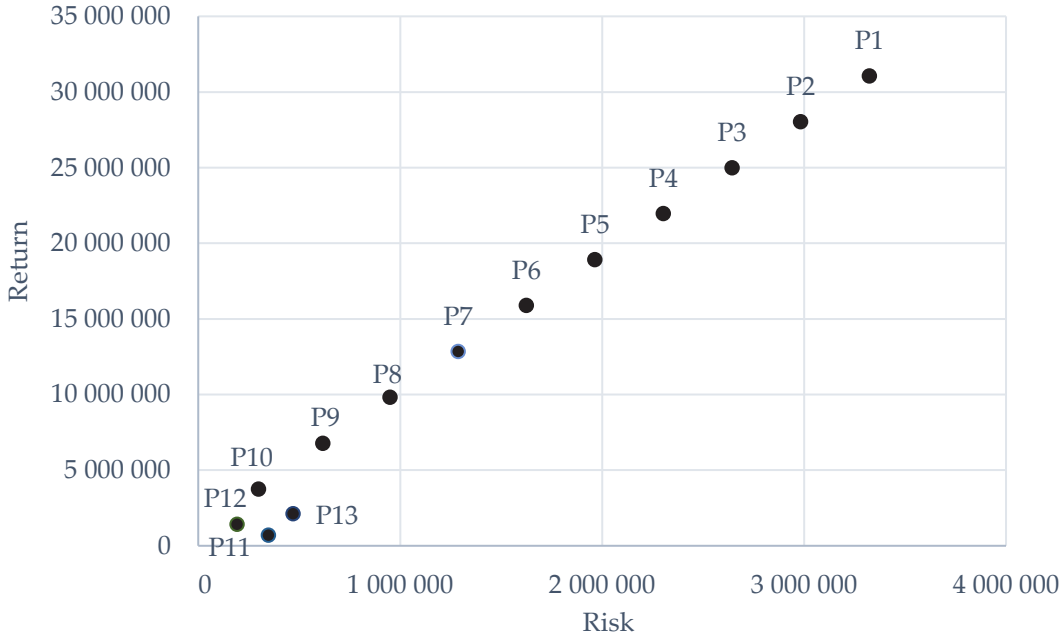

Figure 2. Behavior of the return on investment and risk of the portfolios evaluated.

system in which 50 % of the raw material was destined to the production of inulin and 50 % to the production of tequila, with the use of residues to obtain biogas and bioethanol, in comparison with portfolio P12, with the difference being that the vinasse and bagasse residues were not managed.

It is important to note that P12 was the portfolio with the lowest risk compared to the others. The use of residues increased its risk but also its return. The products with the highest added value maintained a higher risk, since they imply innovation, technological development, access to new markets, greater funding, and new regulations (Brambila-Paz *et al*., 2019; Feng *et al*., 2024; Pender *et al*., 2024). The prices of bioethanol and inulin (Table 2) turned out to be the most expensive, with values of 1.59 and 1.43, respectively, which elevates the level of risk of the portfolios that use waste to manufacture these products.

These results show that the production system in a biorefinery can be implemented in other value chains, such as cereals (ElMekawy *et al*., 2013), oil crops (Chojnacka, 2023), and citrus fruits (Rojas-Rojas *et al*., 2025a), among others. Nevertheless, it is important to have enough information, since a limitation of this investigation was the availability of a robust database.

CONCLUSIONS

The tequila industry is highly profitable. However, diversification in the use of agave as a raw material for the production of inulin and tequila, within a biorefinery system,

helps disperse risk. The hypothesis was confirmed that managing waste from the biomass generated during the processing of agave for tequila production enhances the return on investment portfolio and increases risk. This increase in risk is attributed to innovations in production processes and the development of higher-value products. Nevertheless, this risk can be effectively managed in scenarios involving price volatility.

REFERENCES

Acosta-Salazar E, Fonseca-Aguiñaga R, Warren-Vega WM, Zárate-Guzmán AI, Zárate-Navarro MA, Romero-Cano LA, Campos-Rodríguez S. 2021. Effect of age of *Agave tequilana* Weber blue variety on quality and authenticity parameters for the tequila 100 % agave silver class: Evaluation at the industrial scale level. Foods 10: 3103 https://doi.org/10.3390/foods10123103

Brambila-Paz JJ, Martínez-Damián MA, Rojas-Rojas MM, Pérez-Cerecedo V. 2013. La bioeconomía, las biorefinerías y las opciones reales: el caso del bioetanol y el azúcar. Agrociencia 47 (3): 281–292.

Brambila-Paz JJ, Rojas-Rojas MM, Pérez-Cerecedo V. 2019. Evaluación financiera de los proyectos de biorrefinerías con la metodología de opciones reales. *In* Carrillo-González G, Torres-Bustillos L. (eds.), Biorrefinerías y Economía Circular. Universidad Autónoma Metropolitana: Ciudad de México, México, pp: 37–56.

Cardona-Alzate CA, Ortiz-Sanchez M, Solarte-Toro JC. 2023. Design strategy of food residues biorefineries based on multifeed stocks analysis for increasing sustainability of value chains. Biochemical Engineering Journal 194: 108857. https://doi.org/10.1016/j.bej.2023.108857

Carrillo-González G, Ponce-Sánchez JI. 2019. Economía circular, bioeconomía y biorrefinerías. *In* Carrillo-González G, Torres-Bustillos BL. (eds.), Biorrefinerías y Economía Circular. Universidad Autónoma Metropolitana: Ciudad de México, México, pp: 15–35.

Chojnacka K. 2023. Valorization of biorefinery residues for sustainable fertilizer production: A comprehensive review. Biomass Conversion and Biorefinery 13: 14359–14388. https://doi.org/10.1007/s13399-023-04639-2

CRE (Comisión Reguladora de Energía). 2024. Historial de precios promedio al público de gas LP reportados por los distribuidores. Gobierno de México. Comisión Reguladora de Energía. Ciudad de México, México. https://www.gob.mx/cre/documentos/historial-de-precios-promedio-al-publico-de-gas-lp-reportados-por-los-distribuidores (Retrieved: June 2024)

CRT (Consejo Regulador del Tequila). 2019. Manual del técnico tequilero. Consejo Regulador del Tequila. Tequila, Jalisco. 637 p.

CRT (Consejo Regulador del Tequila). 2024. Estadísticas. Tequila, Jalisco https://old.crt.org.mx/EstadisticasCRTweb/ (Retrieved: June 2024).

Cruz-Ramírez AS, Martínez-Gutiérrez GA, Escamirosa-Tinoco C. 2023a. Las fluctuaciones de precios del agave tequilero y mezcalero en México, para el periodo 1982-2019. *In* Rojas-Rojas MM, Valencia-Sandoval K, Ybarra-Moncada MC. (eds.), Competitividad en las Cadenas de Valor Agroalimentarias: Conceptos y Herramientas Metodológicas. Editorial Plaza y Valdés: Ciudad de México, México, pp: 189–209.

Cruz-Ramírez AS, Martínez-Gutiérrez GA, Martínez-Hernández AG, Morales I, Escamirosa-Tinoco C. 2023b. Price trends of agave mezcalero in Mexico using multiple linear regression models. Ciência Rural 53 (2). https://doi.org/10.1590/0103-8478cr20210685

del Real-Olvera J, López-López A. 2012. Biogas production from anaerobic treatment of agro-industrial wastewater. *In* Kumar S. (ed.), Biogas. InTech: Rijeka, Croacia, pp: 91–112.

Díaz-Carreño MA, Juárez TR, Gómez-Chagoya MC. 2007. Conformación de una cartera de inversión óptima de cultivos agrícolas para México. Economía Sociedad y Territorio 7 (25): 49–63. https://doi.org/10.22136/est002007231

Díaz-Castellanos R. 2023. The price of agave in Mexican states holding Designation of Origin of Tequila status, and its systematic depreciation over the forthcoming decade (2000-2031). The Anáhuac Journal 23 (2): 12–37. https://doi.org/10.36105/theanahuacjour.2023v23n2.01

ElMekawy A, Diels L, de Wever H, Pant D. 2013. Valorization of cereal based biorefinery by products: Reality and expectations. Environmental Science and Technology 47 (16): 9014–9027. https://doi.org/10.1021/es402395g

Estrada-Maya A, Weber B. 2022. Biogás y bioetanol a partir de bagazo de agave sometido a explosión de vapor e hidrólisis enzimática. Ingeniería Investigación y Tecnología 23 (2): 1–10. https://doi.org/10.22201/fi.25940732e.2022.23.2.009

Feng J, Tang J, Qi Z, Liu J. 2024. Supply chain finance and innovation investment: Based on financing constraints. Finance Research Letters 63: 105349. https://doi.org/10.1016/j.frl.2024.105349

Francis JC, Kim D. 2013. Modern portfolio theory: Foundations, analysis, and new developments. John Wiley and Sons: Hoboken, NJ, USA. 557 p.

Gujarati DN, Porter DC. 2010. Econometría (Quinta edición). McGraw-Hill: Ciudad de México, México. 921 p.

Herrera-Pérez L, Valtierra-Pacheco E, Ocampo-Fletes I, Tornero-Campante MA, Hernández-Plascencia JA, Rodríguez-Macías R. 2018. Esquemas de contratos agrícolas para la producción de *Agave tequilana* Weber en la región de Tequila, Jalisco. Agricultura, Sociedad y Desarrollo 15 (4): 619–637.

Hoz-Zavala MEE, Nava-Diguero P. 2017. Los residuos de agave como factor de corrosión del suelo donde se vierte. Revista del Desarrollo Tecnológico 1 (2): 11–24.

INEGI (Instituto Nacional de Estadística y Geografía). 2024a. Balanza comercial de mercancías. Aguascalientes, México. https://www.inegi.org.mx/programas/comext/#tabulados (Retrieved: June 2024).

INEGI (Instituto Nacional de Estadística y Geografía). 2024b. Índice nacional de precios al consumidor. Aguascalientes, México. https://www.inegi.org.mx/temas/inpc/ (Retrieved: June 2024).

Markowitz H. 1952 Portfolio selection. Journal of Finance 7 (1): 77–91. https://doi.org/10.2307/2975974

Montañez-Soto J, Venegas-González J, Vivar-Vera M, Ramos-Ramírez E. 2011. Extracción, caracterización y cuantificación de los fructanos contenidos en la cabeza y en las hojas del *Agave tequilana* Weber azul. Bioagro 23 (3): 199–206.

Muñoz-González S, Saldaña-Carro C, Becerra-Díaz JC. 1992. Administración de portafolios de inversión y la aplicación de recocido simulado con restricciones. Ecorfan: Ciudad de México, México. 57 p.

Pender A, Kelleher L, O`Neill E. 2024. Regulation of the bioeconomy: Barriers, drivers and potential for innovation in the case of Ireland. Cleaner and Circular Bioeconomy 7: 100070. https://doi.org/10.1016/j.clcb.2023.100070

Quezada-Chico G, Vargas-Inclán M, Loza-Ramírez L. 2022. Efecto de la planta del cultivo de *Agave tequilana* con relación a las propiedades del suelo en inmediaciones de la cabecera

municipal de Cuquío, Jalisco. Desarrollo Urbano, Metropolización y el Medio Ambiente 2 (4): 61–77.

Rodríguez-Hernández R, Barrios-Ayala A, Flores-López HE, Sánchez-Vásquez V, Ariza-Flores R. 2016. Economic feasibility of bioethanol production with three species of *Agave* spp. in producing areas from Mexico. Revista Mexicana de Ciencias Agrícolas 7 (6): 1439–1453.

Rojas-Rojas MM, Godínez-Montoya L, Valencia-Sandoval K. 2025a. Explorando opciones para una diversificación sostenible de la cadena de valor: el caso de los cítricos en México. *In* Quiroga-Canaviri JL, Menéndez-Gámiz CR, Becerra-Guzmán FJ, Ramírez-Hernández BC, Zúniga-González CA. (eds.), Bioeconomía en Latinoamérica: Desafíos para la Sostenibilidad y el Desarrollo. Universidad de Guadalajara: Guadalajara, México, pp: 188–209. https://doi.org/10.32870/9786075815107

Rojas-Rojas MM, Valencia-Sandoval K, Brambila-Paz JJ. 2025b. Circular bioeconomy, an opportunity to add value and increase the competitiveness of the milk-cheese value chain in Mexico. Nova Scientia 16 (33): 1–12. https://doi.org/10.21640/ns.v16i33.3455

Rojas-Rojas MM, Valencia-Sandoval K, Ybarra-Moncada MC, Brambila-Paz JJ. 2021. Competitiveness and innovation in the pulquera industry, an economic analysis. Nova Scientia 13 (26). https://doi.org/10.21640/ns.v13i26.2810

SENER (Secretaría de Energía). 2015. Precios máximos aplicables de gas LP. Gobierno de México. Secretaría de Energía, Ciudad de México, México. https://www.gob.mx/cre/documentos/precios-maximos-aplicables-de-gas-lp?idiom=es (Retrieved: June 2024).

SIAP (Servicio de Información Agroalimentaria y Pesquera). 2024a. Panorama Agroalimentario 2024. Gobierno de México. Servicio de Información Agroalimentaria y Pesquera. Ciudad de México, México. https://www.gob.mx/siap/acciones-y-programas/panorama-agroalimentario-258035 (Retrieved: June 2024).

SIAP (Servicio de Información Agroalimentaria y Pesquera). 2024b. Base de datos del SIACON. Gobierno de México. Servicio de Información Agroalimentaria y Pesquera. Ciudad de México, México. https://www.gob.mx/siap/documentos/siacon-ng-161430 (Retrieved: June 2024).

Valencia-Sandoval K, Rojas-Rojas MM, Alvarado-Lagunas E, Duana-Avila D. 2020. Agroindustrial agave innovation (*Agave tequilana* Weber var. Blue): Financial assessment for the obtaining of inulin. Agroproductividad 13 (3): 19–24. https://doi.org/10.32854/agrop.vi.1632

Agrociencia

GEOSTATISTICAL ANALYSIS OF THE PHYSICAL PROPERTIES OF GLEYSOL SOIL IN TABASCO, MEXICO

Manuel David **Sosa-García**[1], Maximiano Antonio **Estrada-Botello**[1*], Rufo **Sánchez-Hernández**[1], Carlos Alberto **Pérez-Cabrera**[2], Areli **Carrera-Lanestosa**[1], Pedro **García- Alamilla**[1]

[1]Universidad Juárez Autónoma de Tabasco. Carretera Villahermosa-Teapa km 25, Ranchería La Huasteca 2da. Sección, Villahermosa, Tabasco, Mexico. C. P. 86298.
[2]Colegio Superior Agropecuario del Estado de Guerrero. Avenida Vicente Guerrero 81, Colonia Centro, Iguala de la Independencia, Guerrero, Mexico. C. P. 40000.
* Author for correspondence: maximiano.estrada@ujat.mx

Citation: Sosa-García MD, Estrada-Botello MA, Sánchez-Hernández R, Pérez-Cabrera CA, Carrera-Lanestosa A, García-Alamilla P. 2026. Geostatistical analysis of the physical properties of Gleysol soil in Tabasco, Mexico. **Agrociencia** 60(2): 253-268. https://doi.org/ 10.47163/agrociencia.v60i2.3406

Editor in Chief:
Dr. Fernando C. Gómez Merino

Received: June 17, 2025.
Approved: March 05, 2026.
Published in Agrociencia: March 23, 2026.

ABSTRACT

The water content stored in soil depends on its physical properties and spatial variation. Unfortunately, in the Sierra de Tabasco region, no studies provide information on the spatial variability of water in the soil. Therefore, the objective of this study was to apply geographic information systems to the physical variables of the soil and the water table stored in Gleysol soil on the "La Victoria" farm, in the municipality of Teapa, Tabasco. The physical properties of texture, bulk density (Da), field capacity humidity content (FC), permanent wilting point (PWP), and saturation point (Psat) of the soil were evaluated. The water tables stored at depths of 0–30, 30–60, and 60–90 cm were also assessed. A descriptive statistical analysis was performed, and maps and semivariograms were produced. The results showed that at all three depths, there was a higher percentage of clay content and an average Da of 1.14 g cm^{-3}. The soils had high humidity content, which affects the stored water sheets. For soil properties, the models varied at all three depths and had the lowest R^2 values, while for stored water variation, the R^2 values were greater than 0.9. The construction of maps using geographic information systems is an important tool for understanding the spatial distribution of stored water and determining potential areas with water deficits or excesses.

Keywords: water, semivariograms, field capacity, permanent wilting point.

INTRODUCTION

The spatial distribution of soil physical properties affects the uniform distribution of irrigation water applied in agricultural areas. In addition, the humidity retention capacity of soils affects the availability of water for crops and is the basis for the proper management of water resources and the management and scheduling of irrigation water (Núñez-Ramírez *et al*., 2020). The physical characteristics of soils show complex spatial variability for each soil type, which is influenced by the way they are managed agronomically (Pérez-Zapata *et al*., 2024).

To understand the components of horizontal and transverse water distribution, it is necessary to determine physical characteristics such as texture, structure, porosity, bulk density (Lince-Salazar, 2021), permanent wilting point (PWP), field capacity (FC), and saturation point (Sakaki and Smits, 2015) of the soil. Xu *et al*. (2025) suggest that the permanent wilting point indicates when the soil retains water with such high energy that plants cannot access it, leading to partial or total wilting due to water stress. On the other hand, field capacity is a parameter that indicates how much water a soil can retain against the forces of gravity and is determined by factors linked to soil type, such as texture, structure, the type of clay present, the depth of the wet front, initial humidity, and soil management (Sandoval-García *et al*., 2021).

Soil texture is considered the relative proportion of sand, silt, and clay particles (Márquez, 2021) that influences its water storage capacity, as does bulk density. Some studies indicate that geostatistical techniques in the physical and hydrological properties of soil (bulk density, total porosity, soil humidity and humidity retention) exhibit spatial dependence (Han *et al*., 2024); furthermore, the use of Kriging as a tool determines the spatial variability of soil properties (Awal *et al*., 2019). To make efficient use of water, computational models (Suarez-Muñoz *et al*., 2025) are used with the support of geostatistics, where factors are modeled as spatially correlated random variables (Álvarez-Herrera *et al*., 2021), which helps understand the spatial distribution of water storage in the soil. Several important techniques contribute to this understanding, including geographic information systems (Bautista, 2021).

The Sierra de Tabasco region of Mexico lacks studies on the spatial variability of parameters used to determine the amount of water that soil can store. However, it is assumed that the use of geostatistical tools can help to understand the spatial distribution of soil water content. Therefore, the objective of this study was to utilize geographic information systems techniques to analyze the physical variables of the soil and the water table stored in Gleysol at the "La Victoria" farm in Teapa, Tabasco.

MATERIALS AND METHODS

Study area

The research was conducted at the "La Victoria" banana plantation in the municipality of Teapa, in the state of Tabasco (17° 40′ 59.13" N, 92° 57′ 30.79" W to 17° 41′ 56.32" N, 92° 56′ 39.95" W) (Figure 1). The study area covers 168 ha. The soil corresponds to the mollic Gleysol unit (Palma-López *et al*., 2007). The climate is characterized as hot and humid with rainfall throughout the year (INEGI, 2017). The average annual precipitation is 3085.3 mm, with an average maximum temperature of 32.1 °C, a minimum of 21.1 °C, and a monthly average of 26.6 °C (CONAGUA, 2023), considering the period from 1991 to 2020.

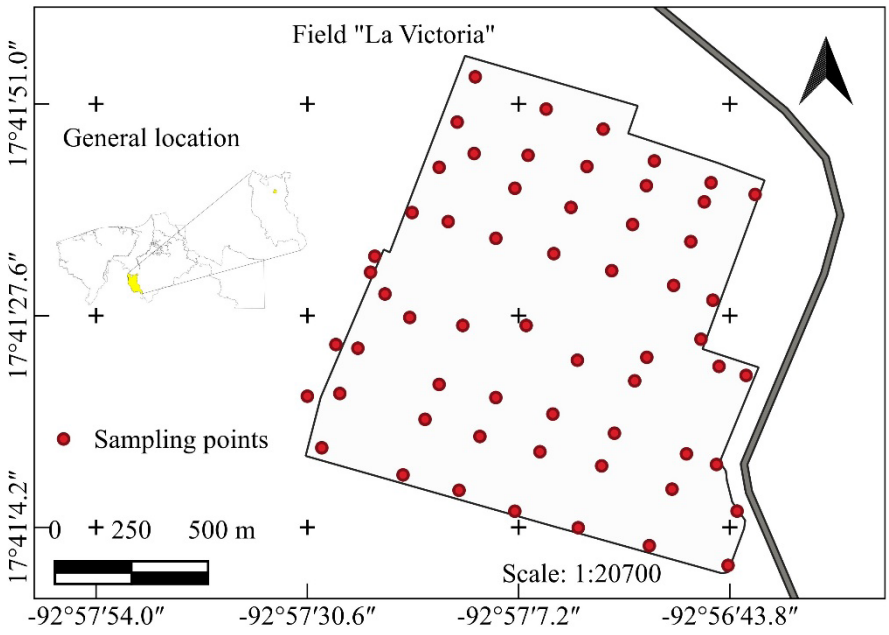

Figure 1. Location of the study area in the municipality of Teapa, Tabasco, Mexico.

Soil sampling

Sampling was carried out during April–May 2023, using a grid system that minimizes the difficulties associated with interpolation, attempting to cover a grid of 180 × 200 m. At some intersections, 55 sampling points were taken, as well as at the periphery of the study area, covering at least one point per 10 ha (Figure 1). Samples were taken at three depths (0–30, 30–60, and 60–90 cm) using an Edelman auger and taken to the Soil and Plant Laboratory of the Academic Division of Agricultural Sciences at the Juárez Autonomous University of Tabasco, where they were dried at room temperature and sieved to determine their physical properties. At the sampling points, the geographical coordinates were determined using a Garmin GPS (GPSMAP 64x) with an accuracy of 3.65 m.

Determination of variables

Texture (Bouyoucos method), bulk density (Da, cylinder method), field capacity (FC, pressure pot method), permanent wilting point (PWP, pressure membrane), and saturation point (Psat, soil saturation) were determined (DOF, 2002). Similarly, the FC sheet, PWP sheet, and Psat sheet were calculated at each of the depths taken.

Calculation of humidity percentage

For the humidity percentage parameters for FC, PWP, and Psat, the wet and dry weights were determined. The humidity percentage was calculated gravimetrically (θw) using the following formula:

$$\theta_w = \frac{(Psh - Pss)}{Pss} * 100$$

where *Psh* is the weight of wet soil (g) and *Pss* is the weight of dry soil (g).

Stored water sheet

The stored leaf area was determined for each stratum using the following formula:

$$Lalmx = \frac{(Px) * Da * Pr}{Dw}$$

where *Lalmx* is the water stored up to the humidity percentage at *FC*, *PWP*, and *Psat* (cm); *Px* corresponds to the gravimetric humidity content (%); *Da* is the bulk density of the soil (g cm^{-3}); *Dw* is the density of water (g cm^{-3}); and *Pr* is the thickness of the soil sheet (cm).

Irrigation sheet

The irrigation sheet was determined for each stratum using the following formula:

$$Lr = \frac{(FC - PWP) * Da * Pr}{Dw}$$

where *Lr* represents the irrigation depth (cm), *FC* the volumetric field capacity (%), *PWP* the volumetric permanent wilting point (%), *Da* the bulk density of the soil (g cm^{-3}), *Dw* the density of water (g cm^{-3}), and *Pr* the thickness of the soil sheet (cm).

Geostatistical analysis

Descriptive statistics were performed using GS+ Version 10 trial software for each of the variables determined. Unmeasured points were estimated using the Kriging method with the following equation:

$$\gamma(h) = \frac{1}{2N(h)} \sum_{i=1}^{n} [Z(X_i) - Z(X_i + h)]^2$$

where $\gamma(h)$ is the semi-variance, $N(h)$ is the number of pairs of points separated by a distance h, $Z(X_i)$ is the heat of the attribute at location Xi, and Z(Xi + h) is the value of the attribute at a distance h from location $X_i + h$.

The best theoretical model was selected according to the structural parameters of the experimental semivariogram: (a) the nugget variance (C_0), which is the Y intercept of the semivariogram model; (b) the sill ($C_0 + C$), which indicates the asymptote of

the curve where the structural variance reaches its maximum values when it remains constant; and (c) the range (A_0), which indicates the distance value (m) at which the maximum soil variance of the parameter is reached, thus defining the area of influence of the autocorrelation (Bautista, 2021).

Map construction

The texture, *FC, PWP*, and *Da* maps were constructed for each stratum, as well as maps of stored water sheets and irrigation in each one. These maps were created using QGIS software and the Kriging interpolation technique. To generate the maps, all variables were classified by range, according to the distribution of cell values resulting from the interpolation.

RESULTS AND DISCUSSION

Descriptive statistics of the soil variables

The statistical parameters (mean, standard deviation, sample variance, maximum and minimum values, skewness, and kurtosis) for the physical properties of the soil (clay, sand, silt, bulk density, field capacity percentage, permanent wilting point percentage, and soil saturation percentage) varied between the depths evaluated (Table 1). For the soil texture components (clay, sand, and silt) in the study area, a minimum percentage of 36.68 % and a maximum of 63.24 % were recorded for clay; for sand, the range was 10.32–36.76 %, while for silt it ranged from 17.44 to 42.01 %. These values correspond to a depth of 60–90 cm.

When comparing the bulk density between depths, the maximum value was found at 60–90 cm and the minimum at 0–30 cm (Table 1). However, in a mollic Gleysol soil in the region, bulk density values of 1.29 to 1.37 g cm^{-3} were reported (Palma-López *et al*., 2007), which are higher than those obtained in this study. The ranges of humidity percentages for *FC, PWP*, and *Psat* were 28.88–46.04, 16.39–29.32, and 53.95–68.78 %, respectively, and varied with depth; in some cases, the values were close to those reported in other studies (Palma-López *et al*., 2007).

The asymmetry values obtained were positive for clay, silt, and permanent wilting point at a depth of 0–30 cm, indicating that the data are distributed to the left of the arithmetic mean. On the other hand, negative asymmetrical values were found in the parameters of sand, bulk density, field capacity, and saturation point, showing that the distribution is skewed to the right in relation to the mean. The kurtosis values were negative in all parameters at a depth of 0–30 cm, indicating a platykurtic distribution. Studies conducted in other locations report asymmetry values of 0.41–0.82 for clay, 0.13–0.46 for sand, and 0.46–0.71 for silt, as well as kurtosis values ranging from -0.55 to 0.43, -0.83 to -0.72, and 0 to 0.33 for clay, sand, and silt, respectively (Varón-Ramírez *et al*., 2022), some of which were similar to those obtained in this study. On the other hand, in a study conducted in Ecuador on Andisol soil, it was found that the kurtosis

Table 1. Descriptive statistics of soil physical properties by depth.

Parameter	Mean	SD	Sample variance	Minimum value	Maximum value	Asymmetry	Kurtosis
				Depth of 0–30 cm			
Clay (%)	46.76	3.90	15.20	40.24	54.52	0.33	-0.80
Sand (%)	26.38	6.18	38.20	11.98	36.76	-0.01	-0.67
Silt (%)	28.98	5.01	25.08	20.72	37.80	0.39	-1.00
Da (g cm^{-3})	1.14	0.05	0.002	1.08	1.22	-0.19	-1.53
FC (%)	37.91	3.46	11.99	30.65	42.87	-0.60	-0.56
PWP (%)	24.01	2.79	7.80	19.02	29.72	0.34	-0.87
Psat (%)	61.74	4.18	17.47	53.95	67.97	-0. 28	-1.31
				Depth of 30–60 cm			
Clay (%)	47.97	6.17	38.13	37.13	60.52	0.21	-0.85
Sand (%)	23.77	5.74	32.95	14.46	36.04	0.16	-0.74
Silt (%)	28.71	5.39	29.02	18.02	30.44	0.24	-0.86
Da (g cm^{-3})	1.13	0.06	0.003	1.04	1.25	0.20	-1.13
FC (%)	39.14	4.01	16.11	31.05	45.99	-0.41	-0.76
PWP (%)	24.14	3.24	10.51	18.80	29.32	0.14	-1.15
Psat (%)	62.19	3.76	14.15	55.00	67.82	-0.33	-1.10
				Depth of 60–90 cm			
Clay (%)	49.41	7.14	51.02	36.68	63.24	0.14	-1.11
Sand (%)	21.75	6.45	41.59	10.32	36.04	0.43	-0.59
Silt (%)	28.41	5.88	36.67	17.44	42.01	0.21	0.59
Da (g cm^{-3})	1.14	0.06	0.06	1.04	1.26	0.17	-1.12
FC (%)	38.79	5.03	25.25	28.88	46.04	-0.37	-0.85
PWP (%)	22.88	3.87	15.00	16.39	29.70	0.06	-1.18
Psat (%)	61.86	3.74	13.98	56.97	68.78	0.19	-1.32

SD: Standard deviation; *Da*: apparent density; *FC*: percentage of humidity at field capacity; *PWP*: percentage of humidity at permanent wilting point; *Psat*: percentage of humidity at saturation point.

and skewness of the bulk density were close to zero at different depths (Salamanca-Jiménez *et al*., 2018), which differs from the results obtained in this study, possibly due to the type of soil.

The results of the descriptive parameters for the depth of 30–60 cm show that all parameters, with the exception of field capacity and saturation, presented positive asymmetry. In terms of kurtosis, all parameters showed negative values, indicating a platykurtic distribution. Likewise, the variables presented differences in asymmetry and kurtosis, without reflecting a clear trend regarding depth.

The descriptive statistical parameters of the water sheets stored in the soil were not similar among the three depths evaluated (Table 2) and varied according to depth. The asymmetry of the variables evaluated was also not similar at the three depths; however, the kurtosis was negative in all variables and depths, indicating platykurtic distributions. On the other hand, the total average water storage was 39.27 cm at field

Table 2. Descriptive statistical parameters of water stored in the soil at different depths.

Parameter	Mean (cm)	SD	Sample variance	Minimum value (cm)	Maximum value (cm)	Asymmetry	Kurtosis
				Depth of 0–30 cm			
Lr_{FC}	12.88	0.68	0.47	11.24	14.31	-0.15	-0.54
Lr_{PWP}	8.24	0.46	0.21	7.26	9.58	0.27	-0.71
Lr_{Psat}	21.33	0.91	0.83	19.23	23.40	-0.12	-0.66
$Lr_{FC\text{-}PWP}$	4.64	0.68	0.46	3.16	6.16	0.53	-0.44
				Depth of 30–60 cm			
Lr_{FC}	13.20	0.57	0.32	11.84	14.39	0.36	-0.54
Lr_{PWP}	8.08	0.54	0.29	6.81	9.51	0.13	-0.41
Lr_{Psat}	20.98	0.64	0.41	19.48	22.60	-0.12	-0.68
$Lr_{FC\text{-}PWP}$	5.12	0.52	0.27	3.58	6.54	0.30	-0.11
				Depth of 60–90 cm			
Lr_{FC}	13.27	0.97	0.94	10.80	15.89	0.06	-0.57
Lr_{PWP}	7.67	0.97	0.95	5.84	10.05	0.17	-0.88
Lr_{Psat}	21.11	0.87	0.75	19.22	23.59	0.25	-0.74
$Lr_{FC\text{-}PWP}$	5.60	0.82	0.66	2.83	7.40	-0.28	-0.50

SD: Standard deviation; Lr_{FC}: sheet stored up to field capacity; Lr_{PWP}: sheet stored up to permanent wilting point; Lr_{Psat}: sheet stored up to saturation point; $Lr_{FC\text{-}PWP:}$ sheet stored between field capacity and permanent wilting point (replacement sheet).

capacity, 23.99 cm at permanent wilting point, and 63.42 cm at saturation, while the replacement water storage (between *FC* and *PWP* humidity) was 15.36 cm.

Semivariograms

Physical properties of the soil

At a depth of 0–30 cm, the Gaussian model provided the best fit for the parameters clay, sand, and saturation point; the spherical model for silt and field capacity; and the exponential model for permanent wilting point and bulk density. In the parameters evaluated, the nugget percentages ranged from 0.00001 to 21.09 %, with R^2 values from 0.536 to 0.919 (Table 3). The sand and permanent wilting point parameters showed the best fit to the statistical model, while clay had the lowest R^2.

At a depth of 30–60 cm, the semivariograms were adjusted to Gaussian and spherical models, depending on the soil property. R^2 values between 0.5 and 0.931 were recorded, ranges between 212 and 1299 m, and nugget percentages from 0.0001 to 14.18 %. At a depth of 60–90 cm, the semivariograms were adjusted to exponential, spherical, and Gaussian models. R^2 values ranged from 0.55 to 0.99, nugget percentages from 0.00015 to 25.2 %, and ranges were between 271 and 6132 m. The sand parameter recorded the highest nugget percentage and the lowest coefficient of determination.

Table 3. Parameters and adjustment of semivariogram models for soil properties and water depth.

Parameter	Model	Nugget (C_0 %)	Sill ($C_0 + C$)	Range (A_0 m)	Structural variance (%)	R^2
			Depth of 0–30 cm			
Clay	Gaussian	0.10	14.680	216.51	99.90	0.54
Sand	Gaussian	21.09	47.100	1039.23	55.20	0.92
Silt	Spherical	0.01	24.650	195.00	100.00	0.73
Da	Exponential	0.00001	0.00244	1038.00	100.00	0.83
FC	Spherical	0.96	12.220	464.00	92.10	0.81
PWP	Exponential	1.17	9.313	990.00	87.40	0.91
Psat	Gaussian	6.60	43.200	1376.98	84.70	0.87
Lr_{FC}	Gaussian	0.001	0.530	464.18	1.00	0.96
Lr_{PWP}	Gaussian	0.0424	0.270	1364.86	0.85	0.98
Lr_{Psat}	Gaussian	0.063	0.986	566.381	0.94	0.99
$Lr_{FC\text{-}PWP}$	Gaussian	0.079	0.538	777.69	0.85	0.92
			Depth of 30–60 cm			
Clay	Gaussian	3.30	38.080	244.21	91.30	0.88
Sand	Spherical	14.18	40.710	1299.00	65.20	0.91
Silt	Spherical	0.01	29.580	212.00	100.00	0.62
Da	Gaussian	0.0001	0.00421	304.84	99.80	0.76
FC	Spherical	5.38	15.200	447.00	66.80	0.50
PWP	Spherical	2.77	12.380	858.00	77.60	0.90
Psat	Spherical	2.29	26.020	732.00	85.70	0.93
Lr_{FC}	Gaussian	0.012	0.368	464.19	0.97	0.90
Lr_{PWP}	Gaussian	0.005	0.376	748.24	0.99	0.99
Lr_{Psat}	Gaussian	0.058	0.467	642.59	0.88	0.98
$Lr_{FC\text{-}PWP}$	Gaussian	0.0109	0.316	519.62	0.98	0.98
			Depth of 60–90 cm			
Clay	Gaussian	0.10	47.410	259.81	99.80	0.70
Sand	Exponential	25.2	81.400	6132.00	69.00	0.60
Silt	Spherical	0.10	38.430	271.00	99.70	0.74
Da	Spherical	0.0002	0.004	388.00	96.10	0.94
FC	Gaussian	0.54	26.320	462.45	80.00	0.98
PWP	Spherical	0.01	20.330	978.00	100	0.98
Psat	Spherical	5.23	21.130	2110.00	75.20	0.92
Lr_{FC}	Spherical	0.081	1.746	2602.00	0.954	0.99
Lr_{PWP}	Gaussian	0.039	1.196	862.56	0.97	1.00
Lr_{Psat}	Gaussian	0.153	0.933	1066.94	0.84	0.97
$Lr_{FC\text{-}PWP}$	Gaussian	0.139	0.668	762.10	1.00	0.99

Da: bulk density; *FC*: percentage of humidity at field capacity; *PWP*: percentage of humidity at permanent wilting point; *Psat*: percentage of humidity at saturation point; Lr_{FC}: leaf stored up to field capacity; Lr_{PWP}: leaf stored up to permanent wilting point; Lr_{Psat}: leaf stored up to saturation point; $Lr_{FC\text{-}PWP}$: leaf stored between field capacity and permanent wilting point (replacement leaf).

For the apparent density variable, Li *et al*. (2019) report that the best fit model was exponential in the 0–20 cm layer, spherical at depths of 20–40 and 40–60 cm, and Gaussian at a depth of 60–100 cm. In addition, the R^2 values were lower and the nugget percentages were higher than those recorded in this study. Salamanca-Jiménez *et al*. (2018) point out that the spherical model presented the best fit in their research, which is consistent only with the 60–90 cm depth in this study.

Stored water sheets

The semivariograms of the water sheets stored at field capacity, at the point of permanent wilting, and at replacement, at all three depths, were adjusted to the Gaussian model, with R^2 values greater than 0.9. Meanwhile, the sheet stored at field capacity at a depth of 60–90 cm was adjusted to a spherical model.

The nugget effect should not be interpreted as a direct measure of error. It is more accurately defined as a phenomenon that represents the randomness inherent in regionalized variables and their values (Camana and Deutsch, 2019); however, it contributes to determining data quality. Even when the spatial separation between samples is minimal, variability exists, and the discrepancy between samples taken very close together complicates the interpolation process due to the high variability of the parameter. Therefore, the nugget effect can be considered a quantitative measure of the level of variability between samples located at very short distances (Yu *et al*., 2025). Parameters with low nugget percentages have less variability and a more homogeneous and predictable distribution; conversely, high nugget values indicate high randomness and, consequently, less reliable predictions.

The nugget effect describes whether a parameter, when sampled again at the same location, will produce similar results or not (Behrens *et al*., 2019). In this study, the sand variable had the highest nugget percentages at all three depths. The model with the lowest fit corresponded to field capacity at a depth of 30–60 cm; however, this same parameter at a depth of 60–90 cm recorded the highest R^2 value.

Construction of maps

Texture

Clay occupied the largest surface area at all three depths, ranging from 43 to 48 % (Figure 2). Clay was the predominant fraction at all depths, with the largest surface area in the 0–30 cm stratum, which is consistent with the report by SEMARNAT (2024), which classifies the soils in the study area as clayey. CONABIO (2020) classifies the soils in the area as Gleysols, coinciding with Palma-López *et al*. (2007), who identify them as mollic Gleysols. In this type of soil, clay contents of 34.3, 40.1, and 21.4 % were reported at depths of 0–38, 38–70, and 70–99 cm, respectively, values that differ from those obtained in this study and from the sampling depths considered.

According to the clay content predictions proposed by CONABIO (2020), percentages of 24.3–26.48 % were reported in the study area at a depth of 0–5 cm, 24.5–26.83 % at

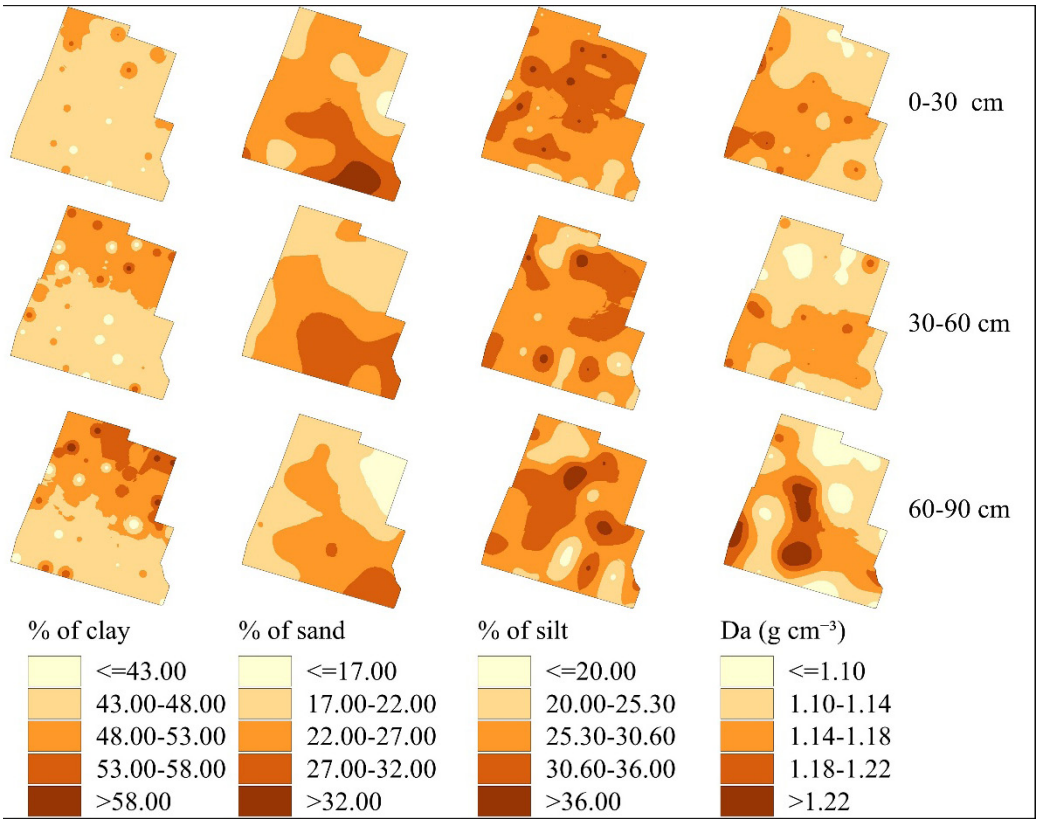

Figure 2. Spatial distribution of soil texture (clay, sand, and silt) and bulk density (*Da*) at the three depths evaluated.

5–15 cm, 28.08–30. 2 % at 15–30 cm, 32.33–33.37 % at 30–60 cm, and 33.9–35.36 % at 60–90 cm, which are lower than those obtained in this research. This difference is due to the fact that these studies are carried out with sampling points established in grids with separations exceeding 1 km between points.

Sand

The sand content at a depth of 0–30 cm was present in more than 50 % of the study area, varying between 22 and 27 %. At a depth of 30–60 cm, this same range occupied the largest surface area (39.78 %), while the rest of the area was distributed between the ranges of 17–22 and 27–32 %, as no values lower than 17 % or higher than 32 % were recorded at this depth. At a depth of 60–90 cm, no values above 32 % were observed; however, more than 80 % of the study area had sand contents between 17 and 27 %. In contrast, CONABIO (2020) reports sand percentages in the study area ranging from 40–56.38, 39.64–41.29, 40.32–40.96, 35.79–36.86, and 34–44.04 % at depths of 0–5, 5–15, 15–30, 30–60, and 60–90 cm, respectively. On the other hand, based on the soil profile corresponding to the soil type, sand percentages of 40.7, 39.3, and 38.75 %

are reported at depths of 0–38, 38–70, and 70–99 cm, respectively (Palma-López *et al*., 2007), which are higher than those found in this research.

Silt

As for the percentage of silt, at all three depths (0–30, 30–60, and 60–90 cm), the class of 25.3–30.6 % predominated, with 57.56, 59.43, and 48.16 % of the total area, respectively. In the study area, 24.6, 20.6, and 39.4 % of silt are reported at depths of 0–38, 38–70, and 70–99 cm, respectively (Palma-López *et al*., 2007), which is close to the data obtained in this research when considering the class with the largest surface area occupied. On the other hand, CONABIO (2020) reports, for the depth of 0–5 cm, percentages of silt in the range of 17.73–33.51 %; from 32.49–34.52 % at 5–15 cm; from 29.30–30.96 % at 15–30 cm; 30–31.60 % at 30–60 cm; and 20.59–32.11 % at 60–90 cm.

Bulk density

The bulk density at a depth of 0–30 cm showed two classes (1.10–1.14 and 1.14–1.18 g cm^{-3}) covering more than 90 % of the area (Figure 2). Similar behavior was observed at depths of 30–60 and 60–90 cm, where these ranges covered 68 % of the surface. These values indicate a variation between the strata evaluated and show that they are not homogeneous, contrary to what has been reported in other studies. This parameter is relevant because of its relationship with other physical and chemical properties of the soil and because it provides information on its use and management, which has a direct effect on plant growth (Salamanca-Jiménez *et al*., 2018).

Percentage of humidity at field capacity

At a depth of 0–30 cm, the highest field capacity values were concentrated in the northern and southeastern parts of the study area (Figure 3); at a depth of 30–60 cm, these values were mainly distributed in the western and southeastern areas; and at a depth of 60–90 cm, the highest values were located in the northern area, which is related to the clay content present. In terms of field capacity percentages, values of 13.91, 16.02, and 8.57 % are reported for depths of 0–38, 38–70, and 70–99 cm, respectively (Palma-López *et al*., 2007), which are lower than those obtained in this study. Conversely, both field capacity and the permanent wilting point increased significantly with sampling depth, aligning with the values reported by Amsili *et al*. (2024).

Percentage of humidity at the point of permanent wilting

In the 0–30 and 30–60 cm strata, the permanent wilting point showed the highest percentage in the range of 21–23.6 % humidity. In contrast, at a depth of 60–90 cm, the highest percentage corresponded to a value of 21 %. In terms of spatial distribution, the lowest PWP values are located in the southern part of the study area (Figure 3), which is associated with a lower apparent density in this zone, a condition that influences PWP, as has been noted in other studies (Chicas-Soto *et al*., 2014).

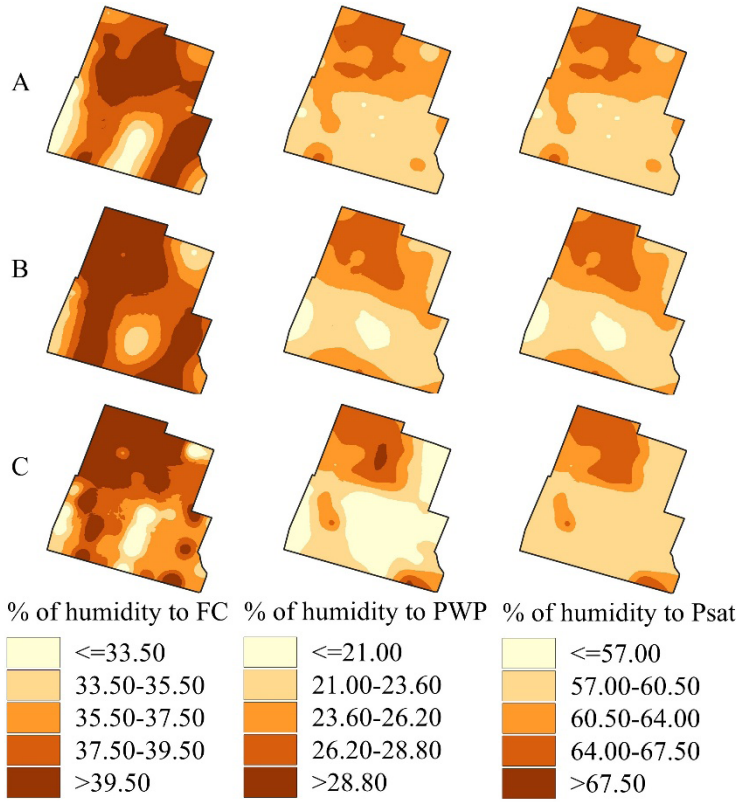

Figure 3. Spatial distribution of the percentage of humidity at field capacity (FC), permanent wilting point (PWP), and saturation point (Psat). A: Depth 0–30 cm; B: depth 30–60 cm; C: depth 60–90 cm.

Percentage of humidity at saturation point

At all three depths, the percentage of humidity saturation ranged between 57 and 67.5 %, which is associated with the high clay content of the soils and directly influences humidity retention (Chicas-Soto *et al*., 2014). Furthermore, as soil bulk density increased, so did the saturation humidity content (Alonso-Báez *et al*., 2023). At depths of 30–60 and 60–90 cm, no areas with saturation humidity content above 67.5 % were recorded. The lowest values of saturation humidity at the three depths were mainly concentrated in the southwest of the study area, while the highest values were associated with the north and northwest, particularly at a depth of 60–90 cm (Figure 3), where the highest clay content was found.

Water sheet stored in the soil

In this study, the replacement sheet was grouped into five classes: ≤12.9, 12.9–14.59, 14.59–16.28, 16.28–17.97, and >17.9 cm; nearly 90 % of the total area has a replacement sheet between 12.9 and 17.97 cm. This result implies the existence of a variable irrigation

rate and the need to avoid problems of water stress in plants, as noted in other studies (Reza *et al*., 2016). The information obtained from the maps allows the modeling of the humidity retention capacity of soils and shows the presence of spatial variation.

The sheet stored in the soil to the point of permanent wilting showed the highest values in the northwestern part of the study area. The humidity content at field capacity showed a distribution very similar to that of the 30–60 cm depth for this same parameter, with the highest values in the western and southeastern parts of the study area. Meanwhile, the humidity content at saturation showed its highest values in the northern part of the study area (Figure 4).

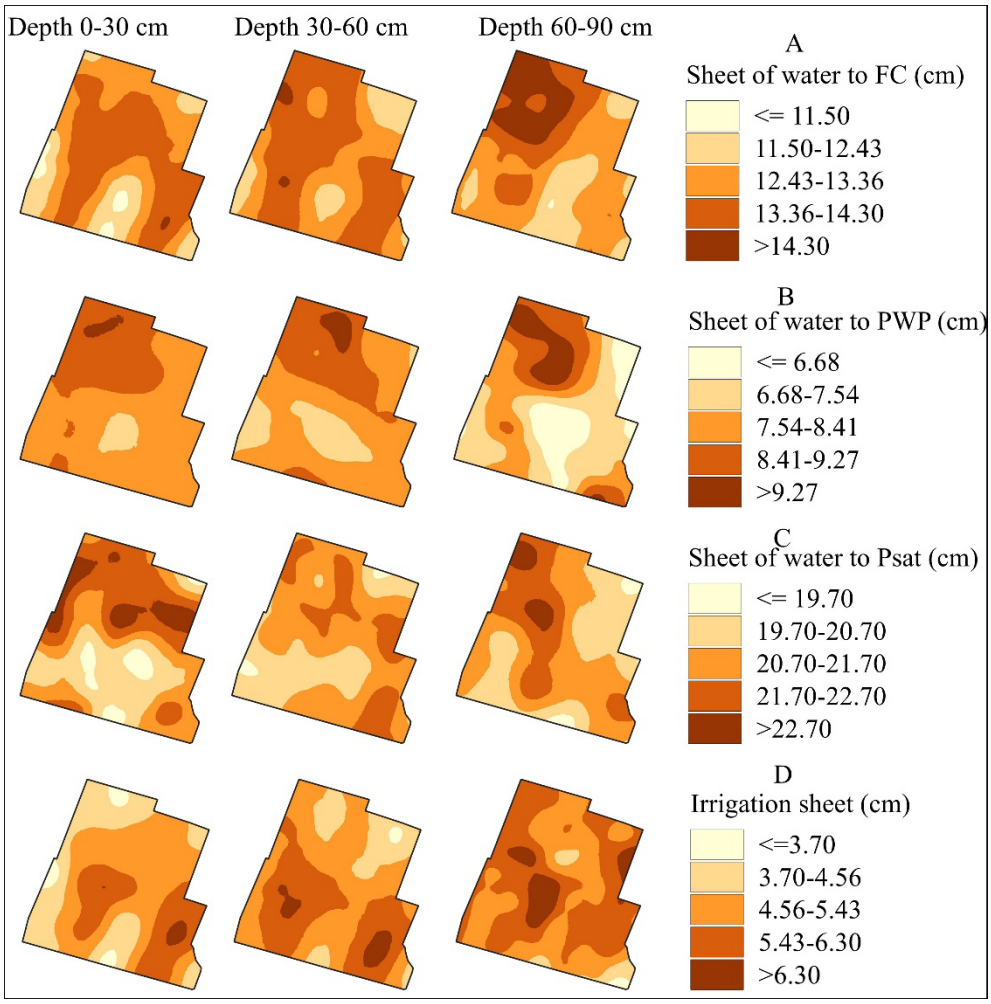

Figure 4. Spatial distribution of stored water depth (in cm). A: field capacity (FC) B: permanent wilting point (PWP) C: saturation point D: depth between CC and PWP (irrigation depth).

CONCLUSIONS

The water storage sheets for the 0–90 cm stratum showed a non-homogeneous spatial distribution in the 168 ha study area of the "La Victoria" farm in Teapa, Tabasco, both for the sheets corresponding to field capacity humidity content, permanent wilting point, saturation humidity, and replacement sheet. The application of geographic information systems made it possible to identify the areas with the greatest water storage potential at different depths. The creation of maps helped to visualize the areas with the highest and lowest amounts of water stored in the farm's soil. In addition, the physical properties of the soil determined the water content stored in the stratum, which was influenced by bulk density, field capacity, permanent wilting point, and saturation point.

ACKNOWLEDGEMENTS

We would like to thank the Juárez Autonomous University of Tabasco for its support in carrying out the project "Water requirements for banana cultivation in a river floodplain area in the municipality of Teapa," code 20221158.

REFERENCES

Alonso-Báez M, López-Guillen G, Grajales-Solís M. 2023. Mejoramiento de las propiedades hidráulicas del suelo en el cultivo de soya mediante el subsuelo. Revista Mexicana de Ciencias Agrícolas 14 (5): 78–89. https://doi.org/10.29312/remexca.v14i5.3102

Álvarez-Herrera JG, Ruiz-Berrío HD, Acosta-Tova DF. 2021. Evaluación geoestadística de atributos hidrofísicos del suelo en la granja Tunguavita, Paipa, Colombia. Ciencia e Ingeniería Neogranadina 31 (1): 127–138. https://doi.org/10.18359/rcin.5396

Amsili JP, van Es HM, Schindelbeck RR. 2024. Pedotransfer functions for field capacity, permanent wilting point, and available water capacity based on Random Forest models for routine soil health analysis. Communications in Soil Science and Plant Analysis 55 (13): 1967–1984. https://doi.org/10.1080/00103624.2024.2336573

Awal R, Safeeq M, Abbas F, Fares S, Deb SK, Ahmad A, Fares A. 2019. Soil physical properties spatial variability under long-term no-tillage corn. Agronomy 9 (11): 750. https://doi.org/10.3390/agronomy9110750

Bautista F. 2021. Geostatistical analysis of soil properties of the karstic sub-horizontal plain of the Yucatan Peninsula. Tropical and Subtropical Agroecosystems 24 (1). https://doi.org/10.56369/tsaes.3540

Behrens T, Viscarra-Rossel RA, Kerry R, MacMillan R, Schmidt K, Lee J, Scholten T, Zhu AX. 2019. The relevant range of scales for multi-scale contextual spatial modelling. Scientific Reports 9 (1). https://doi.org/10.1038/s41598-019-51395-3

Camana FA, Deutsch CV. 2019. The nugget effect. *In* Deutsch JL. (ed.), Geostatistics Lessons. http://geostatisticslessons.com/lessons/nuggeteffect (Retrieved: December 2025)

Chicas-Soto RA, Vanegas-Chacón EA, García-Álvarez N. 2014. Determinación indirecta de la capacidad de retener humedad en suelos de la subcuenca del río Torjá, Chiquimula, Guatemala. Revista Ciencias Técnicas Agropecuarias 23 (1): 41–46.

CONABIO (Comisión Nacional para el Conocimiento y Uso de la Biodiversidad). 2020. Edafología. Mapeo digital de suelos, propiedades del suelo. 1000m. Catálogo de metadatos geográficos. Ciudad de México, México. http://www.conabio.gob.mx/informacion/gis/?vns=gis_root/edafo/edfmdsuelo/edfmscsue/edfmscsu1m/cly_05cm_pgw (Retrieved: December 2025).

CONAGUA (Comisión Nacional del Agua). 2023. Normales climatológicas por estado. Gobierno de México. Comisión Nacional del Agua. Ciudad de México, México. https://smn.conagua.gob.mx/es/climatologia/informacion-climatologica/normales-climatologicas-por-estado?estado=tab (Retrieved: December 2025).

DOF (Diario Oficial de la Federación). 2002. NORMA Oficial Mexicana NOM-021-RECNAT-2000. Que establece las especificaciones de fertilidad, salinidad y clasificación de suelos. Estudios, muestreo y análisis. Gobierno de México. Secretaría del Medio Ambiente y Recursos Naturales. Ciudad de México, México. http://www.ordenjuridico.gob.mx/Documentos/Federal/wo69255.pdf (Retrieved: December 2025).

Han L, Wang C, Meng J, He Y. 2024. Variabilidad espacial de las propiedades físicas y hídricas del suelo en los bosques subtropicales del sur de China. Forests 15 (9): 1590. https://doi.org/10.3390/f15091590

INEGI (Instituto Nacional de Estadística y Geografía). 2017. Anuario estadístico y geográfico de Tabasco 2017. Ciudad de México, México. 443 p.

Li S, Li Q, Wang C, Li B, Gao X, Li Y, Wu D. 2019. Spatial variability of soil bulk density and its controlling factors in an agricultural intensive area of Chengdu Plain, Southwest China. Journal of Integrative Agriculture 18 (2): 290–300. https://doi.org/10.1016/s2095-3119(18)61930-6

Lince-Salazar LA. 2021. Capacidad de almacenamiento de agua en suelos cultivados en café y otras propiedades edáficas relacionadas. Revista Cenicafé 72 (1): e72101. https://doi.org/10.38141/10778/72101

Márquez K. 2021. Caracterización de la textura de suelo en la subcuenca del río Zaratí para la evaluación del sistema de agua subterránea. *In* Congreso Nacional de Ciencia y Tecnología. Asociación Panameña para el Avance de la Ciencia. Ciudad de Panamá, Panamá, pp: 271–277. https://doi.org/10.33412/apanac.2021.3203

Núñez-Ramírez F, Escobosa-García I, Cárdenas-Salazar V, Santillano-Cázares J, Ruelas-Islas J, Preciado-Rangel P, Díaz-Ramírez JB. 2020. Tensión de humedad del suelo, crecimiento, eficiencia en el uso del agua y rendimiento de maíz cultivado en el noroeste de México. Revista Terra Latinoamericana 38 (4): 805–815. https://doi.org/10.28940/terra.v38i4.763

Palma-López DJ, Cisneros-Domínguez J, Moreno-Cáliz E, Rincón-Ramírez A. 2007. Suelos de Tabasco: su uso y manejo sustentable. Colegio de Postgraduados. Fundación Produce Tabasco. Villahermosa, México. 195 p.

Pérez-Zapata J, Delgado BL, Osorio CJ, Bernal MM, Zapata HS. 2024. Variabilidad espacial de propiedades fisicoquímicas en suelos bananeros de Urabá-Colombia. Acorbat Revista de Tecnología y Ciencia 1 (1). https://doi.org/10.62498/artc.2407

Reza S, Nayak D, Chattopadhyay T, Mukhopadhyay S, Singh S, Srinivasan R. 2016. Spatial distribution of soil physical properties of alluvial soils: a geostatistical approach. Archives of Agronomy and Soil Science 62 (7): 972–981. https://doi.org/10.1080/03650340.2015.1107678

Sakaki T, Smits KM. 2015. Water retention characteristics and pore structure of binary mixtures. Vadose Zone Journal 14 (2): 1–7. https://doi.org/10.2136/vzj2014.06.0065

Salamanca-Jiménez A, Lince-Salazar LA, Alzate SNA. 2018. Variabilidad espacial de la densidad aparente del suelo a nivel de lote en café. Revista Cenicafé 69 (2): 47–59.

Sandoval-García C, Cantú-Silva I, González-Rodríguez H, Yánez-Díaz MI, Marmolejo-Monsiváis JG, Gómez-Meza MV. 2021. Efecto de diferentes usos del suelo en las propiedades físicas e hidrológicas de un Luvisol en Oaxaca. Revista Mexicana de Ciencias Forestales 12 (68): 151–177. https://doi.org/10.29298/rmcf.v12i68.982

SEMARNAT (Secretaría de Medio Ambiente y Recursos Naturales). 2024. Mapa con los diferentes grupos de suelos por textura que existen en el territorio mexicano. Gobierno de México. Secretaría de Medio Ambiente y Recursos Naturales. Subsistema de Información sobre el Ordenamiento Ecológico. Ciudad de México, México. https://gisviewer.semarnat.gob.mx/aplicaciones/uga_oe2/ (Retrieved: December 2025).

Suarez-Muñoz BS, Flores-Cadena CA, Cedeño-Bermeo JE, Chóez-Acosta LA. 2025. Modelos matemáticos no lineales aplicados a la agricultura. Revisión sistemática. RECIMUNDO 9 (2): 180–200. https://doi.org/10.26820/recimundo/9.(2).abril.2025.180-200

Varón-Ramírez VM, Araujo-Carrillo GA, Guevara-Santamaría MA. 2022. Colombian soil texture: Building a spatial ensemble model. Earth System Science Data 14 (10): 4719–4741. https://doi.org/10.5194/essd-14-4719-2022

Xu Y, He Q, Lu H, Yang K, Entekhabi D, Gianotti DJ. 2025. A global dataset of remote sensing-based soil critical point and permanent wilting point. Scientific Data 12 (1). https://doi.org/10.1038/s41597-025-05048-y

Yu H, Li X, Zhang Y, Wang J, Chen T. 2025. Spatiotemporal variability of precipitation extremes and their relationship with large-scale climate indices in China. Atmosphere 16 (2): 191. https://doi.org/10.3390/atmos16020191

Agrociencia

SLOW-FORMING TERRACES IN A MILPA SYSTEM INTERCROPPED WITH FRUIT TREES IN THE NORTHWEST OF THE STATE OF MEXICO: BIOPHYSICAL AND SOCIOCULTURAL FACTORS

Adrian **Plata-Cruz**[1], Adolfo **López-Pérez**[2], Horacio **Santiago-Mejía**[1*], Idelfonso **Ronquillo-Cedillo**[1], María Consuelo **Marín-Togo**[1], Blanca Estela **Santiago-Mejía**[3], Eladio **Moreno-González**[4]

[1]Universidad Intercultural del Estado de México. Maestría en Gestión de la Innovación Rural Sustentable. Libramiento Francisco Villa S/N, Colonia Centro, San Felipe del Progreso, State of Mexico, Mexico. C. P. 50640.
[2]Colegio de Postgraduados Campus Montecillo. Postgrado en Edafología. Carretera México-Texcoco km 36.5, Montecillo, Texcoco, State of Mexico, Mexico. C. P. 56264.
[3]Instituto Nacional de Investigaciones Forestales, Agrícolas y Pecuarias. Matamoros 61, Colonia Primero de mayo, Río Bravo, Tamaulipas, Mexico. C. P. 88900.
[4]Tecnológico de Estudios Superiores San Felipe del Progreso. Avenida Instituto Tecnológico S/N, Ejido Tecnológico, San Felipe del Progreso, State of Mexico, Mexico. C. P. 50640.
* Author for correspondence: horacio.santiago@uiem.edu.mx

Citation: Plata-Cruz A, López-Pérez A, Santiago-Mejía H, Ronquillo-Cedillo I, Marín-Togo MC, Santiago-Mejía BE, Moreno-González E. 2026. Slow-forming terraces in a milpa system intercropped with fruit trees in the northwest of the State of Mexico: Biophysical and sociocultural factors. **Agrociencia** 60(2): 269-284. https://doi.org/ 10.47163/agrociencia.v60i2.3259

Editor in Chief:
Dr. Fernando C. Gómez Merino

Received: September 15, 2025.
Approved: March 09, 2026.
Published in Agrociencia: March 17, 2026.

ABSTRACT

In the State of Mexico, 24 % of the soil suffers from severe water erosion. The Intercropped Milpa with Fruit Trees (MIAF) system creates Slow-Forming Terraces (SFT) through the row of fruit trees and the runoff filter. Sociocultural and biophysical factors have been identified in soil conservation that determine the effectiveness of technologies applied by farmers. The objective of this research was to analyze the biophysical and sociocultural factors that influence FPT in the MIAF system in the northwestern State of Mexico. FPT was analyzed through two topographic surveys of six MIAF plots on hillsides. To identify sociocultural and biophysical factors in FPT, six semi-structured interviews were conducted with farming families, and erodibility, erosivity, topography, and vegetation cover indices were obtained. To identify related factors, the data were analyzed using Spearman's rank correlation coefficient ($p \leq 0.05$). A predictive model was generated using multiple linear regression for the statistically significant factors. The 21 identified sociocultural factors were subjected to cluster analysis to observe their grouping. Three biophysical and eight sociocultural factors associated with FPT were identified in the MIAF. The factors of erosivity, erodibility, topography, income, livestock farming, agricultural education, and agriculture as the main source of income predict the SFT ($R^2 = 0.83$). Plots with soil fertility were distinguished from those without by the factors of income, livestock farming, agricultural education, and agriculture as the main source of income. The consideration of biophysical and sociocultural factors is crucial for the successful implementation of soil conservation strategies in agricultural regions.

Keywords: Runoff filter, socioeconomic factors, Mazahua area, peasant agriculture, living wall barrier.

INTRODUCTION

In Mexico, water erosion affects 76 % of the national territory, with mild (37.06 %) and moderate (26.37 %) erosion predominating (Bolaños-González *et al*., 2016). In the northwestern region of the State of Mexico, 24 % of the soil presents severe erosion problems (INEGI, 2023). The Intercropped Milpa with Fruit Trees (MIAF) system addresses this problem through the gradual formation of living wall terraces (Cadena-Iñiguez *et al*., 2018). These terraces retain soil, store moisture, and improve working conditions without the cost of terrace construction, since they form over time (Kraemer *et al*., 2019).

The variability in the Slow-Forming Terraces (SFT) in the MIAF of the northwestern State of Mexico raises questions about the influence of sociocultural and biophysical factors. Although previous studies indicate that both types of factors influence MIAF (Turrent-Fernández *et al*., 1995; Camas-Gómez *et al*., 2012; Pillado-Albarrán *et al*., 2021), their combined analysis has not been addressed. Furthermore, their results cannot be generalized, as they depend on location and social context (Lapar and Pandey, 1999). Understanding which factors influence the slow formation of living wall terraces in this region is necessary for proposing management improvements that are appropriate to local conditions and moving toward more effective soil conservation.

Biophysical and sociocultural factors have both direct and indirect effects on the SFT. Specifically, biophysical factors influence sediment production (Yu *et al*., 2021), while sociocultural factors shape producers' decisions regarding the adoption of conservation technologies (Barrantes-Aguilar *et al*., 2024). Sklenicka *et al.* (2015) report that tenant farmers implement fewer conservation practices than landowners. Similarly, Sklenicka *et al*. (2019) found greater soil loss in plots with older producers who lack post-secondary education and rent their land.

Martínez-Castro *et al*. (2020) indicated that experience, education, economic resources, and plot size are positively associated with the adoption of conservation technologies. Likewise, Siyum *et al*. (2022) showed that the number of livestock and access to extension services influence the likelihood of adopting the technology under study. Regarding biophysical factors, studies report that the original slope (Turrent-Fernández *et al*., 1995; Camas-Gómez *et al*., 2012), erodibility, erosivity (Camas-Gómez *et al*., 2012; Liu *et al*., 2013), and vegetation cover (Bolaños-González *et al*., 2016) affect sediment production and retention.

Based on the biophysical and sociocultural characteristics documented by CONABIO (2023) and INEGI (2023) for the northwest region of the State of Mexico, as well as previous research on the MIAF (Turrent-Fernández *et al*., 1995; Camas-Gómez *et al*., 2012) and studies that incorporate sociocultural aspects (Sklenicka *et al*., 2019; Barrantes-Aguilar *et al*., 2024), several factors differentiate the SFT in living wall

terraces within the MIAF system. These factors include poverty, migration, livestock practices, agricultural education, stubble management and pruning, erodibility, topography, and erosivity. The objective of this study was to analyze the biophysical and sociocultural factors that influence the SFT in MIAF plots of Mazahua peasant families in the State of Mexico to allow the development of collaborative strategies with the producers that focus on efficiency, sustainability, and adaptation to the biophysical and social context of the region.

MATERIALS AND METHODS

Study site

In the northwest of the State of Mexico, six hillside plots were established using the MIAF system (Figure 1). The first was established in 2018 in San Juan Coajomulco, Jocotitlán, with the producer Horacio Santiago-Mejía (SJC-HSM) (19° 44′ 19′′ N, 99° 57′ 18.7′′ W, altitude of 2650 m, precipitation of 825 mm, on Luvisol soil). Three plots were established in 2019 in Jaltepec, San José del Rincón, with María del Carmen Mateo-Salamanca (J-MCMS) (19° 35′ 37.3′′ N, 100° 5′ 51.3′′ W, altitude of 2718 m and precipitation of 811 mm), Francisco Vilchis-Maya (J-FVM) (19° 35′ 35.2′′ N, 100° 5′ 55.4′′ W, altitude of 2720 m and precipitation of 811 mm), and María del Carmen Marín-González (J-MCMG) (19° 36′ 24.8′′ N, 100° 6′ 23.6′′ W, altitude of 2713 m and precipitation of 840 mm). In 2020, another plot was established in Jaltepec, with Gloria Cárdenas-Morales (J-GCM) (19° 36′ 36.5′′ N, 100° 6′ 9.9′′ W, altitude of 2746 m and precipitation of 820 mm). The four plots in Jaltepec have Andosol soil. The last plot was established in 2020 in San Pablo Tlalchichilpa, San Felipe del Progreso, with Manuel Téllez-Hernández (SPT-MTH) (19° 42′ 58.98′′ N, 99° 59′ 6.19′′ W, altitude of 2669 m and precipitation of 831 mm, on Andosol soil).

Soil analyses indicate low levels of organic matter, with an average of 0.68 % in the surface layer (0–30 cm), and loam texture in all sites (Table 1). The six farming families who own these plots are members of the MIAF learning community and receive monthly training on technology. As part of the system, all plots are cultivated in strips of milpa with maize (*Zea mays* L.), beans (*Phaseolus vulgaris* L.), squash (*Cucurbita* spp.), tomatoes (*Solanum lycopersicum* L.), marigold (*Tagetes erecta* L.), and faba beans (*Vicia faba* L.), interspersed with strips of fruit trees such as peach (*Prunus persica* (L.) Batsch), apple (*Malus domestica* Borkh.), tejocote (*Crataegus mexicana* Moc. and Sessé ex DC.), plum (*Prunus domestica* L.), pear (*Pyrus communis* L.), and walnut (*Juglans regia* L.).

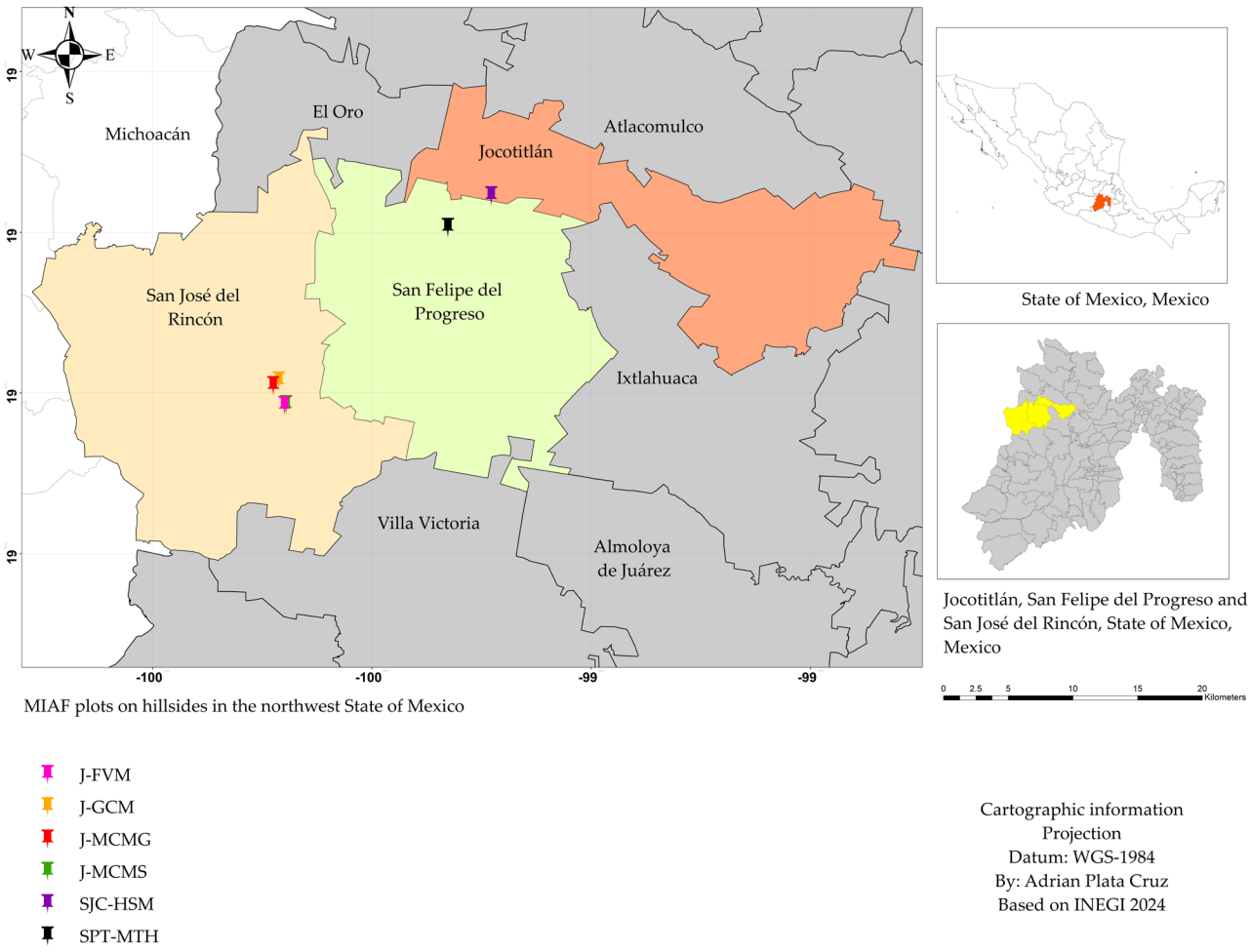

Figure 1. Location of the six Milpa Intercropped with Fruit Trees (MIAF) plots established on hillsides in three municipalities in the northwest of the State of Mexico, Mexico.

Table 1. Texture and organic matter (OM) of six plots with Intercropped Milpa with Fruit Trees (MIAF) in three municipalities of the northwest area of the State of Mexico, Mexico.

Plot	Sand (%)	Lime (%)	Clay (%)	OM (%)	Texture
SJC-HSM	41.55	43.83	14.61	0.59	Frank crumb
SPT-MTH	35.38	51.26	13.24	0.55	Lime frank
J-MCMS	33.19	36.01	30.79	1.05	Lime frank
J-GCM	30.13	57.31	12.55	0.91	Frank crumb
J-MCMG	35.01	49.85	15.12	0.49	Clayey loam
J-FVM	44.99	40.15	14.85	0.54	Frank crumb

SJC-HSM: San Juan Coajomulco, with Horacio Santiago-Mejía; SPT-MTH: San Pablo Tlalchichilpa, with Manuel Téllez-García; J-MCMS: Jaltepec, with María del Carmen Mateo-Salamanca; J-GCM: Jaltepec, with Gloria Cárdenas-Morales; J-MCMG: Jaltepec, with María del Carmen Marín-González; J-FVM: Jaltepec, with Francisco Vilchis-Maya.

Experiment management

Two types of modules were established: for plots with lower slopes (14.4 m) (SPT-MTH) and slopes greater than 10.6 m at 20 % (SJC-HSM, SPT-MTH, J-GCM, J-MCMS, and J-MCMG). Although the number of modules varied according to the size of the plot, only the first three were taken into account for this study, starting upstream. Each plot was managed in accordance with the technical recommendations (Cortés *et al*., 2005) provided during the MIAF learning community training sessions and in line with the criteria of each farming family.

Variables evaluated

Slow-forming terraces (SFT)

To evaluate the SFT, the following variables were calculated: 1) the original slope, 2) soil retention and loss in the MIAF modules for the years 2023 and 2024, and 3) changes in the slope of the terraces in the years 2023 and 2024. To determine the original slope, a topographic survey was conducted using a total station (Kolida KTS-442R6LC) that took readings every meter on the sides of the MIAF module where the system had not been altered by technology (Turrent-Fernández *et al*., 1995). Subsequently, the coordinates and profile of the original slope were projected using AutoCAD (Autodesk, Mill Valley, CA, USA) and CivilCAD 2021 software (CivilCAD, Tijuana, Mexico).

The estimation of soil retention and loss in the donor and recipient areas of the MIAF modules was carried out using two topographic surveys, the first in March 2023 and the second in March 2024. A total station (Kolida KTS-442R6LC) was used for this purpose. Readings were taken every meter or at each notable change in the topography of the terrain in five specific areas of the MIAF module (Figure 2).

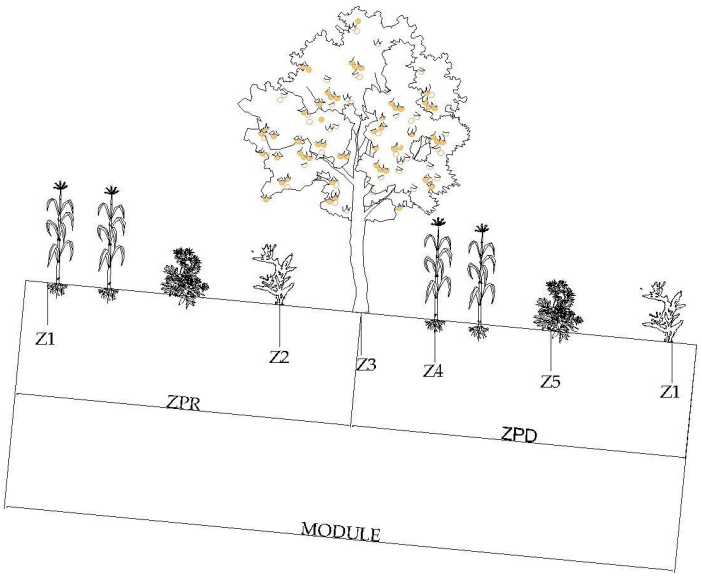

Figure 2. Cross-section of the Intercropped Milpa with Fruit Trees (MIAF) module, showing the points where topographic surveys were conducted on the six plots. Z1: start of the MIAF module; Z2: sediment receiving area; Z3: row of fruit trees; Z4: donor area; Z5: transport area. ZPR: potential sediment receiving area; ZPD: potential sediment donor area.

Using the readings from the topographic surveys, 1) the profiles of the original slope and the topography for 2023 and 2024 were projected; 2) the areas of soil loss and gain for both years were calculated; and 3) soil retention and loss (in Mg ha^{-1}) were obtained using the following formulas:

For modules with a slope >20 %,

$$ST = \frac{A * D * (5000/5.3)}{1000}$$

where ST is total soil (in Mg ha^{-1}), A is the area given by the profile comparison (in m^2), D is the soil bulk density (in kg m^{-3}), 5000 is the potential area of sediment loss or retention (in m^2) in one hectare of MIAF according to Turrent-Fernández *et al*. (1995), 5.3 is the length of the potential area of sediment loss or gain (in m) in a MIAF module with a slope >20 % (Turrent-Fernández *et al*., 1995), and 1000 is the conversion factor from kg to Mg.

For modules with a slope <20 %,

$$ST = \frac{A * D * (5000/7.2)}{1000}$$

where ST is total soil (in Mg ha^{-1}), A is the area given by the comparison of profiles (in m^2), D is the soil bulk density (in kg m^{-3}), 5000 is the potential area of sediment loss or gain (in m^2) in one hectare MIAF (Turrent-Fernández *et al*., 1995), 7.2 is the length of the potential area of sediment loss or gain (in m) in a MIAF module with a slope <20 % (Turrent-Fernández *et al*., 1995), and 1000 is the conversion factor from kg to Mg.
The slope changes in 2023 and 2024 were analyzed using profiles obtained from the areas where milpa is cultivated, without considering the barrier or the row of fruit trees, with the help of AutoCAD software.

Biophysical characterization of the plots

Erodibility

Soil samples were taken from the 0–30 cm layer for each of the six MIAF plots. These samples were analyzed following the method described by van Reeuwijk (1999). Data on texture, density, and organic matter content were obtained. Soil susceptibility to erosion was assessed using the K factor from the universal soil loss equation proposed by Wischmeier and Smith (1978), using the following formula:

$$K = 0.1317 * f_{csand} * f_{cl-si} * f_{organic} * f_{hisand}$$

where f_{csand} is the factor related to sand content, $f_{cl\text{-}si}$ is the factor related to silt and clay content, $f_{organic}$ is the factor related to organic carbon content, f_{hisand} is the parameter related to sand content, and 0.1317 is the conversion factor.

Rain erosivity

A rain gauge was installed in each of the six plots, and precipitation was recorded. To evaluate this parameter, the *R* factor of the Universal Soil Loss Equation (USLE) was selected according to Wischmeier and Smith (1978), using the method of Cortés-Torres *et al.* (1992), who divided the country into 14 zones and assigned a regression equation to each. The northwestern zone of the State of Mexico corresponds to zone V, which is defined by the following formula:

$$R = 3.4880P + 0.00088P^2$$

where *P* is the average annual precipitation, which in this case corresponds to the precipitation recorded in each rain gauge in a year.

Topography

The slope grade and length were evaluated using the USLE dimensionless slope-length (*LS*) factor for uniform slopes, according to Wischmeier and Smith (1978). Its calculation was performed using the topographic survey processed in AutoCAD and CivilCAD 2021. The *LS* topographic factor was obtained with the following formula:

$$LS = \left(\frac{X}{22.13}\right)^m (65.41 + 4.56s + 0.065s^2)$$

where *L* is the slope length factor, *S* is the slope inclination factor, *X* is the slope length (in m), *m* is the constant that depends on the slope inclination, and *s* is the inclination (in percent).

Plant cover

Given the difficulty of continuously monitoring the six plots, a structured questionnaire was used to record the species cultivated. Each plot could include one or more crops to which a vegetation cover index was assigned (Lianes *et al*., 2009). The values for the crops present in each plot were averaged to obtain a representative vegetation cover index per plot.

Sociocultural characterization of peasant families

Using a semi-structured questionnaire based on the guidelines proposed by Geilfus (2005), the information on various sociocultural variables was gathered among peasant

families. The questionnaire addressed topics such as migration, economic income, livestock, agricultural education, primary and secondary economic activities, health, cultural practices related to the milpa, beliefs, ethnicity, time spent with technology, challenges in attending the MIAF community, scheduling of milpa-related activities, types of machinery or animals utilized, available labor, the influence of various stakeholders, crop management practices, ownership status (owner or tenant), perceptions of erosion, pruning management, and stubble management.

Statistical analysis

A descriptive analysis was performed to evaluate the data related to the gradual formation of terraces. Sediment retention levels and the 25 sociocultural and biophysical soil factors were analyzed using Spearman's bivariate correlation in InfoStat 2020. A multiple linear regression model was constructed using the statistically significant variables in Past 2022. Finally, a cluster analysis was carried out with the 21 sociocultural factors using Ward's method and squared Euclidean distance, using InfoStat 2020.

RESULTS AND DISCUSSION

Gradual formation of terraces

Slow-forming terraces (SFT) varied among the six plots evaluated. In order of efficiency, SJC-HSM, J-MCMS, and SPT-ETH exhibited FPT due to soil loss and gain in the donor and recipient areas, respectively, and to the reduction of their original slopes. In the 2023 and 2024 topographic surveys, the three plots showed a similar pattern: in the donor area of the first module, soil loss was greater and gradually decreased toward the third module; in the recipient areas, the greatest retention was recorded in the second module. This indicates that the system is not closed and that the soil coming from the upper part (module 1) is mainly retained in the middle part (module 2) (Table 2).

In SJC-HSM, the amount of soil gained or lost decreased over time, coinciding with slope reductions of 50.14 and 33.39 % compared to the original slope and with stabilization. In contrast, in SPT-MTG and J-MCMS, the amounts of soil gained or lost were not yet stabilized, which is reflected in smaller slope reductions (20 and 14.42 %, respectively) (Table 3).

In the plots without SFT (in descending order, J-MCMG and J-FVM), soil movement was indiscriminate between receiving and donor zones. Transport was observed only from the first module to the third (Table 2), exhibiting a pattern of gain and loss over time. Although the slope temporarily decreased in both plots, the terraces returned to their original slope as the gained soil was lost; therefore, there was no stabilization of the slope changes (Table 3). In plot J-GCM, the gradual formation of terraces was partial, as it appeared in the first two modules but not in the third. Furthermore, the

Table 2. Slow-forming terraces in six plots with Intercropped Milpa with Fruit Trees (MIAF) in three municipalities of the northwest area of the State of Mexico.

Plot	Year	Module 1 (PAL)		Module 2 (PML)		Module 3 (PBL)	
		Recipient (Mg ha^{-1})	Donor (Mg ha^{-1})	Recipient (Mg ha^{-1})	Donor (Mg ha^{-1})	Recipient (Mg ha^{-1})	Donor (Mg ha^{-1})
SJC-HSM	2023	663.57	-521.62	851.92	-173.44	623.37	-39.71
	2024	130.06	-129.64	203.29	-47.37	150.52	-9.37
SPT-MTH	2023	196.99	-117.64	276.28	-51.27	85.98	-51.42
	2024	37.73	-41.27	124.67	-28.51	37.26	-14.86
J-MCMS	2023	290.79	-224.91	404.93	-157.27	227.99	-116.08
	2024	103.48	-69.74	139.73	-52.82	68.62	-34.26
J-GCM	2023	139.37	-82.85	143.41	-68.33	110.66	65.41
	2024	100.69	-64.91	122.57	-55.97	-79.21	-64.74
J-MCMG	2023	665.50	379.52	1274.31	46.70	-189.86	-438.81
	2024	-177.74	-417.84	-593.98	-298.60	660.98	633.88
J-FVM	2023	-216.39	-482.15	-253.40	-141.82	852.48	920.49
	2024	377.97	125.96	-213.16	-483.35	-992.97	-1020.12

SJC-HSM: San Juan Coajomulco, with Horacio Santiago-Mejía; SPT-MTH: San Pablo Tlalchichilpa, with Manuel Téllez-García; J-MCMS: Jaltepec, with María del Carmen Mateo-Salamanca; J-GCM: Jaltepec, with Gloria Cárdenas-Morales; J-MCMG: Jaltepec, with María del Carmen Marín-González; J-FVM: Jaltepec, with Francisco Vilchis-Maya; PAL: upper part of the slope; PML: middle part of the slope; PBL: lower part of the slope.

soil entering through the first module was not retained in any of them (Table 2), and the change in slope in the cultivable area was minimal between the first and second modules and nonexistent between the second and third (Table 3).

Spearman's bivariate correlation analyses between the total levels of retained soil and the 25 sociocultural and biophysical factors showed significant correlations ($p \leq 0.05$) only for erodibility (0.56), erosivity (0.61), topography (0.64), economic income (0.65), livestock (-0.61), agricultural education (0.51), agriculture as the main source of income (0.56), years with MIAF (0.61), external labor (0.56), stubble use (0.58), and pruning residues in the runoff filter (0.58). With these factors, the multivariate linear regression analysis showed that erosivity, erodibility, topography, economic income, livestock, agricultural education, and agriculture as the main source of income generate a prediction equation for soil retention levels ($R^2 = 0.83$), with a greater contribution from sociocultural factors compared to biophysical ones:

$$SR = 1599.5 - 0.2276\,ES + 20035\,ED + 184.42\,T + 300.99\,IE + 918.15\,G - 529.04\,EA + 1474.1\,AP$$

Table 3. Percentage change in slope on the terrace in the cultivable areas between strips of fruit trees in plots with Intercropped Milpa with Fruit Trees (MIAF) in three municipalities of the northwest of the State of Mexico, Mexico.

		Module 1	Module 2	Module 2	Module 3
Plot	Year	Donor Recipient (%)		Donor Recipient (%)	
SJC-HSM	PO	10.51		10.51	
	2023	5.24		7.00	
	2024	5.24		7.00	
SPT-MTH	PO	8.75		8.75	
	2023	7.00		7.00	
	2024	7.00		7.00	
J-MCMS	PO	12.28		12.28	
	2023	10.51		10.51	
	2024	10.51		10.51	
J-GCM	PO	12.28		12.28	
	2023	10.51		12.28	
	2024	10.51		12.28	
J-MCMG	PO	21.26		21.26	
	2023	17.63		21.26	
	2024	21.26		19.39	
J-FVM	PO	10.51		10.51	
	2023	10.51		7.00	
	2024	10.51		10.51	

SJC-HSM: San Juan Coajomulco, with Horacio Santiago-Mejía; SPT-MTH: San Pablo Tlalchichilpa, with Manuel Téllez-García; J-MCMS: Jaltepec, with María del Carmen Mateo-Salamanca; J-GCM: Jaltepec, with Gloria Cárdenas-Morales; J-MCMG: Jaltepec, with María del Carmen Marín-González; J-FVM: Jaltepec, with Francisco Vilchis-Maya; PO: Original pending.

where *SR* is the retained soil, 1599.5 is the constant, *ES* represents erosivity, *ED* erodibility, *T* topography, *IE* economic income, *G* livestock, *EA* agricultural education, and *AP* agriculture as the main source of income.

In plots where slow terraces formation was not observed, the biophysical factors did not show a consistent relationship. For example, in J-FVM and J-MCMG, current erosion differs considerably (19.13 and 62.56 Mg ha^{-1} $year^{-1}$, respectively), but this was not reflected in differences in the SFT (Table 4). Similarly, in the adjacent plots J-MCM and J-FVM, which share biophysical factors and similar upstream conditions, one presented SFT and the other did not (Figure 3).

Table 4. Biophysical factors and potential erosion in six plots with Intercropped Milpa with Fruit Trees (MIAF) in three municipalities in the northwest area of the State of Mexico.

Plot	Erodibility (dimensionless)	Erosivity (MJ ha^{-1} mm h^{-1})	Topography* (dimensionless)	Vegetation cover index	Adoption of conservation practices	Current erosion (Mg ha^{-1} year^{-1})
SJC-HSM	0.028	2278.65	2.135	0.407	0.60	32.69
SPT-MTH	0.022	2290.00	1.174	0.407	0.60	14.19
J-MCMS	0.025	2250.00	2.369	0.407	0.60	31.98
J-GCM	0.022	2268.30	1.882	0.407	0.60	22.54
J-MCMG	0.024	2310.30	3.526	0.407	0.80	62.56
J-FVM	0.026	2250.00	1.363	0.407	0.60	19.13

*Topography: topographic length-slope (LS) factor of the Universal Soil Loss Equation (USLE). SJC-HSM: San Juan Coajomulco, with Horacio Santiago-Mejía; SPT-MTH: San Pablo Tlalchichilpa, with Manuel Téllez-García; J-MCMS: Jaltepec, with María del Carmen Mateo-Salamanca; J-GCM: Jaltepec, with Gloria Cárdenas-Morales; J-MCMG: Jaltepec, with María del Carmen Marín-González; J-FVM: Jaltepec, with Francisco Vilchis-Maya.

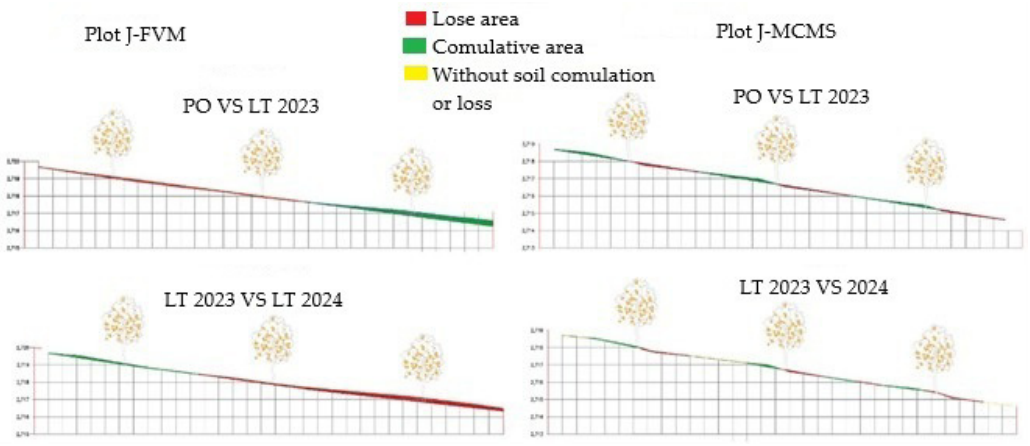

Figure 3. Profile contrast of two adjacent plots with Intercropped Milpa with Fruit Trees (MIAF) in the third (2023) and fourth year (2024) after their installation.

Sociocultural factors

Similarly, cluster analysis applied to sociocultural factors showed that plots with terraced fields (SFT) clustered together and were distinct from those with no or low terrace formation (Figure 4). Among the 21 sociocultural factors evaluated, it was the socioeconomic factors that differentiated production units exhibiting gradual terrace formation (SJC-HSM, SPT-ETH, and J-MCMS). Common factors included income, livestock, agricultural education, agriculture as the main source of income, years of implementation of MIAF, use of external labor, and management of runoff filters.

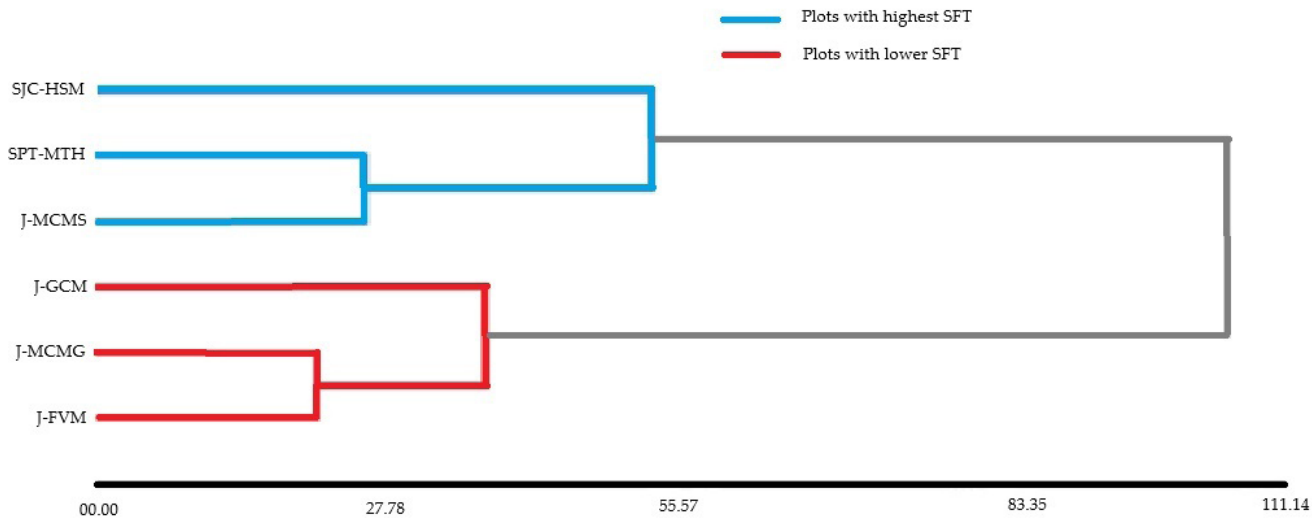

Figure 4. Grouping based on sociocultural factors of plots with Intercropped Milpa with Fruit Trees (MIAF) with and without Slow-Forming Terraces (SFT) in the northwest of the State of Mexico, Mexico.

The soil loss pattern in the donor areas of the plots with SFT coincided with that reported by Turrent-Fernández *et al*. (1998), where the greatest losses were concentrated in the upstream modules and decreased downstream. Sediment input into the system was documented, as soil loss was lower than the amount retained. In the SJC-HSM plot, which was managed according to the recommendations of the MIAF system, the practices included the placement of a runoff filter and the verification of soil turning downstream. Soil retention in this plot ranged from 542.45 to 756.7 m^3 ha^{-1} with 825 mm of annual precipitation.

In experimental plots with living wall terraces, where the filter and tillage were also controlled, the reported retention was 720 to 937 m^3 ha^{-1} with 1750 mm of precipitation (Turrent-Fernández *et al*., 1995). In these experimental contexts, the FPT is attributed to the interaction between biophysical and management factors, such as erosivity, slope, soil type, and tillage (Turrent-Fernández *et al*., 1995; Camas-Gómez *et al*., 2012; Liu *et al*., 2013). The gradual decrease and subsequent stabilization of the slope in the FPT occurred around the fourth year, a period similar to that observed in terraces with living walls of *Gliricidia sepium* (Jacq.) Kunth ex Walp., *Leucaena leucocephala* (Lam.) de Wit (Turrent-Fernández *et al*., 1995), and agroforestry systems with fruit trees (Do *et al*., 2023).

When plots are not experimental and management depends on farming families, socioeconomic factors explain the presence or absence of SFT. Agricultural education in at least one family member was common in plots with SFT, which favored appropriate practices such as the placement of the living wall. In this regard, Lal (2001) and Tesfahunegn *et al*. (2021) point out that agricultural education improves

understanding of the soil ecosystem, strengthens attitudes toward conservation (Lalani *et al*., 2016), and develops practical skills (Cipriano *et al*., 2022). Furthermore, it is associated with higher incomes (Siyum *et al*., 2022) and greater investment capacity and decision-making power (Martínez-Castro *et al*., 2020; Regalado-López *et al*., 2020). Higher incomes provide access to tools that facilitate the management and adoption of conservation technologies (Martínez-Castro *et al*., 2020).

In plots where there was no SFT, families had lower incomes and less access to resources. In J-FVM, the runoff filter was not installed because the crop residue was used as fodder and the pruning waste as firewood. According to Siyum *et al*. (2022), the adoption of certain plant species in agroecosystems is limited by the need for animal fodder. In J-GCM, the lack of access to LP gas forced the use of pruning waste as fuel. Barrantes-Aguilar *et al*. (2024) indicate that, even with training in soil conservation, families prioritize basic needs over conservation. Morales and Parada (2005) and Cotler *et al*. (2020) maintain that poverty limits the proper management of agroecosystems and perpetuates soil degradation.

CONCLUSIONS

The slow-forming terraces in plots using the Intercropped Milpa with Fruit Trees technology, managed by Mazahua families in the State of Mexico, were influenced by the interaction of sociocultural and biophysical factors. Although erodibility, erosivity, topography, and vegetation cover showed different behaviors among plots, they were not the only factors that influenced terrace formation. Soil retention levels were predicted by erosivity, erodibility, topography, economic income, livestock, agricultural education, and agriculture as the main source of income.

The use of crop residue as fodder or fuel affected the establishment of the runoff filter, preventing the gradual formation of terraces. In the plots where gradual terrace formation did occur, soil losses and gains decreased over time, and the slope stabilized by the fourth year. In the plots without terrace formation, the donor and recipient zones were indistinguishable, and soil movement was temporary and indistinct. For the successful establishment of soil conservation technologies in peasant agroecosystems, it is important to consider biophysical and sociocultural factors, and the latter to a greater extent.

ACKNOWLEDGEMENTS

We thank the Secretariat of Science, Humanities, Technology and Innovation (SECIHTI), for the postgraduate scholarship in Mexico, CVU number: 1236088. We also thank the Technological Institute of Higher Studies of San Felipe del Progreso for the loan of the surveying equipment, and the Colegio de Postgraduados for the fecilities provided to perfom soil analyses.

REFERENCES

Barrantes-Aguilar L, Gómez-Castillo D, Villalobos-Ramos V, Valdés-Salazar R. 2024. Factores que influyen en la adopción de prácticas sostenibles en el cultivo del arroz: el caso de Costa Rica. Agronomía Mesoamericana 35: 56879. https://doi.org/10.15517/am.2024.56879

Bolaños-González MA, Paz-Pellat F, Cruz-Gaistardo CO, Argumedo-Espinoza JA, Romero-Benítez VM, de la Cruz-Cabrera JC. 2016. Mapa de erosión de los suelos de México y posibles implicaciones en almacenamiento de carbono orgánico del suelo. Terra Latinoamericana 34 (3): 271–288.

Cadena-Iñiguez P, Camas-Gómez R, López Báez W, López-Gómez HC, González-Cifuentes JH. 2018. El MIAF, una alternativa viable para laderas en áreas marginadas del sureste de México: caso de estudio en Chiapas. Revista Mexicana de Ciencias Agrícolas 9 (7): 1351–1361. https://doi.org/10.29312/remexca.v9i7.1670

Camas-Gómez R, Turrent-Fernández A, Cortes-Flores JI, Livera-Muñóz M, González-Estrada A, Villar-Sánchez B, López-Martínez J, Espinoza-Paz N, Cadena-Iñiguez P. 2012. Erosión del suelo, escurrimiento y pérdida de nitrógeno y fósforo en laderas bajo diferentes sistemas de manejo en Chiapas, México. Revista Mexicana de Ciencias Agrícolas 3 (2): 231–243. https://doi.org/10.29312/remexca.v3i2.1459

Cipriano IM, Onautsu OD, Tarassoum DT, Adejumobi II, Bolakonga BA. 2022. Redefining conservation agriculture through appropriate use of herbicides and fertilisers to improve crop production in Mozambique. African Journal of Agricultural Research 18 (2): 136–145. https://doi.org/10.5897/ajar2021.15897

CONABIO (Comisión Nacional para el Conocimiento y Uso de la Biodiversidad). 2023. Portal de geoinformación 2023. Gobierno de México. Comisión Nacional para el Conocimiento y Uso de la Biodiversidad. Sistema Nacional de Información sobre Biodiversidad. Ciudad de México, México http://www.conabio.gob.mx/informacion/gis/ (Retrieved: April 2023).

Cortés FJI, Turrent FA, Díaz VP, Hernández RE, Mendoza RR, Acevedes RE. 2005. Manual para el establecimiento y manejo del sistema milpa intercalada con árboles frutales (MIAF) en laderas. Colegio de Postgraduados: Montecillo, México. 27 p.

Cortés-Torres HG, Figueroa-Sandoval CA, Ortiz-Solorio CA, González-Cossio FV. 1992. Caracterización de la erosividad de la lluvia en México utilizando métodos multivariados. Descripción de intensidades máximas e índices de erosividad de la lluvia. Agrociencia 3 (2): 115–138.

Cotler H, Corona JA, Galeana-Pizana MJ. 2020. Soil erosion and food deficiency in Mexico: A first approach. Investigaciones Geográficas 101. https://doi.org/10.14350/rig.59976

Do VH, La N, Bergkvist G, Dahlin AS, Mulia R, Nguyen VT, Öborn I. 2023. Agroforestry with contour planting of grass contributes to terrace formation and conservation of soil and nutrients on sloping land. Agriculture, Ecosystems and Environment 345 (1): 108323. https://doi.org/10.1016/j.agee.2022.108323

Geilfus F. 2005. 80 herramientas para el desarrollo participativo: diagnóstico, planificación, monitoreo y evaluación. Instituto Interamericano de Cooperación para la Agricultura: San José, Costa Rica. 217 p.

INEGI (Instituto Nacional de Estadística y Geografía). 2023. México en cifras. Ciudad de México, México. https://www.inegi.org.mx/app/areasgeograficas/default.aspx (Retrieved: June 2023).

Kraemer N, Dercon G, Cisneros P, Arango LF, Wellstein C. 2019. Adding another dimension: Temporal development of the spatial distribution of soil and crop properties in slow-forming

terrace systems. Agriculture, Ecosystems and Environment 283 (1). https://doi.org/10.1016/j.agee.2019.05.002

Lal R. 2001. Soil degradation by erosion. Land Degradation and Development 12 (6): 519–539. https://doi.org/10.1002/ldr.472

Lalani B, Dorward P, Holloway G, Wauters E. 2016. Smallholder farmers' motivations for using Conservation Agriculture and the roles of yield, labour and soil fertility in decision making. Agricultural Systems 146: 80–90. https://doi.org/10.1016/j.agsy.2016.04.002

Lapar LAL, Pandey S. 1999. Adoption of soil conservation: The case of the Philippine uplands. Agricultural Economics 21 (3): 241–256. https://doi.org/10.1111/j.1574-0862.1999.tb00598.x

Lianes E, Marchamalo M, Roldan M. 2009. Evaluación del factor C de la RUSLE para el manejo de coberturas vegetales en el control de la erosión en la cuenca del Río Birrís, Costa Rica. Agronomía Costarricense 33 (2): 217–235.

Liu SL, Dong YH, Li D, Liu Q, Wang, J, Zhang XL. 2013. Effects of different terrace protection measures in a sloping land consolidation project targeting soil erosion at the slope scale. Ecological Engineering 53: 46–53. https://doi.org/10.1016/j.ecoleng.2012.12.001

Martínez-Castro JC, Ramirez-Seañez AR, Marina-Clemente JA. 2020. Factores socioeconómicos y nivel de adopción tecnológica en unidades de producción de piña en Loma Bonita, Oaxaca, México. Investigación y Ciencia 28 (80): 70–79.

Morales C, Parada S. 2005. Pobreza, desertificación y degradación de los recursos naturales. Comisión Económica para América Latina y el Caribe: Santiago de Chile, Chile. 267 p.

Pillado-Albarrán KV, Albino-Garduño R, Santiago-Mejía H. 2021. MIAF como motor de desarrollo sustentable en la región mazahua del norponiente del Estado de México. *In* Martínez-Pellegrini SE, Sarmiento-Franco JF, Valles-Aragón MC. (eds.), Recuperación Transformadora de los Territorios con Equidad y Sostenibilidad. Universidad Nacional Autónoma de México, Instituto de Investigaciones Económicas y Asociación Mexicana de Ciencias para el Desarrollo Regional: Ciudad de México, México. 18 p.

Regalado-López J, Castellanos-Alanís A, Pérez-Ramírez N, Méndez-Espinoza JA, Hernández-Romero E. 2020. Modelo asociativo y de organización para transferir la tecnología milpa intercalada en árboles frutales (MIAF). Revista de Alimentación Contemporánea y Desarrollo Regional 30 (56). https://doi.org/10.24836/es.v30i56.983

Siyum N, Giziew A, Abebe A. 2022. Factors influencing adoption of improved bread wheat technologies in Ethiopia: Empirical evidence from Meket district. Heliyon 8 (2): e08876. https://doi.org/10.1016/j.heliyon.2022.e08876

Sklenicka P, Molnarova KJ, Salek M, Simova P, Vlasak J, Sekac P, Janovska V. 2015. Owner or tenant: Who adopts better soil conservation practices? Land Use Policy 47: 253–261. https://doi.org/10.1016/j.landusepol.2015.04.017

Sklenicka P, Zouhar J, Janeckova KM, Vlasak J, Kottova B, Petrzelka P, Gebhart M, Walmsley A. 2019. Trends of soil degradation: Does the socio-economic status of land owners and land users matter. Land Use Policy 95: 103992. https://doi.org/10.1016/j.landusepol.2019.05.011

Tesfahunegn GB, Ayuk ET, Adiku SGK. 2021. Farmers' perception on soil erosion in Ghana: Implication for developing sustainable soil management strategy. PLOS One 16 (3). https://doi.org/10.1371/journal.pone.0242444

Turrent-Fernández A, Francisco-Nicolás N, Uribe-Gómez S, Camacho-Castro R. 1998. La terraza de muro vivo, tecnología para la explotación prosostenible de laderas roturadas del trópico subhúmedo de México. Agricultura técnica de México 24: 67–81.

Turrent-Fernández A, Uribe-Gómez S, Francisco-Nicolás N, Camacho-Castro R. 1995. La terraza de muro vivo para laderas del tropico subhumedo de México. I. Ánalisis del desarrollo de la terraza durante 6 años. TERRA 13 (3): 276–298.

van Reeuwijk LP. 1999. Procedimientos para análisis de suelos. Colegio de Postgraduados: Montecillo, México. 145 p.

Wischmeier W, Smith D. 1978. Rainfall erosion losses: A guide to conservation planning. United States Departament of Agriculture. Washington, DC, USA. 58 p.

Yu S, Xie C, Jinsong Z, Wang Z, Wang L, Shi Z. 2021. Socioeconomic development mitigates runoff and sediment yields in a subtropical agricultural watershed in southern China. Environmental Research Letters 16 (2) 1–12. https://doi.org/10.1088/1748-9326/abdd5a

Agrociencia

FEATHERS AS INDICATORS OF EXPOSURE TO METALS: STUDY IN *Anas crecca* AND *Anser caerulescens* IN DURANGO, MEXICO

Martín Emilio **Pereda-Solís**[1], Manuel Armando **Salazar-Borunda**[1], José Hugo **Martínez-Guerrero**[1], Andrea **Vargas-Duarte**[1], Fernando **Flores-Morales**[1], Jaime **Rendón-von Osten**[2], Daniel **Sierra-Franco**[1*]

[1]Universidad Juárez del Estado de Durango. Facultad de Medicina Veterinaria y Zootecnia. Carretera Durango-Mezquital km 11.5, Durango, Durango, Mexico. C. P. 34307.
[2]Universidad Autónoma de Campeche. Instituto de Ecología, Pesquerías y Oceanografía del Golfo de México. Campus VI, Campeche, Campeche, Mexico. C. P. 24029.
* Author for correspondence: dan_1015@hotmail.com

Citation: Pereda-Solís ME, Salazar-Borunda MA, Martínez-Guerrero JH, Vargas-Duarte A, Flores-Morales F, Rendón-von Osten J, Sierra-Franco D. 2026. Feathers as indicators of exposure to metals: Study on *Anas crecca* and *Anser caerulescens* in Durango, Mexico. **Agrociencia** 60(2): 285-301. https://doi.org/ 10.47163/agrociencia.v60i2.3277

Editor in Chief:
Dr. Fernando C. Gómez Merino

Received: September 30, 2025.
Approved: January 21, 2026.
Published in Agrociencia: February 26, 2026.

ABSTRACT

The aim of this study was to evaluate the presence of inorganic elements in feathers of green-winged teals (*Anas crecca* Linnaeus, 1758) and snow geese (*Anser caerulescens* Linnaeus, 1758) that hibernate at Laguna de Santiaguillo in Durango. Additionally, the use of feathers as exposure indicators to metallic pollutants was determined. The hypothesis proposed was that the feathers of both bird species contain detectable concentrations of metals, indicating varying levels of exposure to environmental pollutants based on their habits and migration routes. During the 2021–2022 hunting season, a total of 30 green-winged teals and 27 snow geese were collected. The primary P9 and P10 feathers from the left wing of each bird were gathered for analysis. The feathers were cleaned, dehydrated, and analyzed using voltammetry to quantify the concentrations of Zn, Cd, Pb, Cu, Cr, Sn, Al, As, Ni, and Hg. The results revealed significant differences between species. The teals displayed higher concentrations of As, Cr, and Ni, whereas the geese had higher levels of Ni and Cu. Although essential elements like Zn and Cu were present in high concentrations, non-essential elements such as Cd and Pb were also detected. Particularly, Pb levels in some teal individuals were concerning due to their potential toxicity. Significant correlations were identified between certain metals (As-Cr and Pb-Zn), suggesting common exposures to anthropogenic sources, possibly related to agricultural and industrial activities. This study confirms that feathers serve as effective and non-invasive biomarkers to detect the exposure to metallic pollutants, providing a "chemical memory" of accumulation during growth. Consequently, the working hypothesis is accepted, establishing a foundation for future research and environmental conservation efforts focused on priority wetlands, such as Laguna de Santiaguillo.

Keywords: Heavy metals, metalloids, biomarkers, migratory aquatic birds.

INTRODUCTION

Heavy metals and other inorganic elements are widely distributed in the environment through the geological cycle (Abbasi *et al*., 2015; Vizuete *et al*., 2018). They are also released by diverse human activities (Abbasi *et al*., 2015; Abraham-Covarrubias and Peña-Cabriales, 2017), such as industrialization (Kolf-Clauw *et al*., 2007; Vizuete *et al*., 2018), combustion (Haygarth and Jones, 2017), smelting processes (Abdullah *et al*., 2015), motor vehicle emissions (Estrada-Guerrero and Soler-Tovar, 2014; Abraham-Covarrubias and Peña-Cabriales, 2017), mining (Abraham-Covarrubias and Peña-Cabriales, 2017; He *et al*., 2019), agricultural runoff (Abdullah *et al*., 2015; Abraham-Covarrubias and Peña-Cabriales, 2017), and petroleum-related activities (Borah and Deka, 2023).

Some inorganic elements, including zinc (Zn), copper (Cu), and selenium (Se), are essential for living organisms and play a crucial role in their biological functions. Cadmium (Cd), mercury (Hg), and lead (Pb), on the other hand, are not necessary for birds and have been shown to be bad for their health. These elements are naturally present in the environment, resulting in stable exposure levels, although birds have evolved to endure this exposure. The concentrations of essential elements in birds are typically balanced, unless exposure is excessively high, disrupting normal homeostatic processes (Custer, 2011).

Feathers serve as effective biomarkers for metal and metalloid exposure, as these elements bind to proteins in the bloodstream (Dauwe *et al*., 2003) and accumulate throughout their development and growth process (Lodenius and Solonen, 2013). Within the feather, the metals bind with the metallothioneins and become immobilized. Once the feather stops growing, it keratinizes and stops interacting with the physiology of the bird, which reflects the levels of metals accumulated during its period of growth or molt (Dauwe *et al*., 2003).

In this context, it was hypothesized that the feathers of green-winged teals and snow geese collected at Laguna de Santiaguillo in Durango, Mexico, contain detectable concentrations of inorganic elements that reflect a differential exposure to environmental contaminants, reflecting their ecological habits and migration routes. Likewise, it was considered that feathers can be used as non-invasive biomarkers to monitor the presence of metallic contaminants in migratory birds. The aim of this study was to evaluate the presence and concentration of inorganic elements in feathers from both species and determine their use as indicators of environmental exposure to generate information for environmental monitoring and the conservation of priority wetlands.

MATERIALS AND METHODS

Site of study

The study area covers an extension of 2542.16 km^2, encompassing territories within the municipalities of Nuevo Ideal, Canatlán, Santiago Papasquiaro, Coneto de Comonfort,

San Juan del Río, and El Oro in the basin of Laguna de Santiaguillo (Figure 1). The predominant climate in this region is temperate semi-dry, characterized by summer rains and scarce precipitation throughout the rest of the year. A subhumid temperate climate with summer rains is also found, along with a semi-cold subhumid climate. The mean monthly temperature in the region is approximately 17 °C, with a mean annual rainfall of 426.5 mm, concentrated between June and September (RAMSAR, 2012).

The basin of the Laguna de Santiaguillo presents a notable plant diversity, which is attributed to the topographic complexity of the region. Different types of forests are identified, including pine, pine-oak, oak-pine, and oak. There are also areas with riparian vegetation, xerophytic shrubland, grasslands, halophytic vegetation, and aquatic and semi-aquatic vegetation, as well as the typical vegetation of disturbed areas (RAMSAR, 2012).

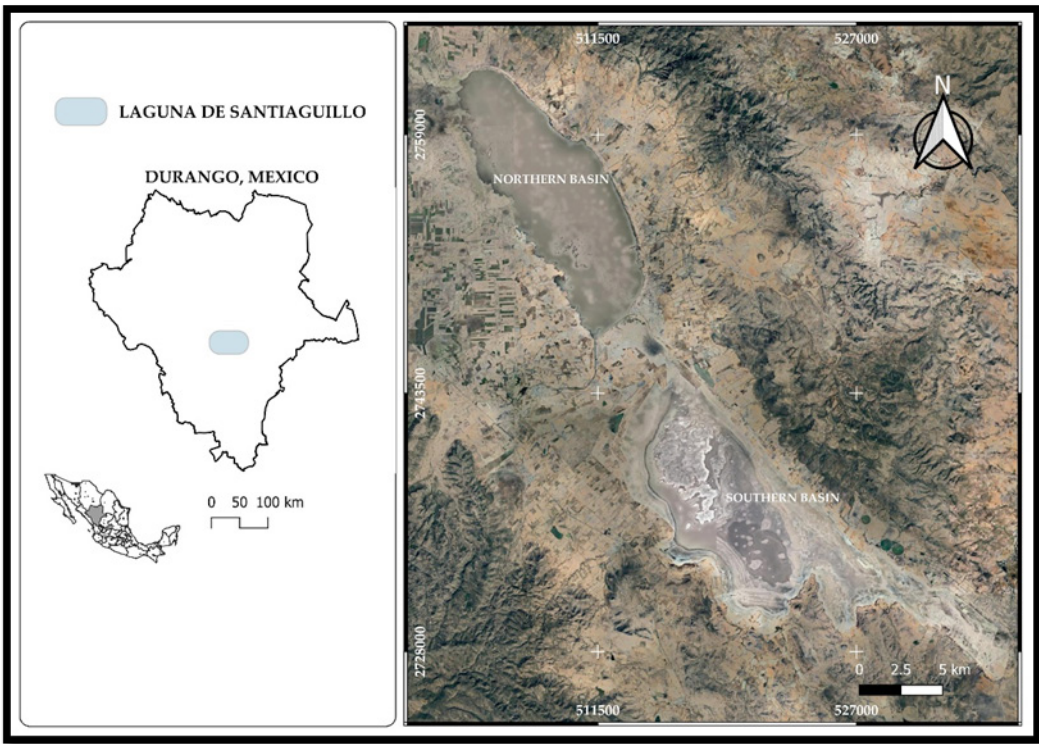

Figure 1. Location of the study site in Laguna de Santiaguillo, Durango, Mexico.

Bird collection

During the 2021–2022 hunting season, 27 snow geese (*Anser caerulescens* Linnaeus, 1758) and 30 green-winged teals (*Anas crecca* Linnaeus, 1758) were captured. The birds were collected with the help of service providers from the Wildlife Conservation

Management Unit, registered under SEMARNAT-UMA-EX-0150-DGO, with authorization document SGPA/DGVS/07540/21. In addition, volunteer hunters helped by donating the birds they hunted to this study.

Analysis of metals

Samples of primary feathers P9 and P10 of the left wings from captured birds were collected and stored in paper envelopes labelled for transportation to the laboratory of the Faculty of Veterinary Medicine and Animal Science (FMVZ) of the Juárez University of the State of Durango. The feathers were cleaned using a 1 % detergent solution (Triton® X-100, CAS 9002-93-1 Biopharm) for 4 h. Then, they were weighed in a fresh state on a precision scale (Sartorius CP224S) and dehydrated in a stove (Thermo Scientific 6964) at 35–45 °C for 48 h.

The dehydrated feathers were packaged and sent to the Institute of Ecology, Fisheries, and Oceanography of the Gulf of Mexico (EPOMEX) of the Autonomous University of Campeche. The samples were cut into small fragments to ensure an even representation of contaminants. From each feather, 0.3 g was transferred to Teflon tubes containing 3 mL of a 9:1 mixture of 65 % nitric acid and 37 % hydrochloric acid. The digestion of the samples was carried out using a MARS 5 microwave digestion system (EPA, 2007). The metals were determined using voltammetry (van den Berg, 1991) with a Metrohm 797 VA Computrace voltamperometer. The analyzed metals and their limits of detection (LOD) were Cd 0.05, Pb 0.03, Cu 0.05, Cr 0.05, Hg 0.02, As 0.02, Zn 0.05, Sn 0.03, Ni 0.4, and Al 0.05 ng g^{-1}.

Statistical analysis

The Minitab 19 (Minitab, LLC 2019) computer program was utilized for analysis. Since the data did not meet the assumptions of normality and homogeneity of variance necessary for parametric tests, the Kruskal-Wallis test was used to compare metal concentrations among species ($p < 0.05$). To identify the most prevalent metals in the feathers of the studied birds, prevalence was calculated as the percentage of samples with detectable concentrations (above LOD). Furthermore, a Spearman correlation analysis was conducted to assess the relationships between metal concentrations detected in both species, which facilitated the identification of shared or divergent bioaccumulation patterns.

RESULTS AND DISCUSSION

The concentrations of inorganic elements (Zn, Cd, Pb, Cu, Cr, Sn, Al, As, Ni, and Hg) found in feathers (Table 1 and Figure 2) varied according to the following pattern: for *A. crecca*, As > Cr > Cu > Ni > Hg > Zn > Sn > Pb > Al > Cd, whereas for *A. caerulescens*, Ni > Cr > Cu > As > Hg > Al > Sn > Zn > Pb > Cd. Coincidentally, in both species, Cr and Cu were found with the highest concentrations (second and third places, respectively), whereas Cd displayed the lowest concentrations. The rest of the elements displayed different distributions among species.

Table 1. Concentration (mg kg^{-1} dry base) of inorganic elements in feathers of green-winged teals (*Anas crecca*) and snow geese (*Anser caerulescens*) collected at Laguna de Santiaguillo, Durango, Mexico.

†Element	*Anas crecca* (n = 30)	*Anser caerulescens* (n = 27)	¶*p*-value
Zn	3.46 (8.53), 0.92–48.31	0.34 (0.13), 0.12–0.65	0.00
Cd	0.13 (0.48), 0.00–2.18	0.00 (0.02), 0.00–0.12	0.33
Pb	1.29 (3.35), 0.00–18.73	0.01 (0.04), 0.00–0.16	0.00
Cu	19.13 (25.57), 0.00–146.44	2.41 (1.12), 0.00–4.91	0.00
Cr	22.65 (20.54), 1.71–87.62	3.49 (3.40), 0.00–12.89	0.00
Sn	2.29 (7.20), 0.00–38.12	0.47 (1.77), 0.00–9.30	0.00
Al	0.56 (1.45), 0.00–7.39	1.49 (1.90), 0.00–6.88	0.05
As	24.64 (30.47), 0.00–122.28	2.01 (1.56), 0.17–5.47	0.00
Ni	18.57 (17.44), 0.71–71.98	4.61 (4.97), 0.00–15.57	0.00
Hg	4.09 (16.07), 0.00–76.52	1.52 (3.80), 0.00–15.08	0.22

†Values are reported as averages, (standard deviation), minimum–maximum.
¶Comparison between species (Kruskal-Wallis, $\alpha = 0.05$).

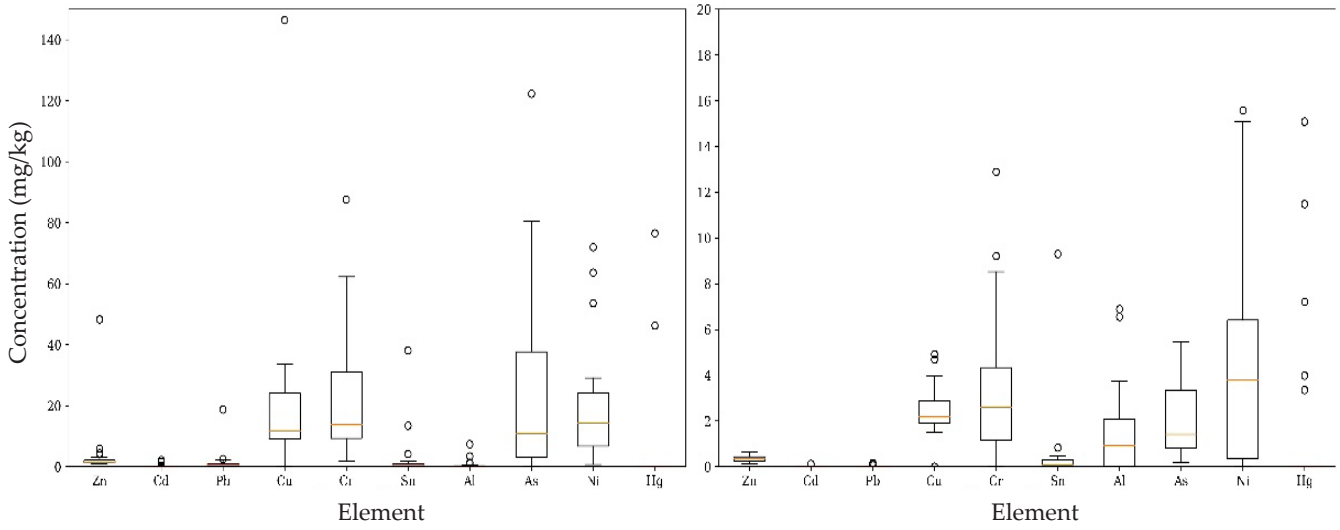

Figure 2. Median, quartiles, and extreme values of inorganic element concentrations (mg kg^{-1} dry base) in feathers of green-winged teals (*Anas crecca*, left) and snow geese (*Anser caerulescens,* right) captured at Laguna de Santiaguillo, Durango, Mexico.

These findings are similar to metal concentrations found in the feathers of two aquatic birds, *Ardea alba* and *Nycticorax nycticorax*, with Cr having the highest concentration. Furthermore, the species were found to accumulate metals in a different order (González *et al*., 2018).

Zinc

Zinc was detected in all samples of each species. The amount in the teal feathers was greater (Kruskal-Wallis, h = 41.9, p = 0.00) compared to those from geese. Zinc is an essential element that plays important parts in diverse metabolic reactions. To date, the effects of chronic exposure to Zn on organisms are not entirely known (Abdullah *et al*., 2015). This element has natural and anthropogenic origins (Ullah *et al*., 2014). It is used as a protective coating and in galvanization processes to prevent corrosion. It is also used in alloys and as a catalyst in the synthesis of certain polymers. In addition, it is less toxic than the other metals analyzed in this study (Newman and Unger, 2003).

Cadmium

The content of Cd in the feathers of teals and geese was below the toxicity threshold (>2 mg kg^{-1} dry base (DB)) (Burger and Gochfeld, 2000). This element was the least prevalent, as it was detected in 10 % of the teals and 3.7 % of the geese. The amount of Cd found in the teal and goose feathers was similar (h = 0.95, p = 0.33). Cd is not essential to organisms, as well as being toxic and carcinogenic (Laws, 1993). The harmful effects on birds include alterations in the formation of eggs, damage to testicles, malfunctioning of the oviduct, and kidney damage (Malik and Zeb, 2009).

This element is used to manufacture alloys, as a plastic stabilizer, in electroplating processes, galvanization, and the production of pigments, batteries, and other products. Cadmium is found in low concentrations in the rocks and soils, but it is chemically similar to Zn. In addition, it is obtained as a byproduct during Zn processing (Laws, 1993). Sewage sludge is often contaminated with Cd, and its application on agricultural soils can significantly contribute to the accumulation of this element (Jackson and Alloway, 1992).

Lead

The prevalence of Pb in teal feathers was 73.33 %, whereas for geese it was 14.81 %. The amount of Pb in teal feathers was higher than in geese (h = 24.03, p = 0.00). Although the average concentration in both species does not seem to indicate a significant exposure to this element, some teal individuals were observed to have concentrations of up to 18.7 mg kg^{-1}, suggesting a certain level of exposure.

Reports that suggest that concentrations of over 4 mg kg^{-1} of Pb in feathers are associated with alterations in behavior, thermoregulation, and locomotion, and consequently, a lower survival of chicks, as well as other physiological alterations such as hemolytic anemia and damage to the digestive tract and nervous system, which can even lead to death (Tsipoura *et al*., 2011; Estrada-Guerrero and Soler-Tovar, 2014). This toxic metal is ubiquitous due to its prolonged and widespread use in gasoline, batteries, welding, pigments, pipes, ammunition, paints, ceramics, and other uses. Bird poisoning can take place due to the ingestion of Pb pellets (Newman and Unger, 2003).

Copper

The prevalence of Cu in teal and geese feathers was 96.67 and 92.59 %, respectively. These values were the highest, considering all the inorganic compounds analyzed in this study. Teals presented a notably higher concentration compared to geese (h = 31.29, p = 0.00). These values are found within the range reported by Pandiyan *et al*. (2020) in feathers from 15 shorebirds in two hibernation sites in their migratory route in central Asia. In that study, the concentration of Cu in feathers had a range of 0.2–82.3 and 0.2–87.2 mg kg^{-1} DB in each location.

Copper is an essential element, required at low concentrations for several physiological processes such as red blood cell formation, blood vessel maintenance, the immune system, bones, glucose and cholesterol metabolism, the contractility of the myocardium, and hormonal development (Calvo-Bruzos *et al*., 2016). However, high doses or chronic exposures can lead to seriously harmful effects, including reproductive, respiratory, gastrointestinal, hematological, hepatic, endocrine, and ocular damage (Chen *et al*., 1993). Copper is widely used in the manufacture of cables, electronic devices, and pipes. It is also used to control the growth of algae, bacteria, and fungi. Although it is toxic in high concentrations, it can easily form complexes with organic matter dissolved in a solution, reducing the biologically available fraction (Newman and Unger, 2003).

Chromium

This element was found in 100 % of teals and in 88.89 % of geese. A concentration comparison between species displayed a higher value in teals (h = 30.76, p = 0.00). The presence of Cr in feathers at levels greater than 4 ppm is considered alarming (Pandiyan *et al*., 2020). In this study, teals displayed a high concentration (22.65 mg kg^{-1} BS), which could be harmful for them (Burger *et al*., 2015). The absorption of Cd, Cr, and Pb in bird feathers can be due to secretions of the uropygial gland and the nasal gland and may be enhanced by the binding affinity of keratin for heavy metals (Morais *et al*., 2012).

Intoxication by Cr is relevant, and some researchers are carrying out complementary studies to understand its impact on bird physiology, particularly on reproductive toxicology, which could provide clues towards wildlife management (Pandiyan *et al*., 2020). This element is used to manufacture alloys, catalysts, pigments, and wood preservatives. It is also used in the tanning of leather products. It can be found in hexavalent [Cr(VI)] and trivalent forms [Cr(III)]. Hexavalent Cr is carcinogenic, and it is the more toxic of the two (Newman and Unger, 2003).

Tin

In teals, the prevalence of this element was 73.33 %, and for geese, it was 59.26 %. Teals presented a higher Sn concentration in relation to the geese (h = 7.05, p = 0.00). Sn has no known function in humans, and the documentation of adverse effects is scarce (Thomas and McGill, 2008). As with some essential elements such as Cu and

Zn, there can be situations in which extreme Sn levels may lead to adverse effects (He *et al*., 2019).

Tin can be released into the environment through diverse anthropogenic and natural sources, including the flow of continental dust, volcanic emissions, and forest fires. The burning of fossil fuels, such as coal and oil, waste burning, and the production of Sn, organotin, iron, steel, and non-ferrous metals are significant sources of contamination. The release of Sn through these processes is approximately 10 times higher than the release from natural sources. These industrial and burning activities contribute to the presence of Sn in the atmosphere and ecosystems, which leads to potentially harmful environmental impacts (Cima, 2011).

Aluminum

This element had a prevalence of 63.33 % in teals and 74.07 % in geese. Average concentrations between species were similar (h = 3.68, p = 0.05) and lower than those reported by Solonen *et al*. (1998) in species in different habitats and trophic chains such as *Columbia livia* (5–250 mg kg^{-1} DB, n = 26), *Strix aluco* (5–200 mg kg^{-1} DB, n = 33), *Buteo buteo* (5–90 mg kg^{-1} DB, n = 21), *Accipiter nisus* (5–94 mg kg^{-1} BS, n = 20), *Accipiter gentilis* (5–140 mg kg^{-1} DB, n = 21), and *Pandion haliaetus* (33–110 mg kg^{-1} BS, n = 17).

Aluminum is the most abundant metallic element in the Earth's crust, accounting for 8 % of its composition. In normal pH conditions, it is found mainly as a component of minerals like gibbsite ($Al_2O_3 \cdot 3H_2O$) and kaolinite ($Al_2Si_2O_5(OH)_4$) (Stumm and Morgan, 1981). However, under low pH conditions, such as those caused by acid rain or drainage from mines, the presence of free Al (Al^{3+}) can increase to unusually high dissolved concentrations, which can be lethal to aquatic species (Newman and Unger, 2003).

Arsenic

The prevalence of As in teals and geese was 96.67 and 100 %, respectively. The concentrations observed in teals were higher than those in geese (h = 14.84, p = 0.00). In teals, As was the element with the highest concentrations in relation to the nine inorganic elements found in feathers (up to 122.28 mg kg^{-1} DB). The average values in the teals (24.6 mg kg^{-1}) in the study site are similar to those reported in two areas contaminated with As in Pakistan, where concentrations of 17–24.5 mg kg^{-1} were reported for herons (*Bubulcus ibis*) (Abdullah *et al.,* 2015).

This element is a metalloid used in the manufacturing of diverse products, such as pesticides, wood preservatives, plant desiccants, and herbicides. It is also linked to coal fly ash and is released when gold and lead are mined. Some fungi can methylate As, producing methylated, demethylated, and trimethylated arsines, which are volatile and highly toxic compounds (Atlas and Barta, 1981). Exposure to As occurs when birds spend their breeding season in areas affected by mining or intensive agriculture, where they eat grains contaminated with pesticides and herbicides.

Arsenic is one of the most toxic inorganic elements, as it can cause serious reproductive, genetic, immunological, cellular, and biochemical disorders (Abdullah *et al*., 2015). It

is also a carcinogenic compound (Newman and Unger, 2003). There are few reports on bird exposure to this element; however, it is important to know the shared risk that can exist with human populations that live near bodies of water where these birds are found.

Nickel

This element was found in 100 % of teal feather samples and 74.07 % from geese. Teals exhibited significantly higher concentrations (h = 18.22, p = 0.00), with some individuals reaching elevated levels (71.98 mg kg^{-1} DB). The average concentrations in geese (4.6 mg kg^{-1} DB) were lower than the values reported by Malik and Zeb (2009) in western cattle egret (*Bubulcus ibis*, 7.8–9 mg kg^{-1} DB) in agricultural areas. High Ni concentrations were recorded in *B. ibis* feathers in places near areas with industrial activity related to the manufacturing of electric devices and Ni-Cd batteries, with ranges of 30–47.5 and 77–89 mg kg^{-1} DB (Abdullah *et al*., 2015). Excess amounts of Ni may have an impact on feather molt (Malik and Zeb, 2009). It is used in alloys such as stainless steel and nickel-plating processes and has countless applications, including the production of batteries. At high enough concentrations, it is toxic and carcinogenic (Newman and Unger, 2003).

Mercury

The prevalence of mercury was 6.67 % in the teals and 18.52 % in the geese. The teals presented extreme values of up to 76.52 mg kg^{-1} DB. A comparison of average values in both species resulted in similar values (h = 1.45, p = 0.22). The average values detected in teal feathers (4 mg kg^{-1}) seem to indicate some level of exposure to this element, as experimental references (Jackson *et al*., 2011) suggest that values of more than 3 ppm (mg kg^{-1}) may generate some signs of intoxication. González *et al*. (2018) conducted measurements in feathers from *Ardea alba, Egretta thula,* and *Nycticorax nycticorax* from Chapala Lake and found maximum values of 1.1 mg kg^{-1}. The source of Hg in aquatic systems may be due to the discharge of industrial wastewater.

Mercury is used in the electronics industry, dental amalgam, gold mining, and paint manufacturing. Phenylmercury compounds and Hg salts are used as fungicides for seed treatments and to inhibit the growth of algae and slime on metallic structures in diverse industries (Atlas and Barta, 1981). This element can be released into the environment as a residue from chemical laboratory products, batteries, fungicides, pharmaceutical products, and as a component in wastewater effluents (Manahan, 2000). When Hg enters water systems, it can remain in the water or sediments (García-Herruzo *et al*., 2010). It is also present in areas where agrochemicals are used (Doadrio-Villarejo, 2004).

Correlation analysis

Results show significant correlations between diverse metals found in the feathers of both species (Figures 3 and 4), which suggests possible sources of contamination or shared bioaccumulation mechanisms.

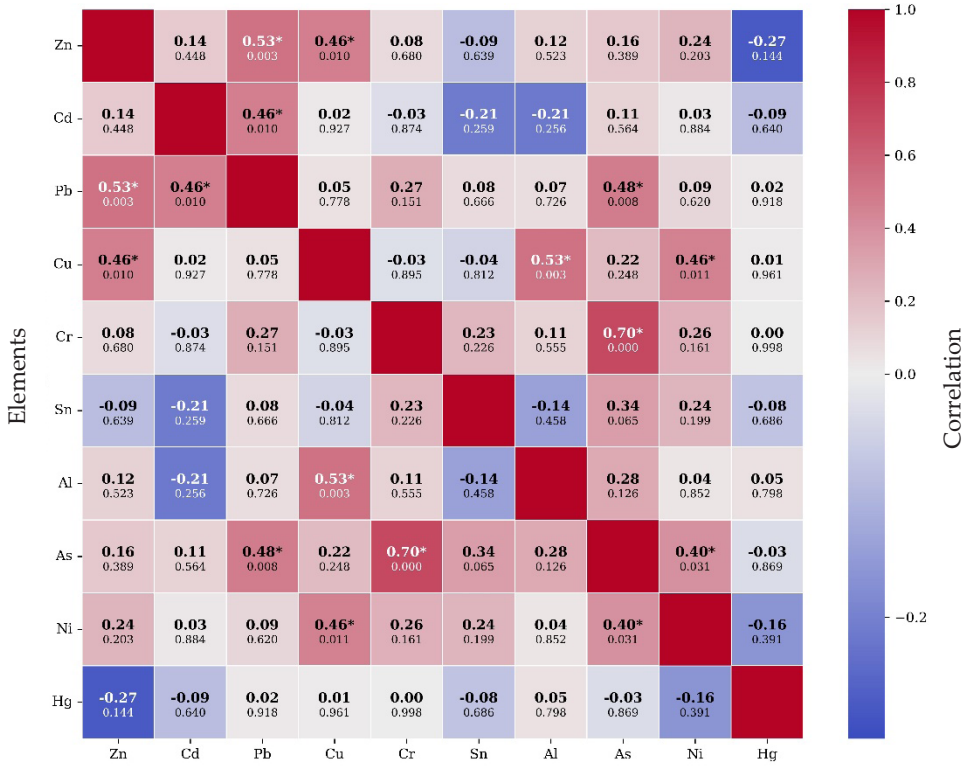

Figure 3. Correlation between the concentrations of metals and metalloids in feathers of green-winged teals (*Anas crecca*) collected at Laguna de Santiaguillo, Durango, Mexico. Each cell shows the Spearman coefficient correlation and *p*-value. Significant correlations ($p < 0.05$) are marked with an asterisk (*).

Correlation of metals in green-winged teals

A significant correlation was identified between Pb and Zn (r = 0.53, p = 0.003), suggesting that both metals could share a common source of exposure. This association can be attributed to anthropogenic activities, such as industrial emissions or urban waste (Newman and Unger, 2003; Ullah *et al*., 2014). On the other hand, As and Cr displayed the strongest correlation among the metals analyzed (r = 0.7, $p < 0.001$), which suggests that these elements come from similar sources, such as pesticides (Atlas and Barta, 1981; Izydorczyk *et al*., 2021) or contaminants found in bodies of water near feeding sites. Likewise, Cu and Al displayed a significant correlation (r = 0.53, p = 0.003), probably related to mining activities or industrial discharges (Izydorczyk *et al*., 2021) that impact the reproduction and resting areas of birds in their migration path. As and Pb showed a moderate yet significant correlation (r = 0.48, p = 0.008), indicating a possible relationship between both metals in the exposure environment. On the other hand, the relation between Ni and Cu (r = 0.46, p = 0.011) suggests possible interactions in bioaccumulation processes or coincidental sources of environmental

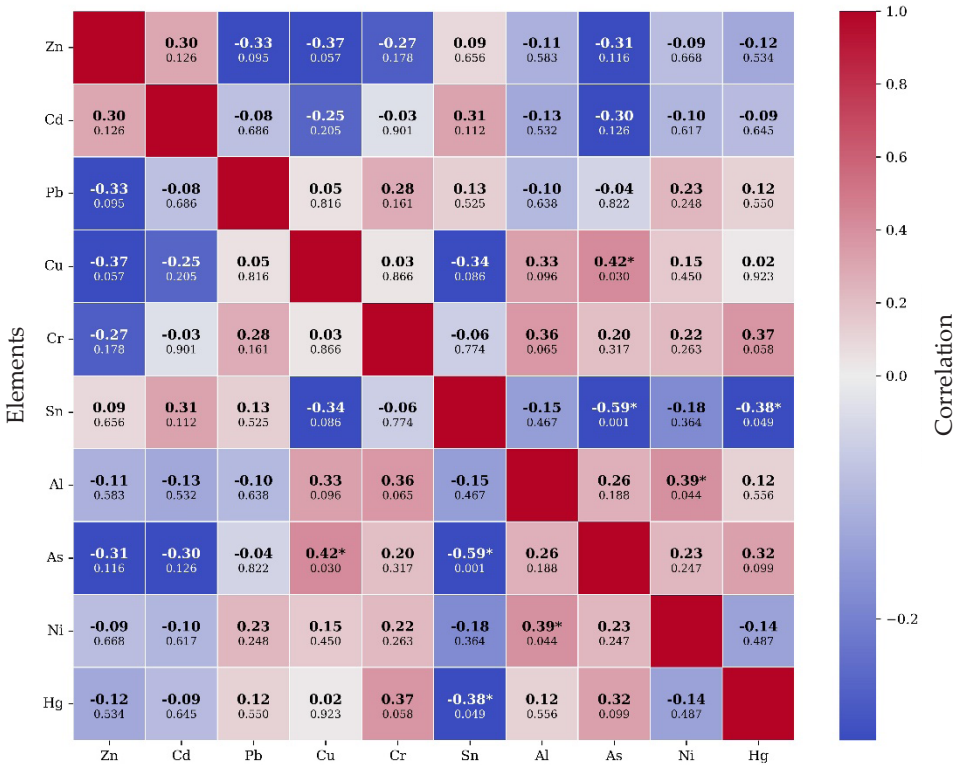

Figure 4. Correlation between the concentrations of metals and metalloids in feathers of snow geese (*Anser caerulescens*) collected at Laguna de Santiaguillo, Durango, Mexico. Each cell shows the Spearman coefficient correlation and *p*-value. Significant correlations ($p < 0.05$) are marked with an asterisk (*).

contamination. Mercury exhibited weak or negative correlations with the majority of the analyzed elements, suggesting distinct sources or bioaccumulation mechanisms, likely associated with atmospheric emissions or accumulation via aquatic food webs (Charvát *et al*., 2020). Tin displayed low and non-significant correlations with the metals analyzed, such as with Pb (r = 0.08, $p = 0.666$); therefore, it could be associated with independent contamination sources, such as electronic waste or specific manufacturing activities (Cima, 2011).

Correlation of metals in snow geese

Cu and As (r = 0.42, $p = 0.03$) presented a significant association that can be attributed to common sources of contamination, such as pesticides or fertilizers used in agricultural fields. Arsenic is a known component in agrochemical products (Atlas and Barta, 1981), while Cu is used as a fungicide (Newman and Unger, 2003) and may be found in the same environments. Geese may be simultaneously exposed to both elements through their diets or the water in wetlands where they feed. Likewise, a significant

correlation was found between Ni and Al (r = 0.39, p = 0.044), which indicates that these elements could share an environmental source, such as industrial emissions or sediments contaminated in wetlands (Newman and Unger, 2003).

Sn and As (r = -0.59, p = 0.001) displayed a significant reverse correlation, which suggests different paths of exposure or bioaccumulation in the environment of the snow geese. While As could be related to agricultural sources (Atlas and Barta, 1998), Sn is usually associated with industrial activities or materials used in construction, such as paints or coatings (Cima, 2011). The low co-occurrence of both metals may be due to their environmental availability or the metabolic processes that regulate their deposition on the feathers.

Hg and Sn (r = -0.38, p = 0.049) also presented a negative relation, which may be due to differences in the environmental distribution of both metals. Mercury is mainly related to contamination from the combustion of carbon and industrial processes (Charvát *et al*., 2020), whereas Sn could come from local specific activities. The interaction between both metals could be competitive or reflect a spatial segregation of the sources of contamination.

Finally, Cr and Al (r = 0.36, p = 0.065) displayed a moderate correlation, though not significant. This suggests a possible coexistence of both metals in the wetlands inhabited by geese. Both Cr and Al are transported through water currents and suspended particles (Newman and Unger, 2003), indicating a simultaneous environmental exposure, although not necessarily a joint accumulation in tissues. From a toxicological perspective, simultaneous exposure to multiple toxic metals can negatively affect the health of birds, including reduced fertility, alterations in migratory behavior, and chronic toxicity.

Use of feathers as biomarkers

Evaluating the presence of contaminants in geese and teals requires careful and specific focus due to the migratory nature of these species and the unique characteristics of their feathers, which reflect the accumulation of contaminants during their growth and provide a temporary "memory" of exposure. Focusing on primary feathers has the advantage of being easy to gather in a non-invasive way and covering an adequate exposure period. Collecting the same feathers (P9 and P10) from different birds helps minimize variability and provides a practical and convenient base for biomonitoring (Jaspers *et al*., 2006). In addition, it is always important to wash the feathers to remove external contaminants.

For the birds studied, the exposure occurs in breeding areas, during hibernation, and throughout the migratory route. Foods and metal concentrations can vary considerably between different areas. The interpretation of metal concentrations in feathers must take into account the metal load found not only in reproductive areas but also the molting patterns of the species involved (Lodenius and Solonen, 2013). The primary feather growth pattern of snow geese and green-winged teals is a well-structured biological and migratory cyclic process. Molting normally takes place after

the breeding season and before migration, ensuring that these birds have new and functional feathers for their migratory flight (Pyle, 2005; Marmillot *et al*., 2016).

In the case of snow geese, molting takes place between June and November (Mlodinow *et al*., 2024). During this period, the synchronized replacement of primary and secondary feathers renders the birds incapable of flying for approximately four weeks. The place in which molting takes place varies depending on individual conditions. In general terms, successful breeders molt near their places of birth. However, in many cases, particularly in birds that did not reproduce successfully, it occurs in places far from their places of birth. Other aquatic birds also exhibit this pattern (Bellrose, 2010). For geese, these specific locations are not yet fully known, although it has been suggested that they could include the Great Arctic Lakes (Reed *et al*., 2003).

The molt of the plumage (or prebasic molt) of the green-winged teal occurs mainly in breeding areas (Johnson *et al*., 2020). During this stage, adults experience a complete molting of their flight feathers after the reproductive season, which produces a flightless period (Sjöberg, 1988). This process is common in breeding regions located in the northern areas of the continent, such as Canada and Alaska, where the green-winged teal breeds. However, some individuals may move to other nearby areas, before molting, in search of safer places with abundant resources. This phenomenon is known as molt migration. In hibernation areas (such as the southern United States, Mexico, and Central America), molting can be less relevant or incomplete, since the alternative plumage does not imply changes as drastic as in the prebasic molt (Johnson *et al*., 2020).

The knowledge of molting patterns helps differentiate exposure to metals in breeding areas and hibernating sites independently (Johnels *et al*., 1979; Burger *et al*., 1992). The analysis of metal and metalloid concentrations in the collected feathers of teals and geese during winter can reflect the exposure levels to these elements in breeding habitats (Ramos *et al*., 2009). Examining these feathers is an important way to check the health of both aquatic and terrestrial habitats, find where pollution is coming from, and learn how it might affect ecosystems and biodiversity.

CONCLUSIONS

This study offers a detailed characterization of the presence of inorganic elements on the feathers of green-feathered teals and snow geese that hibernate at Laguna de Santiaguillo, Durango. Both species displayed significant concentrations of metals and metalloids, although the patterns of accumulation differed between them. Teals displayed higher concentrations of As, Cr, and Ni, while geese had higher levels of Ni and Cu, suggesting differences in their exposure and bioaccumulation pathways. Essential metals such as Zn and Cu were detected in high concentrations, as well as non-essential metals such as Cd and Pb, the latter in concerning levels in some teal individuals. Correlations between elements suggest a common exposure to sources of anthropogenic origin and interspecific differences in bioaccumulation.

ACKNOWLEDGEMENTS

To the North American Wetlands Conservation Act of the U.S. Fish and Wildlife Service for funding the project for Pronatura Noreste (F21AP01277-00), "Conservation of three critical wetlands in the central flyway," from which the results published here derive. To Biologist Velia Patricia Carrillo-Buentello from Pronatura Noreste A.C., for her constant management and logistical support in the development of the project. To Mr. Juan Pablo Jiménez, from the company Durango Hunting, for his support in the collection of birds. To the students of the FMVZ of the Juárez University of the State of Durango, Rebeca Valdez-Abdo, Bryan Alexis Martínez-García, and Andrés Saucedo-Rentería, for their collaboration in fieldwork and bird collection.

REFERENCES

Abbasi NA, Jaspers VLB, Chaudry MJI, Ali S, Malik RN. 2015. Influence of taxa, trophic level, and location on bioaccumulation of toxic metals in bird's feathers: A preliminary biomonitoring study using multiple bird species from Pakistan. Chemosphere 120: 527–537. https://doi.org/10.1016/j.chemosphere.2014.08.054

Abdullah M, Fasola M, Muhammad A, Malik SA, Bostan N, Bokhari H, Kamran MA, Shafqat MN, Alamdar A, Khan M, *et al*. 2015. Avian feathers as a non-destructive bio-monitoring tool of trace metals signatures: A case study from severely contaminated areas. Chemosphere 119: 553–561. https://doi.org/10.1016/j.chemosphere.2014.06.068

Abraham-Covarrubias S, Peña-Cabriales JJ. 2017. Contaminación ambiental por metales pesados en México: Problemática y estrategias de fitorremediación. Revista Internacional de Contaminación Ambiental 33 (1): 7–21. https://doi.org/10.20937/RICA.2017.33.esp01.01

Atlas RM, Barta R. 1998. Microbial ecology: Fundamentals and applications. Addison-Wesley Publishing Company: London, UK. 694 p.

Bellrose FC. 2010. Ducks, geese, and swans of North America (Revised edition). University of Nebraska Press: Lincoln, NE, USA. 387 p.

Borah G, Deka H. 2023. Crude oil associated heavy metals (HMs) contamination in agricultural land: Understanding risk factors and changes in soil biological properties. Chemosphere 310: 136890. https://doi.org/10.1016/j.chemosphere.2022.136890

Burger J, Gochfeld M. 2000. Metal levels in feathers of 12 species of seabirds from Midway atoll in the northern Pacific Ocean. Science of Total Environment 257 (1): 37–52. https://doi.org/10.1016/S0048-9697(00)00496-4

Burger J, Nisbet IC, Gochfeld M. 1992. Metal levels in regrown feathers assessment of contamination on the wintering and breeding grounds in the same individuals. Journal of Toxicology Environmental Health 37 (3): 363–374. https://doi.org/10.1080/15287399209531677

Burger J, Tsipoura N, Niles L, Gochfeld M, Dey A, Mizrahi D. 2015. Mercury, lead, cadmium, arsenic, chromium and selenium in feathers of shorebirds during migrating through Delaware Bay, New Jersey: Comparing the 1990s and 2011/2012. Toxics 3 (1): 63–74. https://doi.org/10.3390/toxics3010063

Calvo-Bruzos SC, Gómez-Candela C, Nomdedeu L, López-Plaza B. 2016. Manual de alimentación. Planificación alimentaria. Universidad Nacional de Educación a Distancia. Madrid, España. 566 p.

Charvát P, Klimes L, Pospísil J, Klemes JJ, Varbanov PS. 2020. An overview of mercury emissions in the energy industry - A step to mercury footprint assessment. Journal of Cleaner Production 267: 122087. https://doi.org/10.1016/j.jclepro.2020.122087

Chen R, Wei L, Huang H. 1993. Mortality from lung cancer among copper miners. Occupational and Environmental Medicine 50 (6): 505–509. https://doi.org/10.1136/oem.50.6.505

Cima F. 2011. Tin: Environmental pollution and health effects. Encyclopedia of Environmental Health 2011: 351–359. https://doi.org/10.1016/b978-0-444-52272-6.00645-0

Custer CM. 2011. Swallows as a sentinel species for contaminant exposure and effect studies. *In* Elliott JE, Bishop CA, Morrisey CA. (eds.), Wildlife ecotoxicology. Springer, New York, NY, USA, pp: 45–91. https://doi.org/10.1007/978-0-387-89432-4_3

Dauwe T, Bervoets L, Pinxten R, Blust R, Eens M. 2003. Variation of heavy metals within and among feathers of birds of prey: Effects of molt and external contamination. Environmental Pollution 124 (3): 429–436. https://doi.org/10.1016/S0269-7491(03)00044-7

Doadrio-Villarejo AL. 2004. Ecotoxicología y acción toxicológica del mercurio. Anales de la Real Academia Nacional de Farmacología 70 (4): 933–959.

EPA (United States Environmental Protection Agency). 2007. Method 3051A (SW-846): Microwave assisted acid digestion of sediments, sludges, and oils. Washington, DC, USA. 30 p.

Estrada-Guerrero DM, Soler-Tovar D. 2014. Las aves como bioindicadores de contaminación por metales pesados en humedales. Ornitología Colombiana 14: 145–160.

García-Herruzo F, García-Rubio A, Gómez-Lahoz C, Vereda-Alonso C, Rodríguez-Maroto JM. 2010. El mercurio: situación actual, problemas y soluciones. Ingeniería Química 480: 84–91.

González D, Álvarez-Bernal D, Mora M, Buelna-Osben HR, Ruelas-Isunza JR. 2018. Biomonitoreo de metales pesados en plumas de aves acuáticas residentes del lago de Chapala, México. Revista Internacional de Contaminación Ambiental 34 (2): 215–224. https://doi.org/10.20937/rica.2018.34.02.03

Haygarth PM, Jones KC. 2017. Atmospheric deposition of metals to agricultural surfaces. *In* Adriano DC. (ed.), Biogeochemistry of Trace Metals. Lewis Publishers. Boca Raton, FL, USA, pp: 249–276.

He C, Su T, Liu S, Jiang A, Goodale E, Qiu G. 2019. Heavy metal, arsenic and selenium concentrations in bird feathers from a region in Southern China impacted by intensive mining of non-ferrous metals. Environmental Toxicology 39 (2): 371–380. https://doi.org/10.1002/etc.4622

Izydorczyk G, Mikula K, Skrzypczak D, Moustakas K, Witek-Krowiak A, Chojnacka K. 2021. Potential environmental pollution from copper metallurgy and methods of management. Environmental Research 197: 111050. https://doi.org/10.1016/j.envres.2021.111050

Jackson AK, Evers DC, Etterson MA, Condon AM, Folsom SB, Detweiler J, Schmerfeld J, Cristol DA. 2011. Mercury exposure affects the reproductive success of a free-living terrestrial songbird, the Carolina wren (*Thryothorus ludovicianus*). The Auk 128 (4): 759–769. https://doi.org/10.1525/auk.2011.11106

Jackson AP, Alloway BJ. 1992. The transfer of cadmium from agricultural soils to the human food chain. *In* Adriano DC. (ed.), Biogeochemistry of Trace Metals. CRC Press: Boca Raton, FL, USA, pp: 109–158.

Jaspers VLB, Voorspoels S, Covaci A, Eens M. 2006. Can predatory bird feathers be used as a non-destructive biomonitoring tool of organic pollutants? Biology Letters 2 (2): 283–285. https://doi.org/10.1098/rsbl.2006.0450

Johnels A, Tyler G, Westermark T. 1979. A history of mercury levels in Swedish fauna. Ambio 8 (4): 160–168.

Johnson K, Carboneras C, Christie DA, M. Kirwan GM. 2020. Green-winged Teal (*Anas crecca*). *In* Billerman SM. (ed.), Birds of the World. Cornell Lab of Ornithology, Ithaca, NY, USA. https://doi.org/10.2173/bow.gnwtea.01

Kolf-Clauw M, Guénin A, Pérez-López M. 2007. Micromamíferos y metales pesados: biomonitorización del medio ambiente. Observatorio Medioambiental 10: 19–37.

Laws EA. 1993. Aquatic pollution: An introductory text (Second edition). John Wiley and Sons: New York, NY, USA. 611 p.

Lodenius M, Solonen T. 2013. The use of feathers of birds of prey as indicators of metal pollution. Ecotoxicology 22 (9): 1319–1334. https://doi.org/10.1007/s10646-013-1128-z

Malik RN, Zeb N. 2009. Assessment of environmental contamination using feathers of *Bubulcus ibis* L., as a biomonitor of heavy metal pollution, Pakistan. Ecotoxicology 18 (5): 522–536. https://doi.org/10.1007/s10646-009-0310-9

Manahan SE. 2000. Environmental chemistry. CRC Press: Boca Raton, FL, USA. 786 p.

Marmillot V, Gauthier G, Cadieux MC, Legagneux P. 2016. Plasticity in moult speed and timing in an arctic-nesting goose species. Journal of Avian Biology 47 (5): 650–658. https://doi.org/10.1111/jav.00982

Mlodinow SG, Mowbray TB, Cooke F, Ganter B. 2024. Snow Goose (*Anser caerulescens*). *In* Rodewald PG, Sly ND. (eds.), Birds of the World. Cornell Lab of Ornithology: Ithaca, NY, USA. https://doi.org/10.2173/bow.snogoo.02

Morais S, Costa FG, Pereira ML. 2012. Heavy metals and human health. *In* Oosthuizen J. (ed.), Environmental Health - Emerging Issues and Practice. IntechOpen: London, UK, pp: 227–246. https://doi.org/10.5772/29869

Newman MC, Unger MA. 2003. Fundamentals of ecotoxicology (Second edition). CRC Press: Boca Raton, FL, USA. 458 p.

Pandiyan J, Jagadheesan R, Karthikeyan G, Mahboob S, Al-Ghanim KA, Al-Misned F, Ahmed Z, Krishnappa K, Elumalai K, Govindarajan M. 2020. Probing of heavy metals in the feathers of shorebirds of Central Asian Flyway wintering grounds. Scientific Reports 10 (1): 22118. https://doi.org/10.1038/s41598-020-79029-z

Pyle P. 2005. Molts and plumages of ducks (Anatinae). Waterbirds 28 (2): 208–219.

Ramos R, González-Solís J, Ruiz X. 2009. Linking isotopic and migratory patterns in a pelagic seabird. Oecologia 160 (1): 97–105. https://doi.org/10.1007/s00442-008-1273-x

RAMSAR. 2012. Ficha informativa del humedal RAMSAR Laguna de Santiaguillo. México. Servicio de Información sobre Sitios Ramsar. https://rsis.ramsar.org/RISapp/files/RISrep/MX2046RIS_2511_es.pdf (Retrieved: December 2024).

Reed ET, Bêty J, Mainguy J, Gauthier G, Giroux JF. 2003. Molt migration in relation to breeding success in greater snow geese. Arctic 56 (1): 76–81. https://doi.org/10.14430/arctic604

Sjöberg K. 1988. The flightless period of free-living male teal (*Anas crecca*) in northern Sweden. Ibis 130 (2): 164–171. https://doi.org/10.1111/j.1474-919x.1988.tb00968.x

Solonen T, Lodenius M, Tulisalo E. 1998. Metal levels of feathers in birds of various food chains in southern Finland. Ornis Fennica 76: 25–32.

Stumm W, Morgan JJ. 1981. Aquatic chemistry: An introduction emphasizing chemical equilibrium in natural waters. John Wiley and Sons: New York, NY, USA. 780 p.

Thomas VG, McGill IR. 2008. Dissolution of copper, tin, and iron from sintered tungsten-bronze spheres in a simulated avian gizzard, and an assessment of their potential toxicity to birds. The Science of the Total Environment 394 (2–3): 283–289. https://doi.org/10.1016/j.scitotenv.2008.01.049

Tsipoura N, Burger J, Newhouse M, Jeitner C, Gochfeld M, Mizrahi D. 2011. Lead, mercury, cadmium, chromium, and arsenic levels in eggs, feathers, and tissues of Canada geese of the New Jersey Meadowlands. Environmental Research 111 (6): 775–784. https://doi.org/10.1016/j.envres.2011.05.013

Ullah K, Hashmi MZ, Malik RN. 2014. Heavy-metal levels in feathers of cattle egret and their surrounding environment: A case of the Punjab province, Pakistan. Archives of Environmental Contamination and Toxicology 66 (1): 139–153. https://doi.org/10.1007/s00244-013-9939-8

van den Berg CMG. 1991. Potentials and potentialities of cathodic stripping voltammetry of trace elements in natural waters. Analytica Chimica Acta 250: 265–276. https://doi.org/10.1016/0003-2670(91)85075-4

Vizuete J, Pérez-López M, Míguez-Santiyán MP, Hernández-Moreno D. 2018. Mercury (Hg), Lead (Pb), Cadmium (Cd), Selenium (Se), and Arsenic (As) in liver, kidney, and feathers of gulls: A review. Reviews of Environmental Contamination and Toxicology 247: 85–146. https://doi.org/10.1007/398_2018_16

VOLUME 60, NUMBER 2 | February 16 - March 31, 2026 | MEXICO